Graduate Theses and Dissertations

12-2021

Formation of Reactive Nitrogen Species During Dichloramine Decay and Their Impact on N Nitrosodimethylamine Formation Under Drinking Water Conditions

Huong Thu Pham
University of Arkansas, Fayetteville

Formation of Reactive Nitrogen Species During Dichloramine Decay and Their Impact on
N-Nitrosodimethylamine Formation Under Drinking Water Conditions

A dissertation submitted in a partial fulfillment
of the requirements for the degree of
Doctor of Philosophy in Engineering

by

Huong Thu Pham
Vietnam National University - Ho Chi Minh City University of Science
Bachelor of Science in Chemistry, 2013
University of Arkansas
Master of Science in Civil Engineering, 2017

December 2021
University of Arkansas

This dissertation is approved for recommendation to the Graduate Council.

_____
Julian Fairey, Ph.D.
Dissertation Director

_____   _____
Wen Zhang, Ph.D.   David Wahman, Ph.D.
Committee Member   Committee Member

_____
Justin Chimka, Ph.D.
Committee Member

Abstract

NDMA occurrence and formation pathways in drinking water systems are reviewed and NDMA yields are compared on the basis of disinfectant type, water chemistry, and precursor category. In chloramination, despite monochloramine being the predominant species between pH 7-9, evidence suggests that dichloramine is the primary species involved in NDMA formation. This is somewhat confounding as NDMA yields are maximal at pH 9, yet at pH 9 dichloramine decays faster than it forms and hence is present at trace levels; additionally, the proposed mechanism involves a spin-forbidden incorporation of dissolved oxygen as a triplet, which is presumably kinetically slow. This review reveals that kinetic data for NDMA formation is lacking, and its influence on chloramine chemistry has not been carefully considered.

In pH 7-10 waters amended with 10 μM total dimethylamine and 800 μeq $Cl_2 \cdot L^{-1}$ dichloramine ($NHCl_2$), NDMA, nitrous oxide (N_2O), dissolved oxygen (DO), $NHCl_2$, and monochloramine (NH_2Cl) were kinetically quantified. $NHCl_2$, N_2O, and DO profiles indicated reactive nitrogen species (RNS) formed during $NHCl_2$ decomposition, including nitroxyl/nitroxyl anion (HNO/NO^-) and peroxynitrous acid/peroxynitrite anion ($ONOOH/ONOO^-$). Experiments with uric acid (an $ONOOH/ONOO^-$ scavenger) implicated $ONOOH/ONOO^-$ as a central node for NDMA formation, which was further supported by concomitant *N*-nitrodimethylamine formation. A kinetic model accurately simulated $NHCl_2$, NH_2Cl, NDMA, and DO concentrations and included (1) the unified model of chloramine chemistry revised with HNO as a direct product of $NHCl_2$ hydrolysis, (2) HNO/NO^- then reacting with (i) HNO to form N_2O, (ii) DO to form $ONOOH/ONOO^-$, or (iii) $NHCl_2$ or NH_2Cl to form nitrogen gas, and (3) NDMA formation via $ONOOH/ONOO^-$ or their decomposition products reacting with (i) dimethylamine (DMA) and/or (ii) chlorinated unsymmetrical dimethylhydrazine (UDMH-Cl), the product of $NHCl_2$ and DMA.

Overall, updated $NHCl_2$ decomposition pathways are proposed, yielding (1) RNS via $NHCl_2 \rightarrow$

$HNO/NO^- \xrightarrow{O_2} ONOOH/ONOO^-$ and (2) NDMA via $ONOOH/ONOO^- \xrightarrow{\text{UDMH-}\atop\text{or DMA}} NDMA$.

The role of DO was further examined at pH 9 by assessing kinetic profiles of $NHCl_2$ and NDMA under ambient DO (~280 µM) and low-DO (< 20 µM) conditions in the presence and absence of 10 µM TOTDMA. Uric acid completely shut down NDMA formation under the low-DO condition, validating $ONOOH/ONOO^-$ as the central node in NDMA formation. Yield experiments with initial $NHCl_2$ of 200-, 400-, and 800 µeq $Cl_2 \cdot L^{-1}$ tracked the formation of NH_3/NH_4^+, NH_2Cl, N_2O, N_2, NO_2^-, and NO_3^-. NH_3/NH_4^+ yields were 20–40% greater under the low-DO condition, implying a reaction occurred between NH_3/NH_4^+ and $ONOOH/ONOO^-$ or its decomposition products. NH_2Cl yields were 16–20% lower under the low-DO condition, revealing a previously unknown NH_2Cl formation reaction. Under ambient DO conditions, about 80% of the nitrogen was accounted for compared to the low-DO conditions in which nitrogen recoveries were 90- and 100% in the absence and presence of 10 µM TOTDMA, respectively. An existing mechanistic model accurately predicted NH_3/NH_4^+, NH_2Cl, and N_2 under ambient conditions but underpredicted N_2O and overpredicted NO_2^- and NO_3^-. The results provide a framework to guide future experiments with $ONOOH/ONOO^-$ generators and revise the mechanistic model to better capture the nitrogenous end-products.

Table of Contents

List of Published Papers

Chapter 2

Pham H., Zhang W., Wahman D., Fairey J., 2019. *N*-nitrosodimethylamine (NDMA) Formation Mechanism in Drinking Water Systems. Wiley Encyclopedia of Water: Science, Technology, and Society. John Wiley & Sons, New York, NY 1 – 14.

Chapter 3

Pham H., Wahman D., Fairey J., 2021. Updated Reaction Pathway for Dichloramine Decomposition: Formation of Reactive Nitrogen Species and N-Nitrosodimethylamine. Environmental Science & Technology, 55 (33), 1740 – 1749.

Chapter 4

Pham H., Wahman D., Chimka J., Fairey J., 2021. Effect of Dissolved Oxygen and Dimethylamine on Dichloramine Decomposition Products: Evidence of Additional Reactions Pathways Revealed by Nitrogen Mass Balances. Environmental Science & Technology, In Progress.

Chapter 1

Introduction

1.1-Problem Statement

The occurrence and control of disinfection byproducts (DBPs) in drinking water systems has been studied for 40 years but remains an ongoing regulatory compliance and chronic toxicity issue throughout the United States. Natural organic matter (NOM) present in source water reacts with disinfectants, such as chlorine or chloramines, to form both halogenated DBPs, such as trihalomethanes (THMs) and dihaloacetonitrile (DHANs), and non-haloagenated DBPs, such as *N*-nitrosamines.

N-nitrosamines are a family of extremely potent carcinogens, of which *N*-nitrosodimethylamine (NDMA) is the most commonly reported species in drinking water systems (Russell et al., 2012). NDMA is a precursor to a carcinogen that has been shown to induce liver cancer in rats (Heath, 1962). The International Agency for Research on Cancer, which operates under the umbrella of the World Health Organization, classified NDMA as a probable human carcinogen (WHO, 2008). The daily tolerate limit for NDMA is 4.0 – 9.3 ng/kg-day and the WHO proposed a drinking water limit of 100 ng/L, which corresponds to approximately 2.9 ng/kg-day (Fitzgerald and Robinson, 2007).

Human exposure routes to NDMA were initially focused on food, consumer products and air. The attention of NDMA to drinking water systems arose after the detection of elevated concentrations of NDMA in the groundwater (as high as 400,000 ng/L on site and 20,000 ng/L offsite) near a rocket engine facility in Sacramento County, California. A subsequent statewide survey at drinking water facilities indicated that NDMA occurrence was not limited to areas near the rocket engine facilities, but also associated with chlorine or chloramine disinfection of water and wastewater (CDHS, 2002). NDMA yields are largely dependent on the type of disinfectant with chloramine > ozone = chlorine dioxide > free chlorine.

The widely accepted NDMA formation pathway through chloramination was proposed by Schreiber and Mitch (2006). The first step is the substitution of dichloramine with the unprotonated amine to formed unsymmetrical dimethylhydrazine (UDMH), which, in the second step, is oxidized by dissolved oxygen to form NDMA. However, with dissolved oxygen as a triplet ($^3O_2$), this reaction is spin-forbidden and, therefore, presumably kinetically slow and rate-limiting. They developed a kinetic model for this reaction mechanism to help explain NDMA formation in waters between pH 6-11 dosed with either preformed monochloramine or dichloramine. While the model fits were good for the waters dosed with monochloramine, for the waters dosed with dichloramine, the model underpredicted NDMA formation between pH 8-11. At pH 9 where NDMA yields in practice are maximal, their model underpredicted NDMA formation by approximately one order of magnitude. In general, the chloramine system is kinetically controlled and at pH 9, dichloramine forms slowly from monochloramine but decays rapidly, and hence dichloramine is present at trace levels (Wahman, 2018). My preliminary data confirmed dichloramine was not present at measurable concentrations at pH 9, casting doubt that dichloramine-proper is the primary reactant in step 1 of the NDMA formation mechanism. Rather, as dichloramine forms slowly and decays rapidly at pH 9, dichloramine decay products are a likely source of nitrosation agents. Additionally, at pH 10 dichloramine completely decays within seconds and tracks with the dissolved oxygen profile, casting doubt on the plausibility that step 2 is rate-limiting. Most importantly, the addition of scavengers of total nitroxyl (HNO/NO^-) and total peroxynitrite ($ONOOH/ONOO^-$) result in depressed NDMA yields by up to 60% in a dose-response relationship, implicating these reactive nitrogen species in the NDMA formation pathway.

Nitroxyl was hypothesized to be a dichloramine decay intermediate by Wei (1972). Peroxynitrite, which is a known nitrosating agent, was experimentally proven to be a product of

the oxidation of nitroxyl by dissolved oxygen (Smulik et al., 2014). Nevertheless, neither nitroxyl nor peroxynitrite have been previously considered in the NDMA formation pathway during chloramination. While nitroxyl may form directly from dichloramine decay, it may also form by a direct reaction between monochloramine and hydroxylamine (NH_2OH) (Wahman et al., 2014), an intermediate in nitrification, which could explain observations of enhanced NDMA formation associated with nitrification (Zeng and Mitch, 2016).

As DO is the primary reactant in the formation of peroxynitrite during $NHCl_2$ decomposition, experiments with lower DO concentration are needed to verify the robustness of the proposed reaction scheme involving the formation of nitroxyl.

1.2-Objective and Approach

1.2.1-<u>Objective 1</u>

The first objective of this research is to critically review the NDMA formation literature in water with different disinfectant types, precursors, and background chemistry. While NDMA formation is primarily associated with chloramination, it can also form by ozonation, in which it is enhanced by bromide, and during chlorine oxide disinfection. Through chloramination, the main precursors of NDMA are secondary amines, such as dimethylamine (DMA), and tertiary and quaternary amines with DMA-based functional groups. These precursors include pharmaceuticals and personal products, anion exchange resins or polyelectrolytes used as coagulants during water treatment, pipeline materials, and veterinary medicines used in agriculture. Ozonation is the most effective disinfectant pretreatment for nitrosamine control. However, NDMA can form in source waters containing compounds with hydrazine-like functional groups, such as daminozide and UDMH, or bromide ion, which acts as a catalyst. Other operational factors such as pH, dissolved oxygen, organic ions can also impact the formation of NDMA.

1.2.2-<u>Objective 2</u>

The second objective of this research is to elucidate the formation of reactive nitrogen species (RNS) generated from dichloramine ($NHCl_2$) hydrolysis and demonstrate these RNS contributed to NDMA formation. The widely accepted reaction mechanism for NDMA formation involves a nucleophilic substitution between $NHCl_2$ and unprotonated amine-based precursors to form an unsymmetrical dimethylhydrazine (UDMH), which then reacts with dissolved oxygen (DO) to form NDMA (Schreiber and Mitch, 2006). However, the latter reaction is spin forbidden, meaning it is likely kinetically unfavorable and therefore unlikely to occur rapidly which runs counter to our preliminary data. The research hypothesis is that nitroxyl (HNO/NO^-) is the key long-stand unidentified intermediate of $NHCl_2$ hydrolysis. HNO/NO^- is known to react with DO to form peroxynitrite ($ONOOH/ONOO^-$) (Smulik et al., 2014), which is a known nitrosating agent, followed by the reaction with base form of dimethylamine (DMA) to form NDMA. Kinetic data of $NHCl_2$, NH_2Cl, DO, N_2O and NDMA were used to validate the model composed of i) the unified model of chloramine chemistry (UF) developed by Jafvert and Valentine (1992), ii) the nitroxyl kinetic reactions that include peroxynitrite formation measured by Lymar and Shafirovich (2007), iii) the decomposition of peroxynitrite developed by Kirsch et al. (2003), and iv) the hypothesized NDMA formation reactions stemming from peroxynitrite. The three underlying models – Jafvert and Valentine (1992), Lymar and Shafirovich (2007), Kirsch et al. (2003) – were previously validated under conditions relevant to this study. However, this work is the first to combine the unified model with the nitroxyl and peroxynitrite models and, as such adjustments to the empirically derived RNS rate expressions were expected. The combined model is referred herein as the UF+RNS model.

The third objective of this research is to examine the role of DO and challenge the robustness of the reaction scheme proposed in Objective 2. As nitroxyl (HNO) was the proven to be the long-standing unidentified intermediate formed by $NHCl_2$ hydrolysis. HNO and nitroxyl anion (NO^-) subsequently reacted with dissolved oxygen (DO) to form peroxynitrous acid/peroxynitrite anion ($ONOOH/ONOO^-$), which in the presence of total dimethylamine (TOTDMA), reacted to form *N*-nitrosodimethylamine (NDMA). As DO is the key reactant for $ONOOH/ONOO^-$ formation, lowering DO concentration can help determine the robustness of the reaction scheme in predicting NDMA and other nitrogen containing end-products such as $TOTNH_3$, NH_2Cl, N_2, N_2O NO_2^-, and NO_3^-. Yields of these compounds can be used to assess the nitrogen mass balances during $NHCl_2$ decomposition.

1.3-Document Organization

Chapter 2 addresses Objective 1. NDMA formation in drinking water is dependent on the disinfectant type, background water chemistry, and precursors, many of which have yet to be identified. Mechanistic insights can explain a portion of the NDMA formation observed in real water systems, but kinetic studies are needed to delineate the roles of chloramine speciation (i.e., the pH-dependent role of dichloramine), reactive intermediates, and the influence of other factors which are frequently present in distribution systems, such as the role of nitrifying bacteria and various inorganic ions.

Chapter 3 addresses Objective 2. A series of batch kinetic experiments with $NHCl_2$ and TOTDMA were conducted at pH 7, 8, 9, and 10 in the presence of dissolved oxygen in head-space free vials. $NHCl_2$, N_2O and DO profiles indicated that RNS formed during $NHCl_2$ decomposition, including HNO/NO^- and $ONOOH/ONOO^-$. Experiments with uric acid (a $ONOOH/ONOO^-$

scavenger) implicated ONOOH/ONOO⁻ as a central node for NDMA formation, which were further supported by the concomitant for NDMA formation. The UF+RNS model accurately simulated $NHCl_2$, NH_2Cl, NDMA and DO kinetic profiles, but not N_2O. Additionally, N_2 gas is a major end-product of $NHCl_2$ decay, indicating the need to complete nitrogen mass balances.

Chapter 4 addresses Objective 3. The role of DO in this reaction scheme was examined at pH 9 by assessing kinetic profiles of $NHCl_2$ and NDMA and nitrogen mass balances under ambient DO (~280 μM) and low-DO (< 20 μM) conditions in the presence and absence of 10 μM TOTDMA. Uric acid, an ONOOH/ONOO⁻ scavenger, completely shut down NDMA formation under the low-DO condition, validating ONOOH/ONOO⁻ as the central node in NDMA formation. Yield experiments with initial $NHCl_2$ of 200-, 400-, and 800 μeq $Cl_2 \cdot L^{-1}$ tracked the formation of NH_3/NH_4^+, NH_2Cl, N_2O, N_2, NO_2^-, and NO_3^-. NH_3/NH_4^+ yields were 20–40% greater under the low-DO condition, implying a reaction occurred between NH_3/NH_4^+ and ONOOH/ONOO⁻ or its decomposition products. An existing mechanistic model accurately predicted NH_3/NH_4^+, NH_2Cl, and N_2 under ambient conditions but underpredicted N_2O and overpredicted NO_2^- and NO_3^-. The results provide a framework to guide future experiments with ONOOH/ONOO⁻ generators and revise the mechanistic model to better capture the nitrogenous end-products.

Chapter 5 summarizes the major conclusions of the research, highlights the novelty of this work, and lists future research opportunities that stem from this study.

1.4-References

CDHS (2002). Studies on the occurrence of NDMA in drinking water. California Department of Health Service.

Fitzgerald, D. J. and Robinson, N. I., *Journal of Toxicology and Environmental Health A*, **70**, 1670-1678 (2007). 10.1080/15287390701434844.

Heath, D. F., *Biochemical Journal*, **85**, 72-91 (1962).

Jafvert, C. T. and Valentine, R. L., *Environ Sci Technol*, **26**, 577-586 (1992). Doi 10.1021/Es00027a022.

Kirsch, M., Korth, H. G., Wensing, A., Sustmann, R. and de Groot, H., *Archives of Biochemistry and Biophysics*, **418**, 133-150 (2003). 10.1016/j.abb.2003.07.002.

Lymar, S. V. and Shafirovich, V., *Journal of Physical Chemistry B*, **111**, 6861-6867 (2007). 10.1021/jp070959+.

Russell, C. G., Blute, N. K., Via, S., Wu, X. Y. and Chowdhury, Z., *Journal American Water Works Association*, **104**, 57-58 (2012). 10.5942/jawwa.2012.104.0037.

Schreiber, I. M. and Mitch, W. A., *Environ Sci Technol*, **40**, 6007-6014 (2006). 10.1021/es060978h.

Smulik, R., Debski, D., Zielonka, J., Michalowski, B., Adamus, J., Marcinek, A., Kalyanaraman, B. and Sikora, A., *Journal of Biological Chemistry*, **289**, 35570-35581 (2014). 10.1074/jbc.M114.597740.

Wahman, D. G., *J Am Water Works Assoc*, **110**, E43-E61 (2018). 10.1002/awwa.1146.

Wahman, D. G., Speitel, G. E., Jr. and Machavaram, M. V., *Water Res*, **60**, 218-227 (2014). 10.1016/j.watres.2014.04.051.

Wei, I. W. (1972). Chlorine Ammonia Breakpoint Reactions: Kinetics and Mechanism. Doctor of Philosophy, PhD Dissertation Harvard University, Cambridge, MA.

WHO (2008). N-nitrosodimethylamine in Drinking Water, Geneva, Switzerland, http://www.who.int/water_sanitation_health/dwq/chemicals/ndma_2add_feb2008.pdf, September 05, 2017.

Zeng, T. and Mitch, W. A., *Environ Sci Technol*, **50**, 2964-2973 (2016). 10.1021/acs.est.5b05668.

Chapter 2

Critical Review of *N*-Nitrosodimethylamine (NDMA) Formation Mechanisms in Drinking

Water Systems

Abstract

N-nitrosodimethylamine (NDMA) occurrence and formation pathways in drinking water systems are reviewed and NDMA yields are compared on the basis of disinfectant type, water chemistry, and precursor category. While NDMA formation is primarily associated with chloramination, it can form by ozonation, in which it is enhanced by bromide, and during chlorine dioxide disinfection. The reaction pathway for NDMA formation during ozonation involves reactive intermediates such as hydroxylamine, which may also be relevant to NDMA formation with other disinfectant types. In chloramination, despite monochloramine being the predominant species between pH 7-9, evidence suggests that dichloramine is the primary species involved in NDMA formation. This is somewhat confounding as NDMA yields are maximal at pH 9, yet at pH 9 dichloramine decays faster than it forms and hence is present at trace levels; additionally, the proposed mechanism involves a spin-forbidden incorporation of dissolved oxygen as a triplet, which is presumably kinetically slow. This review reveals that kinetic data for NDMA formation is lacking, and its influence on chloramine chemistry has not been carefully considered.

2.1-Toxicity Exerted by *N*-Nitrosodimethylamine

N-Nitrosodimethylamine (NDMA) is a precursor to a carcinogen that has been shown to induce liver cancer in rats (Heath, 1962). Specifically, NDMA undergoes enzymatic oxidative reactions (see Figure 2-1) and is converted to the potent carcinogen methanediazohydroxide (Li et al., 2011). The *International Agency for Research on Cancer*, which operates under the umbrella of the *World Health Organization* (WHO), classified NDMA as a *probable human carcinogen* (IARC, 1987). The daily tolerable limit for NDMA is 4.0-9.3 ng/kg-day (Fitzgerald and Robinson, 2007) and the WHO proposed a drinking water limit of 100 ng/L, which corresponds to approximately 2.9 ng/kg-day (WHO, 2008).

2.2-*N*-Nitrosodimethylamine Occurrence

Human exposure to NDMA was initially focused on food (Scanlan, 1983), consumer products (Havery and Chou, 1994), and polluted air (Rounbehler et al., 1981). Concerns over NDMA in drinking water systems arose after the detection of NDMA in the water supply in Ohsweken, Ontario, Canada (Jobb et al., 1993). Subsequently, NDMA was detected in groundwater near a rocket engine testing facility in Sacramento County, California that used unsymmetrical dimethylhydrazine (UDMH)-based rocket fuel. NDMA in the groundwater was as high as 400,000 ng/L onsite and 20,000 ng/L offsite, which spurred occurrence studies. A statewide survey at drinking water facilities in California indicated that NDMA occurrence was not limited to sites nearby those that used UDMH-based fuels, but was also associated with chlorine and chloramine-based disinfection of water and wastewater (CDHS, 2002).

The USEPA, through the *Integrated Risk Information System* (IRIS), has established 10^{-6} lifetime cancer risks for six *N*-nitrosamine species in drinking water (Table 2-1).

NDMA is among the more toxic of the *N*-nitrosamines at a 10^{-6} risk level of 0.7 ng/L. In terms of occurrence of these compounds in US drinking water systems, Russell et al. (2012) analyzed *N*-nitrosamine data collected as part of the second *Unregulated Contaminants Monitoring Rule* (UCMR2). As shown in Table 2-1, NDMA was found in ~10% of the samples (n=17,150) whereas the other *N*-nitrosamines were found in <0.3% of the samples. Of the NDMA occurrences, over two-thirds were in chloraminated systems and many of the others may have been in free chlorine systems with episodic spikes in ammonia that may have been forming chloramines unintentionally. The occurrence data from the UCMR2 are similar to findings in other countries. Charrois et al. (2007) sampled the distribution systems of 20 public water utilities in Canada and found that six systems had NDMA levels above the method detection limit of 5 ng/L. Five of these six utilities were chloramine systems, including one that had NDMA ranging from 66 ng/L near the middle of the distribution system to 100 ng/L at the furthest reach. This finding was in agreement with other studies, such as Wilczak et al. (2003) and Barrett et al. (2003), that showed a direct relationship between NDMA and water age within distribution systems. Charrois et al. (2007) concluded that some distribution systems face serious challenges for reducing NDMA, while a majority of systems appear to have little issue with NDMA or any of the other nitrosamine compounds listed in Table 2-1, but they did not elucidate the underlying cause of these disparities.

2.3-*N*-Nitrosodimethylamine Formation Pathways Relevant to Chloramination

NDMA and other *N*-nitrosamines can be formed by reactions of secondary amines and nitrite. The mechanism shown in Figure 2-2 was proposed to explain the formation of NDMA in the stomach of humans (Mirvish, 1975). The nitrosating agent is nitrous anhydride (N_2O_3) which is generated from two molar equivalents of nitrous acid (HNO_2). In this scenario, the formation of NDMA is pH dependent as its reactants are (1) N_2O_3, which is generated from hydrolysis of nitrous

acid, HNO_2 ($K_1 = 10^{-6.70}$), that exists in acid/base equilibrium with nitrite (HNO_2 is favored at lower pH with a $pK_a = 3.4$) and (2) unprotonated dimethylamine, which is favored at high pH and exists in equilibrium with dimethylammonium ($pK_a = 10.72$). DMA can be found in animals, plants, and many foods. The maximum NDMA formation rate occurs at pH 3.4, which is a typical pH in human stomachs (Beasley et al., 2015). However, the mechanism shown in Figure 2-2 was insufficient to explain the formation of NDMA during the chlorination of drinking water and wastewater because the reaction rate was too slow. Specifically, nitrous acid, with a pK_a of 3.4, is present in its base form (nitrite, NO_2^-) under typical drinking water conditions; importantly, nitrite is readily oxidized by hypochlorous acid to form nitrate with a half-life less than 1 second (Johnson and Margerum, 1991), so it is not available for nitrosation. Even in the absence of hypochlorite, theoretical calculations indicate just 10^{-12} ng/L NDMA would form after 24 hours at pH 7 with initial nitrite and DMA concentrations of 100 μM (Mitch and Sedlak, 2002). During chlorination in the presence of a large excess of nitrite, Choi and Valentine (2003) proposed that dinitrogen tetroxide (N_2O_4) can act as nitrosating and nitrating agent, which is formed as HOCl reacts with nitrite. While the NDMA conversion was dependent on the ratio of free chlorine to nitrite and pH, the overall NDMA yields through this pathway are low (~0.0007% at pH 7 with 0.2 mM nitrite) in comparison to preformed monochloramine at the same conditions (~0.05%).

Early mechanistic research into NDMA formation in chloraminated waters suggested the formation pathway involved the reaction between monochloramine and organic amine precursors (Choi and Valentine, 2002; Mitch and Sedlak, 2002). Subsequent research indicated that dichloramine, rather than monochloramine, was the principal reactant in NDMA formation (see details in Section 3.1.1), and dissolved oxygen also played an important role in the formation mechanism (Schreiber and Mitch, 2006). These authors argued that despite the predominance of

monochloramine under typical chloramination conditions, dichloramine always coexists in equilibrium and most of the NDMA formation in chloramination can be explained by the low concentration of dichloramine proper. However, as demonstrated in Section 4.1, chloramine speciation is kinetically controlled and hence not an equilibrium system; further, the pH-dependence of dichloramine formation and decay does not track with the respective NDMA yields.

2.3.1-*N-Nitrosodimethylamine Precursors*

The precursors of NDMA include secondary amines, such as DMA, and tertiary and quaternary amines with DMA-based functional groups (Mitch and Sedlak, 2004). These precursors include pharmaceuticals and personal products (PPCPs) (Shen and Andrews, 2011a), anion exchange resins used during water treatment (Flowers and Singer, 2013), polyelectrolytes used as coagulants in drinking water treatment (Najm and Trussell, 2001; Kohut and Andrews, 2003; Wilczak et al., 2003), pipeline materials (Morran et al., 2011), humic substances (Chen and Valentine, 2007), veterinary antibiotics used in agriculture (Leavey-Roback et al., 2016), and pesticides and herbicides (Chen et al., 2015). The mechanism for NDMA formation through tertiary amines also starts with a nucleophilic substitution of monochloramine or dichloramine on the DMA functional groups of the precursor (Figure 2-3b, Reaction f). The stability of the carbocations (R^+) have a significant role in the mechanism as they impact the ability of the precursors to form NDMA (Leavey-Roback et al., 2016). It is significant to note that those compounds with aromatic moiety at β-position of dimethylamine functional group can form NDMA at high concentration during chloramination (Selbes et al., 2013). Specifically, if the carbocation is stable, the intermediates will break down to NDMA because of favorable energetics; conversely, if the carbocation is unstable, breakdown to NDMA is energetically unfavorable and thus less will form. Another explanation proposed by Mitch and Sedlak (2004) involves the

cleavage of C-N bond, which results in the formation of DMA which subsequently reacts with a chloramine species, later surmised to be dichloramine (Schreiber and Mitch, 2006), to form NDMA (see Figure 2-3a). The remainder of Section 3.1 details the most intensively studied model precursors associated with NDMA formation.

2.3.1.1-*Dimethylamine*

The NDMA formation pathway proposed by Schreiber and Mitch (2006) for chloramination systems begins with a nucleophilic substitution between dichloramine and unprotonated DMA to form UDMH followed by the oxidation of UDMH by dissolved oxygen to form NDMA (see Figure 2-3a, reaction (d) and (e)). The importance of dissolved oxygen (i.e., the ground state triplet, $^3O_2$) was deduced by ruling out other possible oxidants through the addition of superoxide dismutase, a scavenger for reactive oxygen species, and β-carotene, a scavenger for singlet oxygen, $^1O_2$, neither of which had a significant effect on NDMA formation. However, the oxidation of UDMH by $^3O_2$ is a spin forbidden reaction and thus presumably occurs at a very slow rate (Harvey, 2007). While spin forbidden reactions can occur, they are usually much slower (~ 400 times) than the corresponding spin-allowed reactions, due to their high activation energies (~30-70 Kcal/mol) (Bertini et al., 2007; Swart and Costas, 2016). However, the difference in kinetic rates vary widely between the spin-forbidden and spin-allowed reactions. The energy calculation shows that the spin allowed pathway for the oxidation of UDMH results in the increase in energy of the systems ($\Delta G > 0$, ~ 11 Kcal/mol) (Schreiber and Mitch, 2006). Therefore, more detailed studies are needed to reveal the actual role of dissolved oxygen in NDMA formation during chloramination.

2.3.1.2-<u>Ranitidine</u>

Among NDMA precursors, ranitidine (an antacid and antihistamine sold under the trade name Zantac®) has received considerable attention due to its high yields during chloramination. The NDMA conversion varied in a range of 10-90%, and depends on many factors such as ranitidine to chloramine molar ratio, chloramine speciation, pH, and amount of dissolved oxygen (Le Roux et al., 2011; Shen and Andrews, 2011a; Shen and Andrews, 2011b; Le Roux et al., 2012b; Shen and Andrews, 2013; Jeon et al., 2016; Spahr et al., 2017). Maximal NDMA formation occurs between pH 7 and 8 following a three-phase formation curve, which includes: (1) an initial lag phase, indicating the formation of an intermediate; (2) a period of rapidly increasing NDMA formation; and (3) a plateau region in which the NDMA is constant, indicating the completion of the reaction (Le Roux et al., 2012b; Shen and Andrews, 2013). Although NDMA formation kinetics were impeded in real water matrices (i.e., waters containing natural organic matter, NOM) to which ranitidine was spiked, the final NDMA molar yields were unaffected (Shen and Andrews, 2011a). NOM could have played three possible roles in these systems: (1) it could react with monochloramine, leaving less monochloramine to react with ranitidine, (2) it could react with ranitidine, leaving less ranitidine to react with monochloramine, and (3) it could react with a radical intermediate. As NDMA formation kinetics were slowed but yields were unaffected, Role (1) is most likely, as the NDMA formation potential test was performed with a high dose of monochloramine so there was still a residual present to react with ranitidine after the monochloramine demand of NOM was exerted.

Pre-oxidation of nitrosamine precursors using free chlorine, chlorine dioxide, or ozone is one of the control strategies for nitrosamines in water systems. However, the decomposition of the precursors does not always result in less NDMA formation. Ranitidine has four different moieties

(see Figure 2-4): tertiary amine, furan, thioether and acetamidine, which have different reactivities with chlorine (i.e., acetamidine > thioether >> tertiary amine > furan) (Jeon et al., 2016). Only the attack of chlorine at tertiary amine or furan moieties (i.e., the two least chlorine reactive sites of ranitidine) resulted in less NDMA formation, which requires a chlorine to ranitidine molar ratio of 4 or higher. The same experiments were also conducted with ozone. As ozone has relatively similar reactivities for all functional groups in ranitidine, NDMA formation potential had an inverse linear correlation with ozone dose. Unfortunately, increasing pre-oxidation exposure to control NDMA formation can promote formation of other disinfectants by-products (Krasner et al., 2013).

For monochloramine, only reactions with the tertiary amine or furan moiety (i.e., the two least monochloramine reactive forms of ranitidine) lead to NDMA formation (Jeon et al., 2016). Hence, the decomposition of ranitidine does not always result in the formation of NDMA. Similar to the DMA pathway, dissolved oxygen also has a significant role in this formation pathway as no NDMA was formed in the presence of low (i.e., less than 0.3 mg/L) dissolved oxygen (Le Roux et al., 2011).

The proposed NDMA formation pathway with ranitidine (Figure 2-5) starts with the nucleophilic substitution of monochloramine to the DMA functional group of ranitidine under aerobic conditions to generate amino-peroxyl radicals. The coupling of this intermediate results in the formation of Compound (A) in Figure 2-5, which decays to hydrogen peroxide, H_2O_2, with two equivalents NDMA and a thermodynamically favored stable carbocation (Le Roux et al., 2012b; Spahr et al., 2017). This could be the reason why ranitidine has such a high NDMA yield during chloramination. At pH 8, dichloramine is a relatively minor and short-lived species and therefore is unlikely to contribute to the high conversion to NDMA from ranitidine.

Le Roux et al., (2011) examined the impact of dichloramine on NDMA formation through ranitidine. At pH 8, with the same initial concentration of mono- and dichloramine (1 mM) reacting with 100 nM of ranitidine, the NDMA formation yield with monochloramine was 80% while with dichloramine, it was only 45%. They reasoned their results by proposing that some of the dichloramine formed monochloramine at pH 8, and the monochloramine subsequently reacted with ranitidine to form NDMA. However, kinetic experiments are still needed to assess the importance of dichloramine in NDMA formation in the presence of ranitidine.

2.3.1.3-*Polymers*

DMA can serve as NDMA precursor and is also used as a reagent in the production of many polymers, including polyDADMAC and epi-DMA. Park et al. (2007) compared the residual DMA from several polymers and assessed their NDMA formation potential. A cationic polyacrylamide (PAM) had 0.04-0.14 □g DMA/mg active polymer while polyDADMAC had 0.81-1.84 □g DMA/mg active polymer. Interestingly, the so-called Mannich polymer had 5,800-7,800 □g DMA/mg active polymer which was attributed to the reversibility of the Mannich reaction that releases DMA over time. Park et al. (2007) assessed the NDMA formation potential of these polymers with monochloramine and determined the Mannich polymer >> polyamine > polyDADMAC > cationic PAM. They also tested other oxidants but monochloramine was found to produce the highest NDMA yields compared with free chlorine, chlorine dioxide, or nitrite, but all the oxidants yielded significant levels with the Mannich polymer.

Wilczak et al. (2003) showed that NDMA was formed when water was coagulated with polyDADMAC and then dosed with free chlorine. The testing was performed on the polymers from five different water utilities in California and formed similar concentrations of NDMA upon

exposure to chloramine. The formation of NDMA increased with the increasing contact time (1-15 days) and polymer doses (0.4-10 mg/L).

2.4-Operation and Analysis Factors

The formation of NDMA in chloraminated water is a function of the precursor type, pH, dissolved oxygen, various inorganic ions, and the disinfectant type and dose as detailed in the remainder of this section.

2.4.1-pH

The discussion in this section is restricted to chloramination of antibiotic precursors or those containing amine-like functional groups. This reflects the importance of these oxidant-precursor combinations in terms of NDMA formation but also the lack of studies of other NDMA-generating systems in which pH was an independent variable.

In most cases, the maximal yields of NDMA occur between pH 8 and 9 for amine-based precursors. For the antibiotic precursors studied by Leavey-Roback et al. (2016), maximal NDMA formation was reached at pH 8.4 with yields in the range of 0.9-4.9% and pK_a values between 7.4 and 8.9; the one exception was oleandomycin, which had a maximal NDMA yield at pH 7. NDMA formation is maximal with dimethylamine at pH 9 (Schreiber and Mitch, 2006) and ranitidine at pH 8 (Le Roux et al., 2012b). Shen and Andrews (2013) also studied the effect of pH on kinetics of NDMA formation from the chloramination of two amine-based pharmaceuticals, ranitidine and sumatriptan. The maximum NDMA yields occurred at 1.2-1.6 pH units below the pK_a of the dimethylamine functional group. Conversion of the precursors was maximal at pH 7 for ranitidine (~95%) and pH 8 for sumatriptan (~40%). For both precursors, at pH levels below where the NDMA were maximal, the reactions were slow and NDMA reach steady state levels after

19

approximately 45 hours. In contrast, at higher pH, the kinetics were faster and NDMA reached steady states after approximately 20 hours.

Overall, during chloramination of amines, NDMA yields are typically maximal between pH 7.5 and 9.0 and are impacted by pH due to changes in chloramine speciation and precursor chemistry. In experiments with the precursor dimethylamine (pK_a = 10.71), Mitch and Schreiber (2006) showed NDMA formation was maximal at pH 10.0 and concluded dichloramine was most directly associated with NDMA formation. However, dichloramine is favored at lower pH, and is present in only trace amounts above pH 8, leading to the possibility that some other species, perhaps a product of dichloramine and/or monochloramine decay, may be important in the NDMA formation pathway with dimethylamine. To provide a basis for this supposition, the unified chloramine model used by Schreiber and Mitch (2006) coded in Aquasim was used to interpret their NDMA yields determined with dimethylamine. Figure 2-6a shows chloramine kinetics for a solution initially containing 0.2 mM dichloramine and Figure 2-6b shows that for 0.4 mM monochloramine.

As monochloramine and dichloramine were dosed at a concentration ~40 times higher than DMA (Schreiber and Mitch, 2006), the stability of the chloramine species is not likely to be affected by the presence of DMA. Dichloramine decay (C_0 = 0.2 mM) is strongly pH dependent (pH 7-11, Figure 2-6a), with more rapid decay at higher pH and concomitant formation of monochloramine. While higher pH favors unprotonated DMA (pK_a = 10.7) and hence higher NDMA formation as discussed in the next paragraph, it also accelerates the decomposition of dichloramine. NDMA yields were highest at pH 9 and 10, but as shown in Figure 2-6a, dichloramine completely decays in 50 minutes at pH 9 and just 5 minutes at pH 10. The model simulations in Figure 2-6b show that monochloramine remains stable throughout the 300 minute

simulation period and only low levels of dichloramine are formed after 300 minutes at pH 7 (~0.26 mg/L as Cl_2) and just trace levels between pH 8-10 (10 μg/L as Cl_2 at pH 8, 0.1 μg/L as Cl_2 at pH 9 and 1.8 ng/L as Cl_2 at pH 10). In summary, at pH 10 where NDMA formation is maximal, dichloramine is short-lived and present only at trace levels. As such, it is unlikely that dichloramine proper is the primary reactant in the NDMA formation pathway. Regardless, there is a need to consider other NDMA formation pathways and measure kinetic profiles and likely intermediates under realistic chloramination conditions.

In terms of acid/base chemistry of NDMA precursors, unprotonated amines, which exist predominately at higher pH, are typically favored in NDMA formation. For the seven antibiotic precursors studied by Leavey-Roback et al. (2016), which had pK_a values between 7.4-8.9, maximal NDMA formation was reached at pH 8.4 with yields of 0.9-4.9%; the one exception in this study was oleandomycin, which had a maximal NDMA yield at pH 7.0. However, Selbes et al. (2013) found a contradiction with regard to precursor protonation state and maximal NDMA formation. At pH 7 with pre-formed monochloramine, they showed that two structurally similar precursors with disparate acidity constants – trimethylamine (pK_a = 9.8) and dimethyl-aminoacetonitrile (pK_a = 4.2) – had similar NDMA yields, at yields of 1.9% and 2.4%, respectively. Others have found maximal NDMA formation at lower pH with ranitidine. For example, Le Roux et al. (2012b) showed NDMA was maximal at pH 8 and Shen and Andrews (2013) showed NDMA was maximal at pH 7. Given the contradictory trends regarding precursor protonation, it is clear that additional mechanistic studies are needed in which chloramine speciation and acid/base precursor chemistry is tracked in relation to NDMA formation. However, the literature on the pH dependence of NDMA formation indicates there is a tradeoff in terms of

minimizing NDMA formation between conditions favorable to minimize dichloramine (high pH) and those in which protonated amine-like precursors exist (low pH).

Based on the balance of this literature, we postulate that there are additional NDMA formation pathways relevant to chloramination. Understanding the role of dissolved oxygen is likely important in addition to intermediate species formed during chloramine decay.

2.4.2-*Reagent Addition Sequence*

pH was the most important factor influencing NDMA formation. However, the order of reagent addition is also important and the underlying concepts can be used to help limit NDMA formation. Schreiber and Mitch (2005) observed that at pH 7 and higher, less NDMA was formed when DMA was first mixed with free chlorine prior to the addition of NH_4Cl. They speculated that this sequence of reagent addition resulted in the formation of a less reactive product, chlorinated DMA. In comparison, more NDMA was formed when free chlorine was added to a mixture of DMA and NH_4Cl. They reasoned that as both ammonia and DMA competed for free chlorine, less chlorinated DMA would form, leaving more DMA proper to react to form NDMA. Moreover, preformed monochloramine yielded the highest NDMA formation in the presence of DMA, presumably because no chlorinated DMA was formed. As such, from an operational standpoint, to minimize NDMA formation, free chlorine should be added prior to ammonia to minimize dichloramine and maximize chlorinated DMA. Similar trends were also observed by Wilczak et al. (2003) in their study of the cationic polymers. Preformed monochloramine resulted in higher NDMA formation compared to chloramines formed by free chlorine addition prior to ammonia. Moreover, longer lag times between either chlorine and polymer addition or ammonia and chlorine addition resulted in less NDMA formation. In the study of polyamine and polyDADMAC, Park et

al. (2015) showed that the addition of free chlorine to ammonia should be avoided as this sequence promoted highest NDMA formation, in agreement with Schreiber and Mitch (2005).

2.4.3-*Inorganic Ions*

The presence of metal ions such as copper or bromide can increase the formation of NDMA upon chloramination (Le Roux et al., 2012; Zhang and Andrews, 2013). Metal ions can be present in the source waters or generated from distribution system pipe corrosion and can catalyze monochloramine breakdown (Hawkins and Davies, 2001; Nguyen et al., 2012), although the likely products of these reactions, such as dichloramine, were not measured. Bromide ion can react with monochloramine to generate NHBrCl, which has higher reactivity than mono- and dichloramine (Symons et al., 1998; Luh and Marinas, 2014). Hence, it may form more Br-UDMH, a hypothesized intermediate, that results in higher NDMA yields.

2.4.4-*Catalysis by Activated Carbon*

Small yields of NDMA (0.05-0.29%) were observed when DMA was treated with activated carbon (no chloramine species involved). The formation is strongly influenced by chemical properties of activated carbon, pH conditions (with the highest yields occurring at pH 9), and dissolved oxygen (Padhye et al., 2011). Strong correlations were observed between NDMA conversion and percent carbonyl groups on the activated carbon. While the presence of such oxygen-containing functional groups enhanced adsorption of polar organic compounds, their role in the formation of NDMA remains unclear. Using isotope labeled nitrite, DMA, and N_2O, it was confirmed that nitrite had very little impact on the formation of NDMA. DMA only contributed to one of the nitrogen atoms in the resultant NDMA and the reactive nitrogen species involved in the mechanism is likely to be N_2O. An external source of nitrogen was also required for NDMA to form as lower concentrations were detected with pure oxygen (0.19 nanomoles under a pure

oxygen atmosphere vs. 1.79 nanomoles under an air atmosphere). Hydroxyl radical in this scenario played a significant role in NDMA formation as the final NDMA concentration reduced by more than half with the addition of hydroxyl radical scavenger, 0.62 vs. 1.62 nanomoles (Padhye et al., 2011). Hydroxylamine can also work as a catalyst as the NDMA concentration increased more than two orders of magnitude with the presence of equal molar hydroxylamine with DMA. In short, the formation of NDMA under contact with activated carbon mainly involves reactions with the reactive oxygen species such as hydroxyl radical and reactive nitrogen species. However, the exact formation pathway remains unclear. While the exact formation mechanism remains unclear, the extremely low yields of NDMA formed through this pathway indicate that NDMA measured following solid phase extraction with GAC remains an appropriate analytical procedure.

2.4.5-*Nitrifying Bacteria in the Distribution System*

Nitrification is a potential problem for drinking water systems that use chloramines as a disinfectant. This phenomenon is more likely to occur under excess ammonia, low chloramine residual conditions when coupled with long detention times in the distribution system and appropriate temperature to accelerate the growth of nitrifying bacteria (20-30 °C). Zeng and Mitch (2016) observed elevated NDMA in the presence of the nitrifying bacteria in chloraminated drinking water distribution systems and storage tanks. Through experiments with spiked nitrite, these authors determined that elevated levels of nitrite did not enhance NDMA formation and concluded that *N*-nitrosamine precursors were likely associated with the nitrifying biofilm. Krasner et al. (2012) showed that a nitrified biofilter can serve as NDMA precursors, likely due to the soluble microbial products produced by the nitrifying bacteria. However, the underlying mechanistic pathway was not elucidated.

2.5-Non-chloramine Disinfectant Type and Dose

Among the various NDMA formation pathways in drinking water and wastewater systems, the formation during chloramination is likely to the be the highest yielding and hence most important. However, NDMA formation has been observed in systems using chlorine dioxide (ClO_2) or ozone (O_3) under various conditions, albeit at relatively low yields.

2.5.1-*Chlorine Dioxide*

During treatment with ClO_2, small yields of NDMA were formed with ranitidine (0.050%), DMA (0.016%), and chlorpheniramine (0.036%) (Zhang et al., 2014). However, daminozide (Figure 2-7) has a molar yield of 5%, the highest yield reported from reaction between ClO_2 and amines (Gan et al., 2015). Given these authors found no detectable NDMA in reaction between DMA and ClO_2, DMA is unlikely to be an important intermediate during the reaction between ClO_2 and other amines. On the other hand, UDMH release was observed over the first 10 minutes of the reaction between daminozide (DMZ) and ClO_2 and decreased rapidly thereafter.

With the same initial concentration, NDMA yields from UDMH contributed approximately 95% of the NDMA yield from daminozide at pH 7 under different doses of ClO_2, which indicates that UDMH plays a significant role in NDMA formation, but this also implies the existence of other more minor formation pathways. Similar to other precursors, these NDMA formation pathways are pH dependent with the highest yields between pH 6 and 7.

2.5.2-*Ozone*

Ozonation is the most effective disinfectant pretreatment for nitrosamine control (Selbes et al., 2014; McCurry et al., 2015). However, high NDMA concentrations can be found following ozonation when the source water contains compounds with hydrazine-like functional groups

(Kosaka et al., 2014) or sulfamides (von Gunten et al., 2010). The occurrence of NDMA in water treatment using ozone disinfection was observed in several drinking water treatment plants in Germany (Schmidt and Brauch, 2008) and was associated with the presence of *N,N*-dimethylsulfamide (DMS), a degradation product of the fungicide tolyfluanid (Dalkmann et al., 2012; Trogolo et al., 2015), in surface waters and groundwaters. Ozone-induced NDMA formation was observed in finished water from 5 of 8 wastewater treatment trains monitored at concentrations ranging from <10 to 143 ng/L (Gerrity et al., 2015). However, the variability in NDMA formation and underlying mechanisms were not determined. Therefore, the reason for this abnormally high level of NDMA was not clear.

NDMA can form during the ozonation of DMA and is strongly dependent on the ozone-to-DMA ratio and contact time and significantly increased with pH between 6.5 and 10 (Andrzejewski et al., 2008). However, even the highest NDMA yields with ozone (pH 10.5, O_3:DMA ratio of 2.8 and contact time of 60 minutes) did not exceed 0.4%. Yang et al. (2009) observed similar pH dependence with NDMA formation in the absence of ozone and similar NDMA yields (0.011% at pH 7 after 24 hours) compared to Andrzejewski et al. (2008) (0.018% at pH 7.7, O_3:DMA ratio of 2.6 and contact time of 60 minutes). They proposed that hydroxylamine (NH_2OH) will form from the ozone-induced breakdown of DMA and confirmed NH_2OH reacts with DMA to form UDMH which is then oxidized to NDMA (see Figure 2-8). They speculated that UDMH reacted with molecular oxygen to form NDMA, however, this is spin-forbidden reaction and thus is likely slow kinetically. Marti et al. (2015) confirmed that oxidation of UDMH during ozonation formed NDMA, but did not determine the reaction mechanism or oxidant. Padhye et al. (2013) also observed higher NDMA yields as the pH increased from 5 to 9 in their ozonation study of dithiocarbamates, in agreement with these other studies. This literature points

to the potential importance of NH_2OH in NDMA formation but reveals the need for mechanistic studies to better understand the reaction mechanism.

The mechanism of hydroxylamine formation and the precise role of hydroxylamine during ozonation is also not clear. While Andrzejewski et al. (2008) did not consider hydroxylamine, they ruled out chloramine species in the NDMA formation pathway during ozonation and proposed a formation mechanism through nitrite, as this was detected in ozonated mixtures of DMA. They speculated that hydroxyl radical may help explain the pH dependence of NDMA formation as it is readily formed at higher pH because the decomposition of ozone is promoted by hydroxide ions (von Gunten, 2003). Consequently, more nitrite or other nitrogenous compounds (they suggested N_2O_4) can form as DMA degradation products at higher pH, which may subsequently react with DMA to form NDMA. However, Yang et al. (2009) studied the nitrosation pathway through N_2O_4 but showed this agent alone could not fully explain the pH-dependence of NDMA formation under alkaline conditions because of its instability at high pH. They proposed hydroxylamine, NH_2OH (Figure 2-8) was the proper intermediate. The authors also pointed out that the transformation of nitrogen is a complicated process and can produce more than one nitrosating agent. A series of experiments with DMA and NH_2OH under different pH and dissolved oxygen conditions showed the importance of hydroxylamine in NDMA formation and, further, that NDMA yields were enhanced at higher pH but were mitigated in the absence of dissolved oxygen. However, as none of these reactions were conducted with ozone, the formation of hydroxylamine as a breakdown product of DMA by ozone remains speculative. Andrzejewski et al. (2012) questioned this proposed pathway and conducted a series of experiments to assess the reaction of ozone, DMA, and three sequential intermediates proposed by Yang et al. (2009): *N*-dimethylhydroxylamine, *N*-methylhydroxylamine and hydroxylamine (Figure 2-8). However, only the addition of

hydroxylamine produced more NDMA, indicating the breakdown of DMA likely did not go through the other two intermediates. Therefore, the reaction mechanism responsible for hydroxylamine production has not been fully explained, nor has the relevance of hydroxylamine itself been proven in NDMA formation during ozonation as it was not measured in any of these studies. We speculate that hydroxylamine is itself an intermediate that can react to form the actual nitrosating agent, which can be generated through multiple reaction pathways with various disinfectants, including ozone.

The NDMA molar yields for formaldehyde dimethylhydrazone (FDH), 1-Formyl-2,2-dimethylhydrazine (FDMH), and acetone dimethylhydrazone (ADMH) with ozone are 89%, 85% and 84% respectively (Kosaka et al., 2014). Such high conversion can be explained by the strong reactivity of ozone with the C=N double bond in these compounds and resulted in NDMA formation. Among the six hydrazine compounds in this study, there was no observable difference in NDMA formation in the presence or absence of t-BuOH, a scavenger for hydroxyl radical, except for tetramethyltetrazene (TMT), which had a NDMA yield that doubled in the presence of t-BuOH. Thus, the other five compounds are likely to react directly with ozone to form NDMA. The effect of the water matrix was also studied by comparing ground water, river water, and ultrapure water. For FDH and FDMH, the water matrix did not have any significant effect on NDMA formation yields, indicating these compounds react directly with ozone and not other reactive oxygen species or NOM. However, in the case of TMT in the absence of t-BuOH, NDMA yields were slightly higher in the river water (28%) and groundwater (19%). In the presence of t-BuOH, no significant difference in NDMA formation was observed in the river water sample (31%) while the yield for groundwater sample increased approximately twofold (47%). NDMA formation with the six compounds through chloramination ranged from 0.041-0.39%, indicating

all were NDMA precursors but their roles are more important in ozonation rather than chloramination.

UDMH and daminozide (DMZ) can also generate NDMA upon ozonation (Figure 2-9) at molar yields of 61% and 55% in the absence of hydroxyl radical which was scavenged by t-BuOH or dimethyl sulfoxide, DMSO (Lim et al., 2016). In the presence of t-BuOH, molar NDMA yields were 100% and 84% for DMZ and UDMH respectively, in agreement with previous research (Schmidt and Brauch, 2008). These results indicate that the reaction of hydroxyl radical with UDMH or DMZ forms other products rather than NDMA, leaving less precursors to react with ozone. Hydroxyl radical can also react with the intermediates and form compounds other than NDMA. The reaction initially starts with the ozone attack of the nitrogen next to the *N,N*-dimethylamine group to form an ozone adduct intermediate, which can decompose through three different pathways and form (a) singlet oxygen, $^1O_2$, and an *N*-oxide, (b) superoxide anion radical, $O_2^{\bullet-}$, and *N*-oxide radical, and (c) ozonide radical, $O_3^{\bullet-}$, and amine radical. These reactive oxygen species can further react with ozone to generate hydroxyl radicals. This formation mechanism can explain the high consumption of ozone per mole of UDMH or DMZ and the formation of hydroxyl radical during the ozonation.

In the matrix of wastewater effluent, the formation of NDMA through DMZ during ozonation is unavoidable and the NDMA molar yield was more than 90% at 0.4 g O_3/g DOC.

The formation of NDMA was also observed in the water that contained *N,N*-dimethylsulfamide (DMS) and bromide upon ozonation (Schmidt and Brauch, 2008; von Gunten et al., 2010). Without bromide, low NDMA conversions were observed at pH 7. However, the increasing of bromide in the solution leads to the increasing in NDMA formation and in the presence of 10-20 µg/L bromide – a typical range found in Swiss lakes and drinking water – a

maximum 50% molar yield of NDMA was observed during ozonation. The mechanism, illustrated in Figure 2-8, begins with the oxidation of bromide (Br^-) by ozone to produce hypobromous acid (HOBr). DMS then reacts with hypobromous acid to form a proposed intermediate, Br-DMS, which is then oxidized by ozone to form NDMA and release bromide.

Hence, bromide works as a catalyst in the formation pathway. The rate limiting step is the oxidation of bromide by ozone. The reaction pathway was later confirmed by computational study by Trogolo et al., (2015). Hydroxyl radical hindered the formation of NDMA as it can (a) react directly with DMS to generate other products which do not lead to NDMA formation and (b) promote the transformation of bromide to bromate, BrO_3^-, which is less reactive than HOBr.

2.5.3-*Breakpoint chlorination*

Breakpoint chlorination is used to control taste and odor as well as algae and biofilm growth, remove ammonia, and oxidized metal ions such as iron (Fe^{2+}) or manganese (Mn^{2+}). In a series of batch experiments with different doses of free chlorine to solutions containing ammonia and DMA (Schreiber and Mitch, 2007) or polyDADMAC (Park et al., 2015), elevated NDMA was found near the breakpoint where the free chlorine to ammonia molar ratio was around 1.4-1.8 and neither free chlorine nor chloramines were detected. In sub-breakpoint region, both studies observed increasing NDMA yields with increasing Cl_2:N ratio, which favors dichloramine formation. At the breakpoint, along with enhanced dichloramine formation, reactive species such as peroxynitrite ($ONOO^-$) and hydroxyl radical ($^.OH$) can form and may enhance NDMA formation as the use of their scavengers (i.e., trolox, uric acid, and *tert*-butyl alcohol) significantly lowered NDMA yields (Schreiber and Mitch, 2007). Beyond the breakpoint where most inorganic chloramine species are destroyed, Schreiber and Mitch (2007) showed significantly suppressed NDMA formation while Park et al. (2015) showed only a modest decrease in NDMA. This

somewhat inconsistent behavior may be a result of the complexity of reaction between free chlorine and the polymer.

2.6-Summary

NDMA is the most commonly detected *N*-nitrosamine in drinking water and wastewater systems and can form at toxicologically relevant levels (i.e., low ng/L).

Its various formation pathways result in different yields depending on the disinfectant type (see Table 2-1; in general, chloramine > ozone = chlorine dioxide > free chlorine) and precursors molecular structures (see Figure 2-11), many of which have yet to be identified. In chloraminated water systems, the currently accepted mechanism initially begins with a nucleophilic substitution of dichloramine to the unprotonated amine-based precursors followed by the oxidation of the intermediates by dissolved oxygen to form NDMA. During ozonation, the decomposition of precursors may result in nitrosating agent(s) (like N_2O_4) or hydroxylamine, which subsequently react with residual precursors to yield NDMA. However, the NDMA conversion through ozonation is generally low with the only exception of hydrazine-containing precursors or bromide ion, which acts as a catalyst.

Mechanistic insights can explain a portion of the NDMA formation observed in real water systems but additional studies (especially kinetic experiments) are needed to better understand the role of chloramine speciation (i.e., the pH-dependent role of dichloramine), reactive intermediates, and the influence of other factors which are frequently present in distribution systems, such as the role of nitrifying bacteria and various inorganic ions.

2.7-Disclaimer

This work has been subjected to the United States Environmental Protection Agency's (Agency's) review and has been approved for publication. The views expressed in this manuscript are those of the authors and do not necessarily represent the views or policies of the Agency. Any mention of trade names, products, or services does not imply an endorsement by the Agency. The Agency does not endorse any commercial products, services, or enterprises.

2.8-Tables and Figures

Table 2-1. Epidemiological data from the Integrated Risk Information System (IRIS) database and occurrence data for the EPA 521 *N*-nitrosamines

N-nitrosamine Species	Abbreviation	10^{-6} lifetime cancer risk in drinking water (ng/L)[§]	% Occurrence in UCMR2[¥]
N-nitrosodimethylamine	NDMA	0.7	9.8
N-nitrosomethylethylamine	NMEA	2	0.0
N-nitrosodiethylamine	NDEA	0.2	0.3
N-nitrosodi-n-propylamine	NDPA	5	0.0
N-nitrosodi-n-butylamine	NDBA	6	0.1
N-nitrosopyrollidine	NPYR	20	0.2
N-nitrosopiperidine	NPIP	NA	NS

[§] Concentration that corresponds to one additional lifetime cancer risk per million people; http://www.epa.gov/iris/ accessed February 8, 2018 NA – not available in IRIS

[¥] From Russell et al. (2012), based on 17,150 samples from the second Unregulated Contaminants Monitoring Rule (UCMR2); NS – not sampled

Table 2-2. NDMA conversion of different precursors upon different disinfectants.

Precursor	NDMA molar yields (%)				References
	NH_2Cl	ClO_2	O_3	$HOCl/OCl^-$	
DMA	0.20	0.016	0.011		(Schreiber and Mitch, 2006; Yang et al., 2009; Zhang et al., 2014)
PolyDADMAC	0.1	1.45×10^{-5}		2.95×10^{-6}	(Zhang et al., 2014; Gan et al., 2015)
Pharmaceuticals					
Ranitidine	85.2	0.055		0.050	(Shen and Andrews, 2011a;
Chlorphenamine	5.5	0.005		0.036	Zhang et al., 2014)
Antibiotics					
Minocycline	4.9				(Leavey-Roback et al., 2016)
Spiramycin	3.4				(Leavey-Roback et al., 2016)
Tetracycline	1.7				(Leavey-Roback et al., 2016)
	0.54	0.31			(Gan et al., 2015)
Oxytetracycline	1.4				(Leavey-Roback et al., 2016)
Quinupristin	0.15				(Leavey-Roback et al., 2016)
Hydrazine compounds					
Daminozide	ND	5.01			(Gan et al., 2015)
			84		(Lim et al., 2016)
Unsymmetrical Dimethylhydrazine	0.47	3.42			(Gan et al., 2015)
			61		(Lim et al., 2016)
Formaldehyde dimethylhydrazone	0.041		89		(Kosaka et al., 2014)
1-Formyl-2,2-dimethylhydrazine	0.081		85		(Kosaka et al., 2014)
Tetramethyltetrazene	0.39		19		(Kosaka et al., 2014)
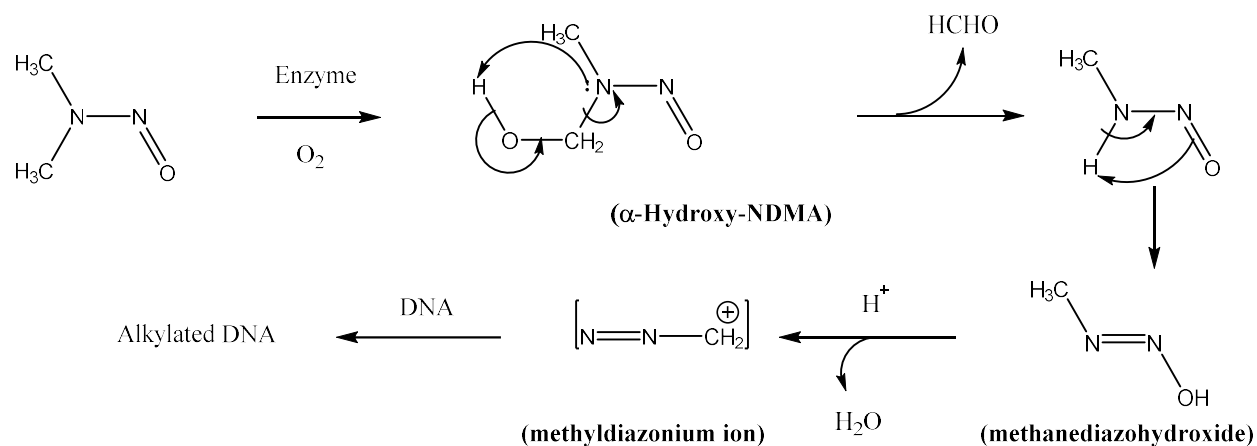
Figure 2-1. Toxicity mechanism showing NDMA undergoing enzymatic reactions to form potent carcinogen methanediazohydroxide. Replication of the alkylated DNA before repair mechanism in the cell has removed the damaged DNA may lead to cancer (Craddock, 1993). Adapted with permission from VM Craddock. Copyright 1993 Cambridge University Press.
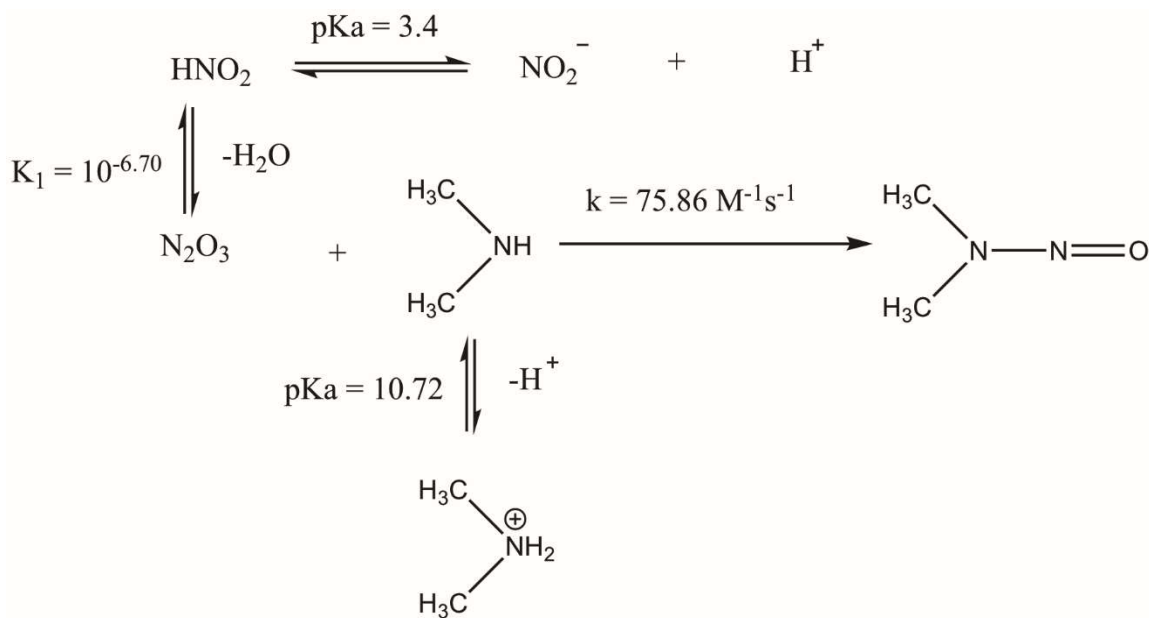
Figure 2-2. NDMA formation mechanism through nitrite.

(A)

(B)
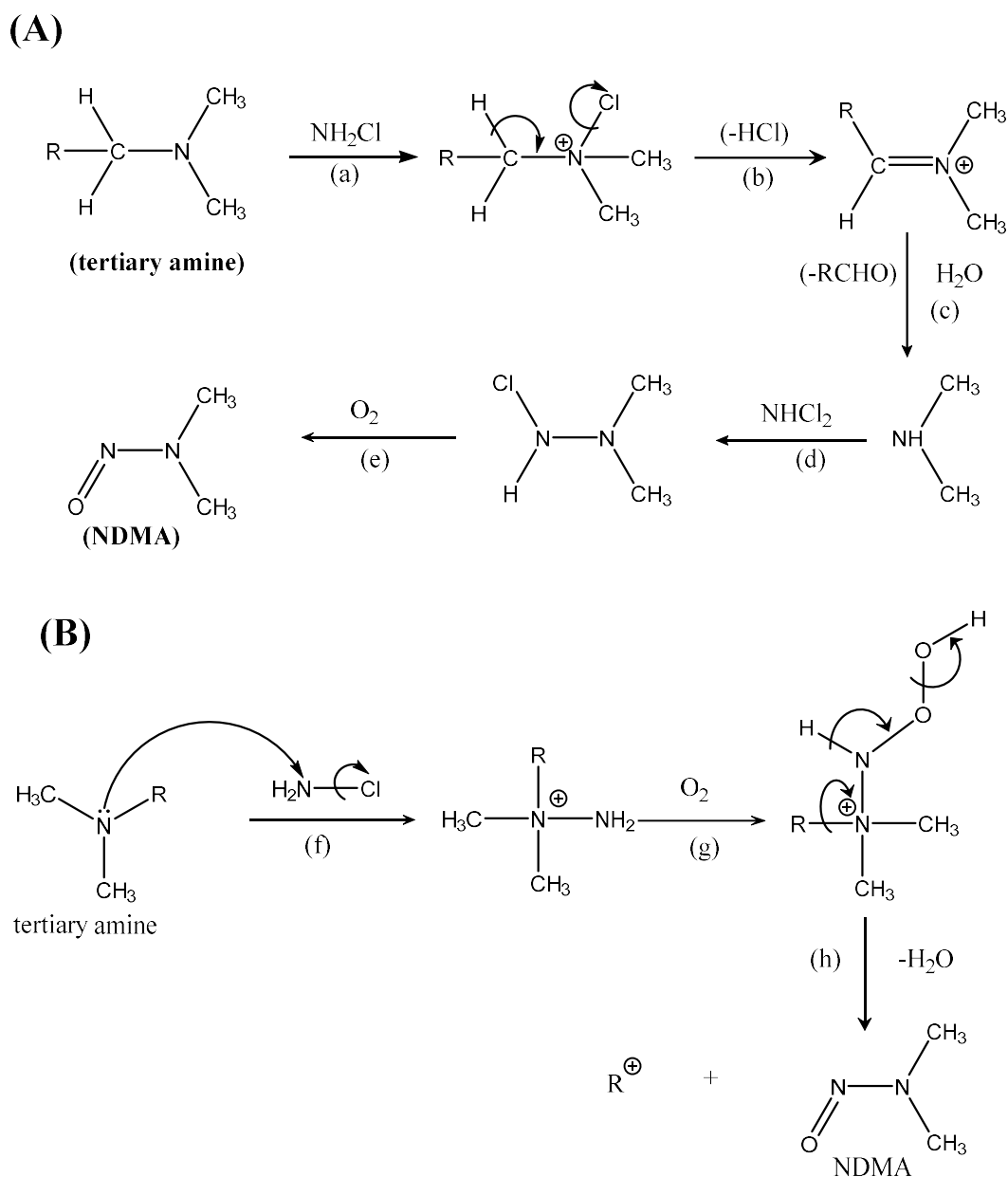
Figure 2-3. Proposed NDMA formation pathways upon chloramination of tertiary amines (Mitch and Sedlak, 2004; Leavey-Roback et al., 2016). (A) Adapted with permission from WA Mitch and DL Sedlak, *Environ. Sci. Technol.*, 2004, 38(5), pp 1445-1454. Copyright 2004 American Chemical Society. (B) Adapted with permission from SL Leavy-Roback, SW Krasner, and IH Suffet, Chemosphere, 164, 330-338. Copyright 2016 Elsevier.
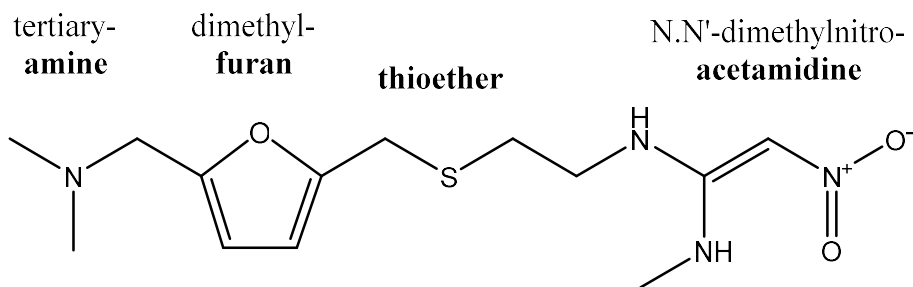
Figure 2-4. Molecular structure of ranitidine (Jeon et al., 2016). Adapted with permission from D Jeon, J Kim, J Shin, ZR Hidayat, S Na, and Y Lee, *Journal of Hazardous Materials*, 2016, 318, pp 802-809. Copyright 2016 Elsevier.
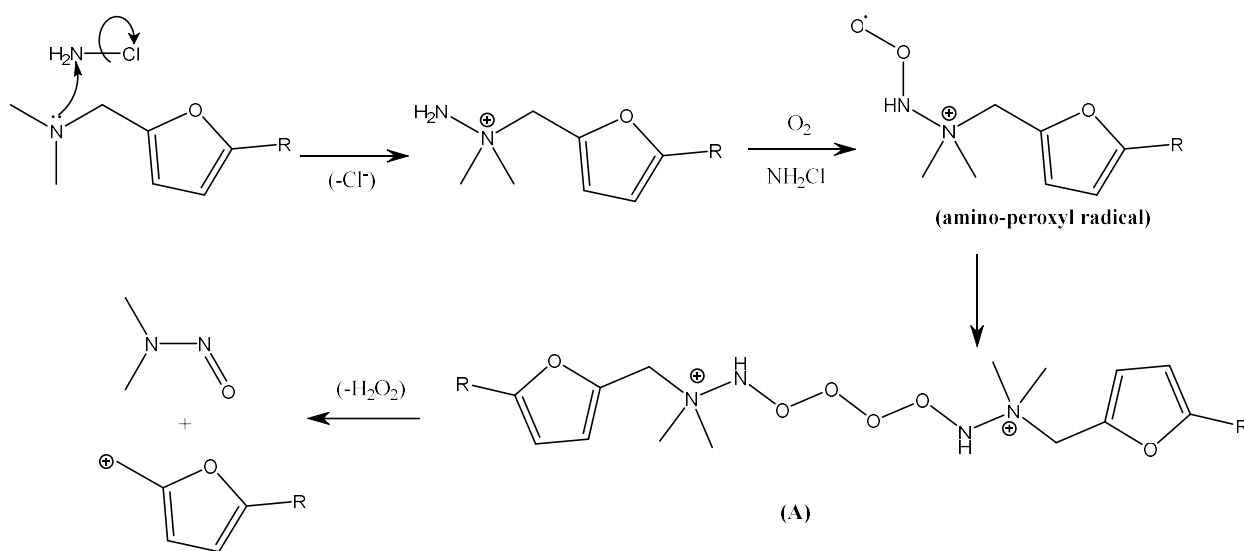
Figure 2-5. Proposed NDMA formation mechanism for ranitidine upon chloramination (Spahr et al., 2017). Adapted with permission from S Spahr, OA Cirpka, U von Gunten, and TB Hofstetter, *Environ. Sci. Technol.*, 2017, 51, pp 280-290. Copyright 2017 American Chemical Society.
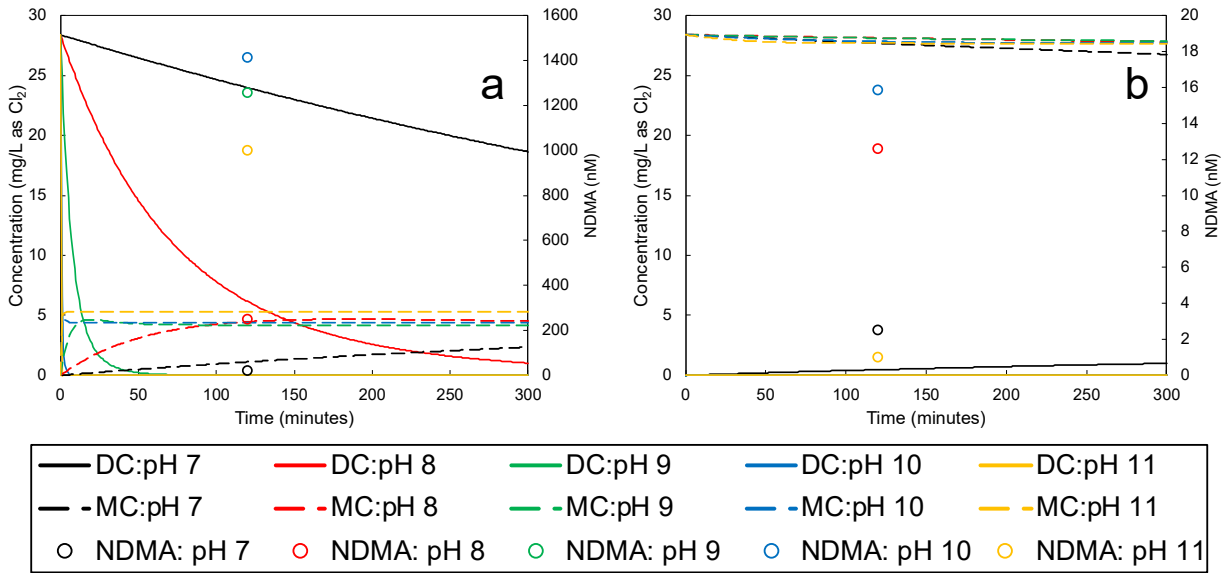
Figure 2-6. Chloramine kinetics simulated in Aquasim with the unified chloramine model used by Schreiber and Mitch (2006). (a) initial concentrations of 0.2 mM dichloramine (DC) and 0.28 mM free ammonia and the concomitant monochloramine (MC) formation at pH 7, 8, 9, 10, and 11; (b) initial concentrations of 0.4 mM monochloramine and 0.08 mM free ammonia and the concomitant dichloramine formation at pH 7, 8, 9, 10, and 11. Measured NDMA values are from Schreiber and Mitch (2006) for the chloramine conditions specified in (a) and (b) and DMA concentrations of (a) 5 μM and (b) 10 μM.
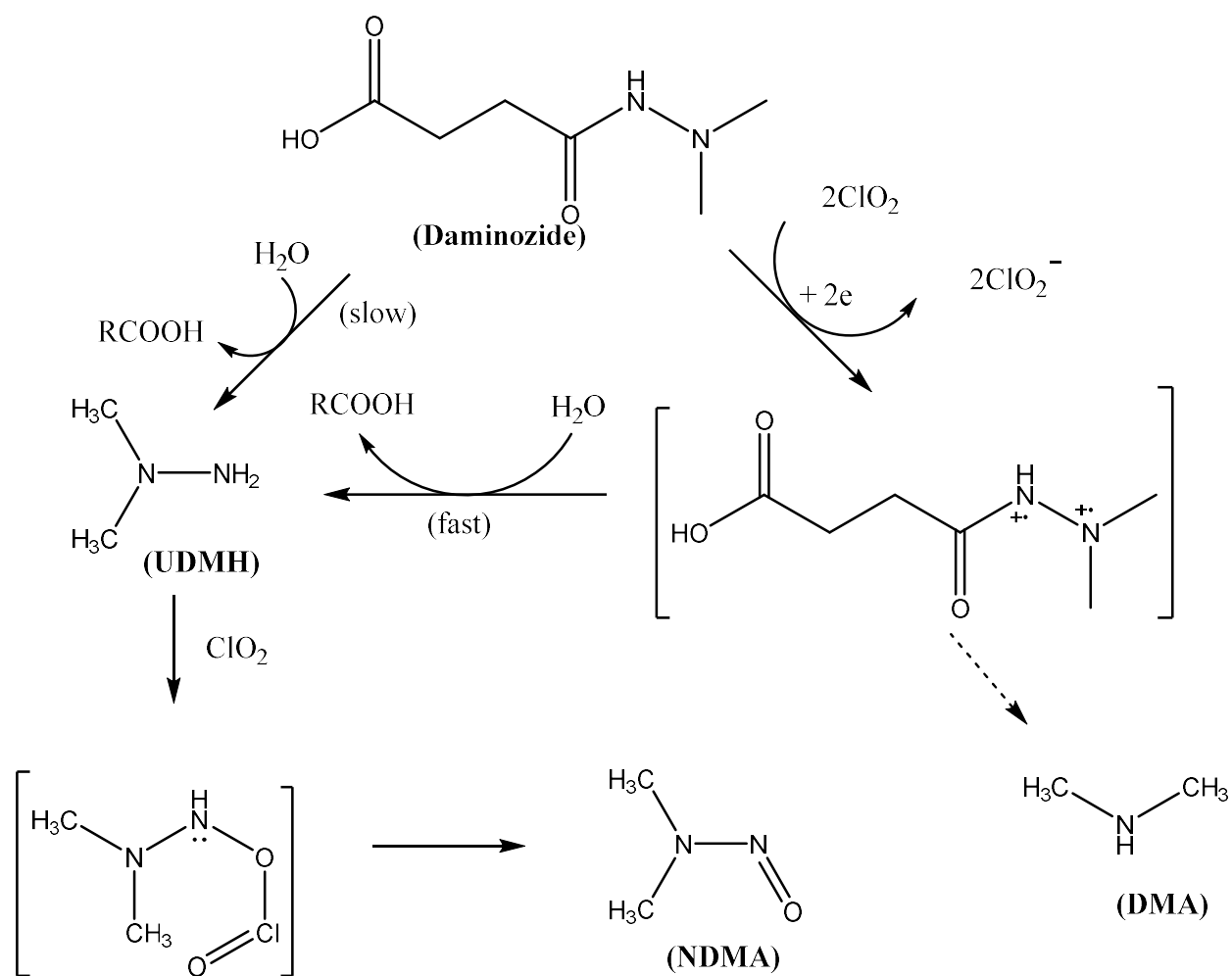
Figure 2-7. Proposed formation pathway for NDMA from the reaction of daminozide with chlorine dioxide (Gan et al., 2015). Adapted with permission from W Gan, T Bond, X Yang, and P Westerhoff, *Environ. Sci. Technol.*, 2015, 49(19), pp 11429-11437. Copyright 2015 American Chemical Society.
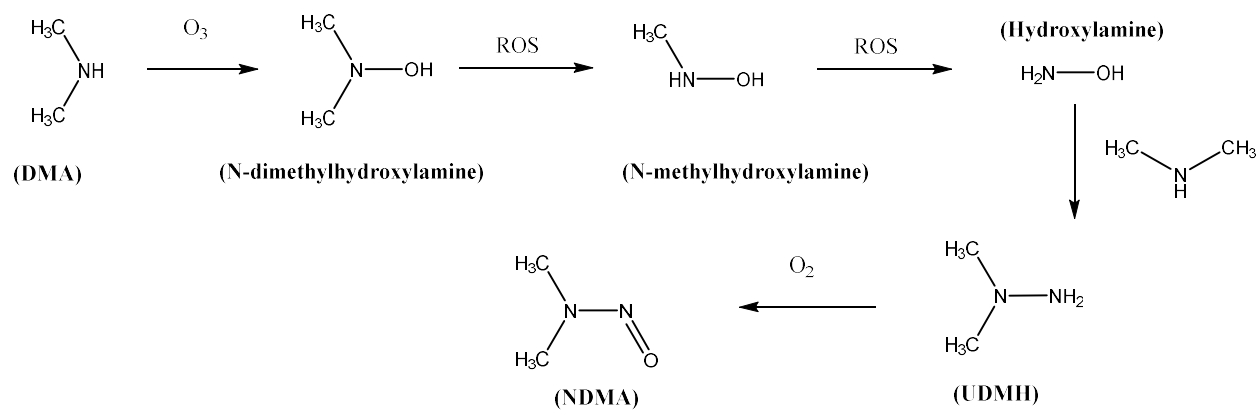
Figure 2-8. NDMA formation pathway from DMA during ozonation, proposed by Yang et al. (2009)
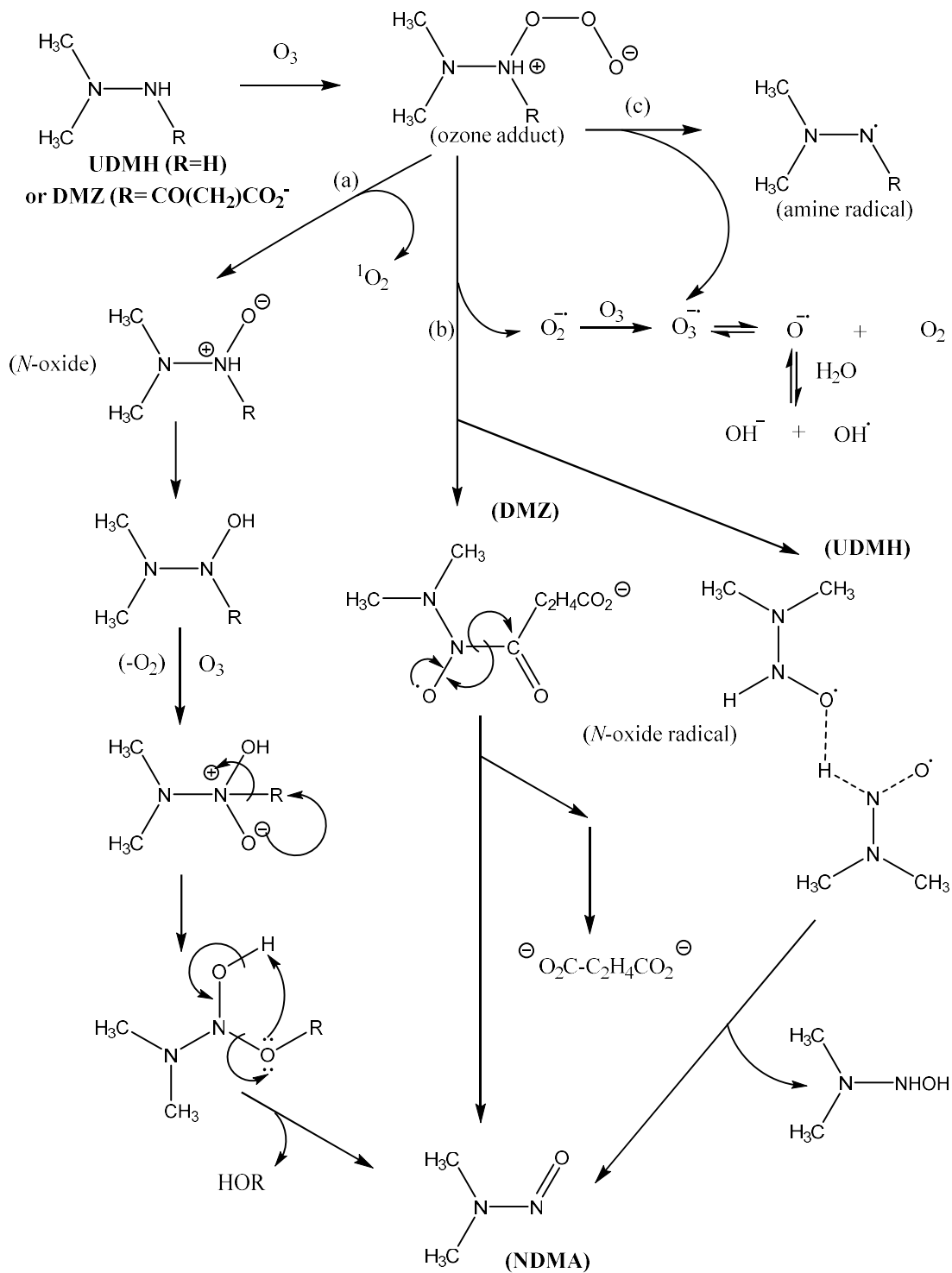
Figure 2-9. NDMA formation pathway of UDMH and DMZ through ozonation (Lim et al., 2016). Adapted with permission from S Lim, W Lee, S Na, J Shin, and Y Lee, *Water Research*, 2016, 105, pp 119-128. Copyright 2016 International Water Association.
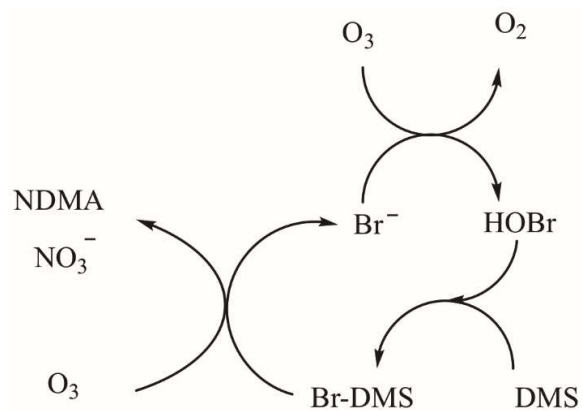
Figure 2-10. NDMA formation pathway with DMS upon ozonation with bromide as a catalyst (von Gunten et al., 2010). Adapted with permission from U von Gunten, E Salhi, CK Schmidt, and WA Arnold, *Environ. Sci. Technol.*, 2010, 44(15), pp 5762-5768. Copyright 2010 American Chemical Society.
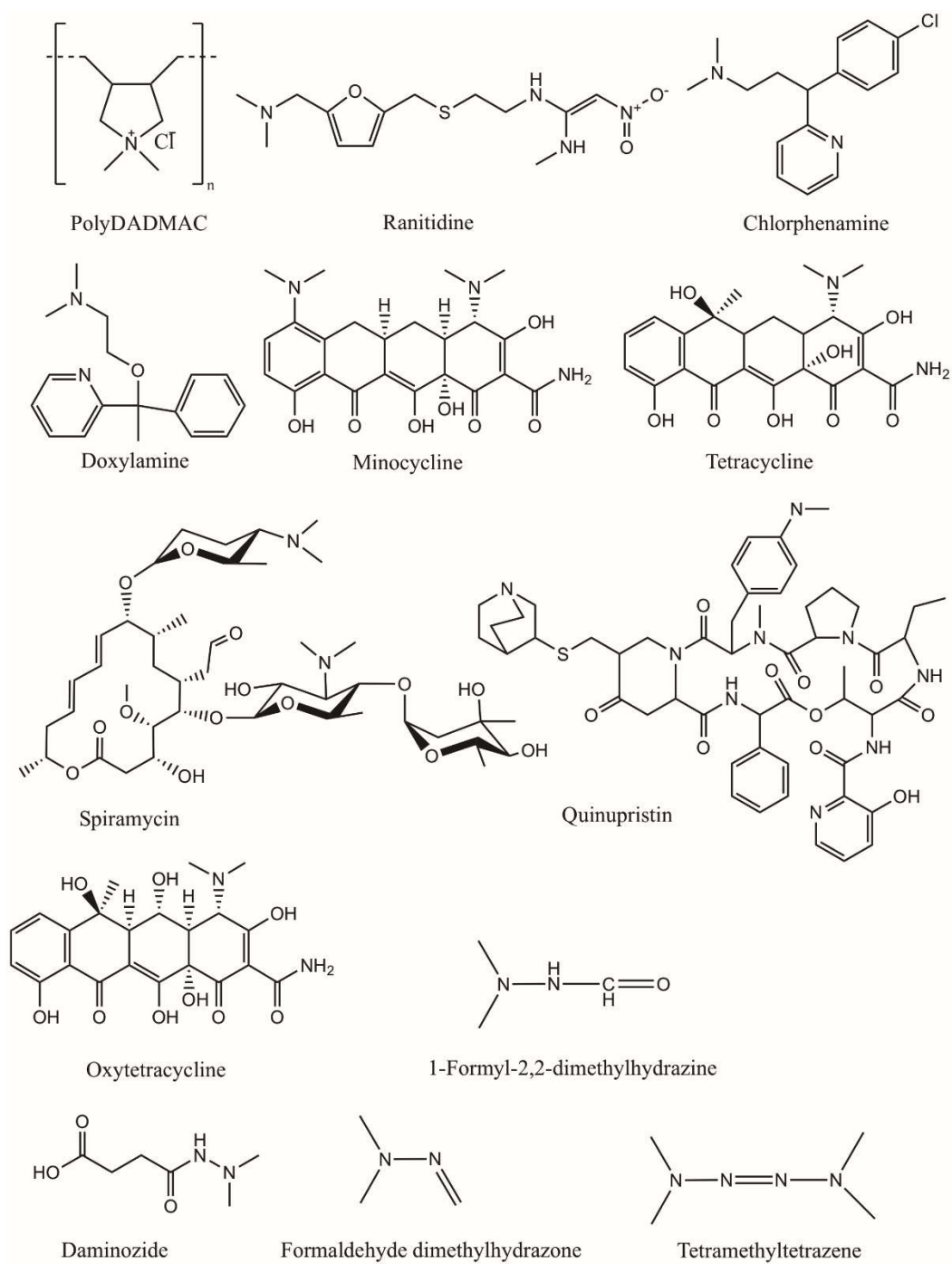
Figure 2-11. Molecular structures of N-nitrosodimethylamine precursors listed in Table 2-2.

2.9- References

Andrzejewski, P., Fijolek, L. and Nawrocki, J., *J Hazard Mater*, **229-230**, 340-345 (2012). 10.1016/j.jhazmat.2012.06.009.

Andrzejewski, P., Kasprzyk-Hordern, B. and Nawrocki, J., *Water Res*, **42**, 863-870 (2008). 10.1016/j.watres.2007.08.032.

Barrett, S., Hwang, C., Guo, Y., Andrews, S. A. and Valentine, R. L. (2003). Occurrence of NDMA in drinking water: A North American survey, 2001-2002. American Water Works Association Annual Conference. Anaheim, CA, AWWA.

Beasley, D. E., Koltz, A. M., Lambert, J. E., Fierer, N. and Dunn, R. R., *PLoS One*, **10**, e0134116 (2015). 10.1371/journal.pone.0134116.

Bertini, I., Gray, H. B., Stiefel, E. I. and Valentine, J. S. *Biological Inorganic Chemistry: Structure and Reactivity*, University Science Books, Sausalito, California, (2007).

CDHS (2002). Studies on the occurrence of NDMA in drinking water. California Department of Health Service.

Charrois, J. W. A., Boyd, J. M., Froese, K. L. and Hrudey, S. E., *Journal of Environmental Engineering and Science*, **6**, 103-114 (2007). 10.1139/s06-031.

Chen, W. H., Yang, Y. C., Wang, Y. H., Li, C. M., Lin, K. Y. and Lou, J. C., *Environmental Science-Processes & Impacts*, **17**, 2092-2100 (2015). 10.1039/c5em00308c.

Chen, Z. and Valentine, R. L., *Environ Sci Technol*, **41**, 6059-6065 (2007). 10.1021/es0705386.

Choi, J. and Valentine, R. L., *Water Research*, **36**, 817-824 (2002). 10.1016/S0043-1354(01)00303-7.

Choi, J. and Valentine, R. L., *Environ Sci Technol*, **37**, 4871-4876 (2003). 10.1021/es034020n.

Craddock, V. M. *Cancer of the esophagus : approaches to the etiology*, Cambridge University Press, Cambridge, NY, (1993).

Dalkmann, P., Menke, U., Schafer, D., Keppler, J. and Patzold, S., *Environmental Toxicology and Chemistry*, **31**, 556-565 (2012). 10.1002/etc.1734.

Fitzgerald, D. J. and Robinson, N. I., *Journal of Toxicology and Environmental Health A*, **70**, 1670-1678 (2007). 10.1080/15287390701434844.

Flowers, R. C. and Singer, P. C., *Environ Sci Technol*, **47**, 7365-7372 (2013). 10.1021/es4003185.

Gan, W. H., Bond, T., Yang, X. and Westerhoff, P., *Environ Sci Technol*, **49**, 11429-11437 (2015). 10.1021/acs.est.5b01729.

Harvey, J. N., *Physical Chemistry Chemical Physics*, **9**, 331-343 (2007). 10.1039/b614390c.

Havery, D. C. and Chou, H. J. *Nitrosamines and Related N-nitroso Compounds*. American Chemistry Society. Washington, DC**:** 20-33 (1994).

Hawkins, C. L. and Davies, M. J., *Chemical Research in Toxicology*, **14**, 1071-1081 (2001). Doi 10.1021/Tx010071r.

Heath, D. F., *Biochemical Journal*, **85**, 72-91 (1962).

IARC (1987). Overall Evaluations of Carcinogenicity: An Updating of IARC Monograph, International Agency for Research on Cancer, Lyon, France, http://monographs.iarc.fr/ENG/Classification/latest_classif.php, September 05, 2017.

Jeon, D., Kim, J., Shin, J., Hidayat, Z. R., Na, S. and Lee, Y., *J Hazard Mater*, **318**, 802-809 (2016). 10.1016/j.jhazmat.2016.06.039.

Jobb, D. B., Hunsinger, R. B., Meresz, O. and Taguchi, V. Y. (1993). In a study of the occurrence and inhibition of formation of NDMA in the Ohsweken water supply. 5th National Conference on Drinking Water on Disinfection Dilemma - Microbiological Control Versus By-Products, Winnipeg, Canada, 241-252.

Johnson, D. W. and Margerum, D. W., *Inorganic Chemistry*, **30**, 4845-4851 (1991). 10.1021/ic00025a031.

Kohut, K. D. and Andrews, S. A., *Water Quality Research Journal of Canada*, **38**, 719-735 (2003).

Kosaka, K., Fukui, K., Kayanuma, Y., Asami, M. and Akiba, M., *Ozone-Science & Engineering*, **36**, 215-220 (2014). 10.1080/01919512.2014.875765.

Krasner, S. W., Lee, C. F. T., Liang, H., Mitch, W. A., Von Gunten, U. and Westerhoff, P. (2012). Impact of a nitrified biofilter on NDMA formation. American Water Works Association Annual Conference and Exposition 2012, ACE 2012, Dallas, Texas, 3919 - 3943.

Krasner, S. W., Mitch, W. A., McCurry, D. L., Hanigan, D. and Westerhoff, P., *Water Research*, **47**, 4433-4450 (2013). 10.1016/j.watres.2013.04.050.

Le Roux, J., Gallard, H. and Croue, J. P., *Water Research*, **45**, 3164-3174 (2011). 10.1016/j.watres.2011.03.035.

Le Roux, J., Gallard, H. and Croue, J. P., *Environ Sci Technol*, **46**, 1581-1589 (2012). 10.1021/es203785s.

Le Roux, J., Gallard, H., Croue, J. P., Papot, S. and Deborde, M., *Environ Sci Technol*, **46**, 11095-11103 (2012b). 10.1021/es3023094.

Leavey-Roback, S. L., Krasner, S. W. and Suffet, I. M., *Chemosphere*, **164**, 330-338 (2016). 10.1016/j.chemosphere.2016.08.070.

Li, L., Lin, X. Y. and Li, Z. H., *Chemical Research in Chinese Universities*, **27**, 1006-1009 (2011).

Lim, S., Lee, W., Na, S., Shin, J. and Lee, Y., *Water Res*, **105**, 119-128 (2016). 10.1016/j.watres.2016.08.054.

Luh, J. and Marinas, B. J., *Environ Sci Technol*, **48**, 2843-2852 (2014). 10.1021/es4036754.

Marti, E. J., Pisarenko, A. N., Peller, J. R. and Dickenson, E. R. V., *Water Research*, **72**, 262-270 (2015). 10.1016/j.watres.2014.08.047.

McCurry, D. L., Krasner, S. W., von Gunten, U. and Mitch, W. A., *Water Res*, **84**, 161-170 (2015). 10.1016/j.watres.2015.07.024.

Mirvish, S. S., *Toxicology and Applied Pharmacology*, **31**, 325-351 (1975). 10.1016/0041-008x(75)90255-0.

Mitch, W. A. and Sedlak, D. L., *Environ Sci Technol*, **36**, 588-595 (2002). 10.1021/es010684q.

Mitch, W. A. and Sedlak, D. L., *Environ Sci Technol*, **38**, 1445-1454 (2004). 10.1021/es035025n.

Morran, J., Whittle, M., Fabris, R. B., Harris, M., Leach, J. S., Newcombe, G. and Drikas, M., *Journal American Water Works Association*, **103**, 76-+ (2011).

Najm, I. and Trussell, R. R., *Journal American Water Works Association*, **93**, 92-99 (2001).

Nguyen, C., Elfland, C. and Edwards, M., *Water Research*, **46**, 611-621 (2012). 10.1016/j.watres.2011.11.006.

Padhye, L. P., Hertzberg, B., Yushin, G. and Huang, C. H., *Environ Sci Technol*, **45**, 8368-8376 (2011). 10.1021/es201696e.

Padhye, L. P., Kim, J. H. and Huang, C. H., *Water Research*, **47**, 725-736 (2013). 10.1016/j.watres.2012.10.043.

Park, S. H., Padhye, L. P., Wang, P., Cho, M., Kim, J. H. and Huang, C. H., *Journal of Hazardous Materials*, **282**, 133-140 (2015). 10.1016/j.jhazmat.2014.07.044.

Park, S. H., Wei, S., Huang, C. H., Mizaikoff, B. and Aral, M. M. (2007). A study of the effect of polymers on potential N-nitrosodimethylamine (NDMA) formation at water and wastewater treatment plants, MESL-03-07, Atlanta, Georgia,

Rounbehler, D. P., Reisch, J. W., R., C. J. and Fine, D. H. *Chemical Hazards in the Workpalce*. American Chemical Society. 343-356 (1981).

Russell, C. G., Blute, N. K., Via, S., Wu, X. and Chowdhury, Z., *Journal American Water Works Association*, **104**, E205-E217 (2012).

Scanlan, R. A., *Cancer Res*, **43**, 2435s-2440s (1983).

Schmidt, C. K. and Brauch, H. J., *Environ Sci Technol*, **42**, 6340-6346 (2008).

Schreiber, I. M. and Mitch, W. A., *Environ Sci Technol*, **39**, 3811-3818 (2005). 10.1021/es0483286.

Schreiber, I. M. and Mitch, W. A., *Environ Sci Technol*, **40**, 6007-6014 (2006). 10.1021/es060978h.

Schreiber, I. M. and Mitch, W. A., *Environmental Science & Technology*, **41**, 7039-7046 (2007).

Schreiber, I. M. and Mitch, W. A., *Environ Sci Technol*, **41**, 7039-7046 (2007). 10.1021/es070500t.

Selbes, M., Kim, D., Ates, N. and Karanfil, T., *Water Research*, **47**, 945-953 (2013). 10.1016/j.watres.2012.11.014.

Selbes, M., Kim, D. and Karanfil, T., *Water Res*, **66**, 169-179 (2014). 10.1016/j.watres.2014.08.015.

Shen, R. and Andrews, S. A., *Water Res*, **45**, 5687-5694 (2011a). 10.1016/j.watres.2011.08.034.

Shen, R. and Andrews, S. A., *Water Res*, **45**, 944-952 (2011b). 10.1016/j.watres.2010.09.036.

Shen, R. and Andrews, S. A., *Water Res*, **47**, 802-810 (2013). 10.1016/j.watres.2012.11.004.

Shen, R. Q. and Andrews, S. A., *Water Research*, **47**, 802-810 (2013). 10.1016/j.watres.2012.11.004.

Spahr, S., Cirpka, O. A., von Gunten, U. and Hofstetter, T. B., *Environ Sci Technol*, **51**, 280-290 (2017). 10.1021/acs.est.6b04780.

Swart, M. and Costas, M. *Spin States in Biochemistry and Inorganic Chemistry: Influence on Structure and Reactivity*, Wiley, (2016).

Symons, J. M., Xia, R., Speitel, G. E., Diehl, A., Hwang, C. J. and Krasner, S. W. *Factors Affecting Disinfection By-Product Formation During Chloramination*, AWWA Research Foundation, Denver, Colorado, (1998).

Trogolo, D., Mishra, B. K., Heeb, M. B., von Gunten, U. and Arey, J. S., *Environ Sci Technol*, **49**, 4163-4175 (2015). 10.1021/es504407h.

von Gunten, U., *Water Res*, **37**, 1443-1467 (2003). 10.1016/S0043-1354(02)00457-8.

von Gunten, U., Salhi, E., Schmidt, C. K. and Arnold, W. A., *Environ Sci Technol*, **44**, 5762-5768 (2010). 10.1021/es1011862.

WHO (2008). N-nitrosodimethylamine in Drinking Water, Geneva, Switzerland, http://www.who.int/water_sanitation_health/dwq/chemicals/ndma_2add_feb2008.pdf, September 05, 2017.

Wilczak, A., Assadi-Rad, A., Lai, H. H., Hoover, L. L., Smith, J. F., Berger, R., Rodigari, F., Beland, J. W., Lazzelle, L. J., Kinicannon, E. G., Baker, H. and Heaney, C. T., *Journal American Water Works Association*, **95**, 94-106 (2003).

Yang, L., Chen, Z., Shen, J., Xu, Z., Liang, H., Tian, J., Ben, Y., Zhai, X., Shi, W. and Li, G., *Environ Sci Technol*, **43**, 5481-5487 (2009). 10.1021/es900319f.

Zeng, T. and Mitch, W. A., *Environ Sci Technol*, **50**, 2964-2973 (2016). 10.1021/acs.est.5b05668.

Zhang, A., Li, Y., Song, Y., Lv, J. and Yang, J., *J Hazard Mater*, **276**, 499-509 (2014). 10.1016/j.jhazmat.2014.05.069.

Zhang, H. and Andrews, S. A., *Chemosphere*, **93**, 2683-2689 (2013). 10.1016/j.chemosphere.2013.08.067.

Chapter 3

Updated Reaction Pathway for Dichloramine Decomposition: Formation of Reactive

Nitrogen Species and *N*-Nitrosodimethylamine

Abstract

The *N*-nitrosodimethylamine (NDMA) formation pathway in chloraminated drinking water remains unresolved. In pH 7-10 waters amended with 10 μM total dimethylamine and 800 μeq $Cl_2 \cdot L^{-1}$ dichloramine ($NHCl_2$), NDMA, nitrous oxide (N_2O), dissolved oxygen (DO), $NHCl_2$, and monochloramine (NH_2Cl) were kinetically quantified. $NHCl_2$, N_2O, and DO profiles indicated reactive nitrogen species (RNS) formed during $NHCl_2$ decomposition, including nitroxyl/nitroxyl anion (HNO/NO^-) and peroxynitrous acid/peroxynitrite anion ($ONOOH/ONOO^-$). Experiments with uric acid (an $ONOOH/ONOO^-$ scavenger) implicated $ONOOH/ONOO^-$ as a central node for NDMA formation, which was further supported by concomitant *N*-nitrodimethylamine formation. A kinetic model accurately simulated $NHCl_2$, NH_2Cl, NDMA, and DO concentrations and included (1) the unified model of chloramine chemistry revised with HNO as a direct product of $NHCl_2$ hydrolysis, (2) HNO/NO^- then reacting with (i) HNO to form N_2O, (ii) DO to form $ONOOH/ONOO^-$, or (iii) $NHCl_2$ or NH_2Cl to form nitrogen gas, and (3) NDMA formation via $ONOOH/ONOO^-$ or their decomposition products reacting with (i) dimethylamine (DMA) and/or (ii) chlorinated unsymmetrical dimethylhydrazine (UDMH-Cl), the product of $NHCl_2$ and DMA. Overall, updated $NHCl_2$ decomposition pathways are proposed, yielding (1) RNS via $NHCl_2 \rightarrow HNO/NO^- \xrightarrow{O_2} ONOOH/ONOO^-$ and (2) NDMA via $ONOOH/ONOO^- \xrightarrow[\text{or DMA}]{\text{UDMH-Cl}} NDMA$.

3.1-Introduction

Chloramines are commonly used drinking water disinfectants in the United States (Cornwell Engineering Group., 2018). While chloramination is associated with decreased formation of regulated trihalomethanes and haloacetic acids, N-nitrosodimethylamine (NDMA) is a concern (Russell et al., 2012) given its formation at toxicologically-relevant levels (Hrudey and Charrois, 2012). Some NDMA precursors are comprised of secondary amines such as dimethylamine (DMA, $(CH_3)_2NH$)(2010-2011) as well as tertiary amines and quaternary ammonium compounds with DMA functional groups. These precursors include pharmaceuticals and personal-care products (Shen and Andrews, 2011), veterinary antibiotics (Leavey-Roback et al., 2016), anion exchange resins (Flowers and Singer, 2013), and unidentified components of pipeline materials (Morran et al., 2011). In conversion of DMA to NDMA, the nitrogen and oxygen in the added NO group have been attributed to chloramines (Choi and Valentine, 2002) and dissolved oxygen (DO), respectively (Schreiber and Mitch, 2006; Le Roux et al., 2011; Spahr et al., 2017).

Early studies with DMA as a model precursor postulated a two-step NDMA formation pathway in which monochloramine (NH_2Cl) and DMA reacted to form unsymmetrical dimethylhydrazine (UDMH), followed by a NH_2Cl and UDMH reaction to form NDMA (Choi and Valentine, 2002; Mitch and Sedlak, 2002). Schreiber and Mitch (2006) cast doubt on this pathway by (i) showing NDMA yields with NH_2Cl and DMA were about one-hundred times greater than with NH_2Cl and UDMH and (ii) noting the rate constant for UDMH formation (Yagil and Anbar, 1962) (0.081 $M^{-1}s^{-1}$) was about one-hundred times lower than needed (6.4 $M^{-1}s^{-1}$) to simulate their NDMA data (Choi and Valentine, 2002). This led to a revision and replacement of the NDMA-chloramine formation pathway (Schreiber and Mitch, 2006) in which dichloramine

(NHCl$_2$) was proposed as the primary reactant. This reaction pathway from Schreiber and Mitch (2006) (SM) combines (i) fourteen reactions from the unified (UF) model of chloramine chemistry (Jafvert and Valentine, 1992) (Table s3-1, U1-U14) with (ii) eight reactions that culminate in NDMA formation (Table s3-2, P1-P8) and associated acid-base chemistry (Table s3-3), referred to herein as the UF+SM model. This model is shown as Pathway A1 of Scheme 1 where, for clarity, only UF model reactions U3–U9 and NDMA formation reactions P5, P7, and P8 are presented. For NDMA formation, the first step is a reaction between NHCl$_2$ and DMA (P5) to form chlorinated unsymmetrical dimethylhydrazine (UDMH-Cl).

Next, UDMH-Cl reacts with DO to form NDMA (P8) or with NHCl$_2$ to form other products (P7). To curb NDMA formation, Pathway A1 emphasizes minimizing the NHCl$_2$ concentration (Schreiber and Mitch, 2005) or removing and/or transforming DMA-like precursors (Krasner et al., 2013). However, P8 (UDMH-Cl + DO) is spin-forbidden and DO consumption was not previously kinetically validated (Schreiber and Mitch, 2006), prompting others to investigate other potential reaction pathways. Subsequent studies have found NDMA yields from NHCl$_2$ and NH$_2$Cl were dependent on pH and precursor type. For example, in waters containing ranitidine – a high-yielding NDMA precursor containing a DMA functional group – NDMA yields at pH 8 were lower with NHCl$_2$ (ca. 47% yield) compared to NH$_2$Cl (ca. 80% yield) (Le Roux et al., 2011). However, at pH 7, Huang et al. (2018) found greater NDMA with NHCl$_2$ compared to NH$_2$Cl with four *N,N*-dimethyl-α-arylamine precursors, including ranitidine. They computationally rationalized contrary findings, attributing these to high NHCl$_2$ doses. Selbes et al. (2013) found NH$_2$Cl preferentially reacted with precursors containing electron-withdrawing groups and NHCl$_2$ with precursors containing electron-donating groups.

Radical species in chloramine systems may also be relevant in NDMA formation. Spahr et al. (2017) studied NH_2Cl and ranitidine reaction kinetics at pH 8 and showed that radical scavengers (e.g., ABTS and Trolox) shut down NDMA formation, concluding that aminyl radicals (from NH_2Cl oxidation of organic amines) and *N*-peroxyl radicals (from aminyl radicals reacting with DO) were part of the NDMA formation pathway. The hypothesized source of the radical was an electron transfer reaction of an amine with NH_2Cl but was not demonstrated experimentally.

A long-standing unknown in the UF model which remained in the UF+SM model is the identity of the reactive intermediate (*I*) from $NHCl_2$ hydrolysis (Jafvert and Valentine, 1992) (Table s3-1, U7). *I* has been hypothesized to be the reactive nitrogen species (RNS) nitroxyl (HNO) (Wei, 1972), but this has not been experimentally proven. HNO and its conjugate base, nitroxyl anion (NO^-) exist in a slow equilibrium because of the spin-forbidden oxygen transition from singlet state HNO to triplet state NO^- (Shafirovich and Lymar, 2003). HNO/NO^- are difficult to measure kinetically because they are short lived and unlikely to accumulate. However, HNO/NO^- may react with HNO to form N_2O (Shafirovich and Lymar, 2002), a stable end-product, via R1 and R2→R3 (see Scheme 1). Real-time N_2O measurements can be made non-destructively using a N_2O microelectrode (Wahman et al., 2014); therefore, N_2O kinetic measurements would serve as a total nitroxyl (HNO plus NO^-) marker. In competition with N_2O formation, DO may react in a pH-dependent manner with HNO or NO^- (Smulik et al., 2014; Hamer et al., 2016) via R5 and R2→R4 (see Scheme 1) to form peroxynitrous acid/peroxynitrite anion ($ONOOH/ONOO^-$), which are also RNS. A microelectrode can be used to measure DO in real-time (Spahr et al., 2017), and DO consumption would support HNO/NO^- and $ONOOH/ONOO^-$ formation.

Once formed, $ONOOH/ONOO^-$ is unstable and known to decompose through a complex series of 117 reactions (Kirsch et al., 2003) to nitrite (NO_2^-) and nitrate (NO_3^-), which would both

further serve as markers for ONOOH/ONOO⁻ formation. With DMA present and competing with NO_2^- and NO_3^- formation, ONOOH/ONOO⁻ may directly react with DMA or decompose to radical species that may react with DMA, forming NDMA and another suspected carcinogen, *N*-nitrodimethylamine (DMNO) (Pliss GB, 1982; Masuda et al., 2000). Uric acid is a known scavenger of ONOOH/ONOO⁻ and its decomposition products (Hooper et al., 1998), including the free radicals $NO_2^\bullet$ and $CO_3^{\bullet-}$ that form by rapid decay of $ONOOCO_2^-$ and $O_2NOCO_2^-$ which are short-lived intermediates generated by the reaction of ONOOH/ONOO⁻ with CO_2 (Squadrito et al., 2000). While uric acid is non-selective and can also scavenge reactive oxygen species such as hydroxyl radical and superoxide radical Schreiber and Mitch (2006), ruled out these species in the NDMA formation pathway through scavenging experiments with superoxide dismutase and tert-butanol (see SI, S0.2 for details). Experiments with uric acid would allow for the evaluation of ONOOH/ONOO⁻ (i) presence from $NHCl_2$ decomposition and (ii) importance in NDMA formation. Taken together, identifying *I* and understanding its fate during $NHCl_2$ decomposition may lead to an updated pathway for RNS and NDMA formation during $NHCl_2$ decomposition and/or a revised interpretation of the UF+SM model.

Based on the previous discussion, the objective of the current study was to evaluate revisions to the chemistry of $NHCl_2$ decomposition and associated NDMA formation with DMA present. To accomplish this, Pathway A1 was first evaluated through kinetic model simulations to assess the accuracy of NDMA formation kinetics in the UF+SM model at pH 7-10. Next, experiments (pH 7-10) were completed with and without 10 μM total DMA (TOTDMA, DMA plus dimethylammonium cation, DMAH⁺) and 800 μeq $Cl_2 \cdot L^{-1}$ $NHCl_2$, measuring NH_2Cl, $NHCl_2$, N_2O, DO, and NDMA kinetically and NO_2^-, NO_3^-, and DMNO at 4 hrs. NH_2Cl, $NHCl_2$, and N_2O data allowed evaluation of the hypothesis that *I* is HNO during $NHCl_2$ decomposition, and DO,

NO$_2^-$, NO$_3^-$, and NDMA data allowed evaluation of ONOOH/ONOO$^-$ formation and its potential relevance in NDMA formation. Furthermore, under drinking water conditions, DMNO most likely forms through a reaction of DMA with radicals that form during ONOOH/ONOO$^-$ decomposition (Uppu et al., 2000; Kirsch et al., 2003). Therefore, DMNO formation would further support a pathway containing ONOOH/ONOO$^-$. Additional experiments with uric acid, an ONOOH/ONOO$^-$ scavenger (Hooper et al., 1998), allowed evaluation of ONOOH/ONOO$^-$ formation and its importance in NDMA formation. Concurrently with the kinetic experiments, a kinetic model was used to evaluate proposed revisions to NHCl$_2$ decomposition and NDMA formation chemistry, including addition of HNO/NO$^-$, DO, and ONOOH/ONOO$^-$. Overall, the current study objectives were to advance fundamental chloramine chemistry by evaluating the identity of I during NHCl$_2$ decomposition, evaluate a pathway for RNS formation and propagation through DO consumption, and demonstrate formation of toxicologically-relevant end-products such as NDMA through RNS-mediated pathways.

3.2-Materials and Methods

The following are detailed in Supporting Information (SI) in Appendix 1: (i) reagent preparation and washing procedures (SI, S1.1), (ii) chloramine preparation (SI, S1.2), and (iii) chloramine (SI, S1.3), NO$_2^-$ and NO$_3^-$ (SI, S1.4), and NDMA and DMNO (SI, S1.5) quantification. This section's remainder details kinetic experiments, analytical techniques, and kinetic parameter estimation methodology.

3.2.1-Chloramine Formation/Quenching, TOTDMA Addition, and NDMA/DMNO Extraction.

NH$_2$Cl stock solutions were freshly prepared before each experiment (Do et al., 2015) at ca. 4 mM to make NHCl$_2$ stock solutions as detailed in the SI (see S1.2). NHCl$_2$ stock solutions

were made by decreasing the pH of the NH_2Cl stock solutions to 3.7-4.0 with 4 N H_2SO_4 and aging for 45 to 60 minutes until all the NH_2Cl was transformed to $NHCl_2$. Because $NHCl_2$ formation consumes protons, H_2SO_4 was added throughout the aging process to maintain the pH between 3.7-4.0.

$NHCl_2$ concentrations were quantified (Shimadzu UV 2450 spectrophotometer) following Schreiber and Mitch (2005) by deconvoluting the 245 and 295 nm absorbance spectra. Within 15 minutes of complete conversion to $NHCl_2$, the $NHCl_2$ solutions were diluted to 0.4 mM $NHCl_2$ (800 µeq $Cl_2 \cdot L^{-1}$) with pH-adjusted buffer to the desired pH which was time zero. For the experiments in which NDMA was measured, this buffer also contained TOTDMA.

The starting experiment concentrations were 40 mM for the phosphate (pH 7 and 8), borate (pH 9), or carbonate (pH 10) buffers and 10 µM for TOTDMA (pH 7-10). The initial TOTDMA and $NHCl_2$ concentrations were twice those used by Schreiber and Mitch (2006) which was done to exceed detection limits for N_2O formation and DO consumption at pH 7 and prolong the temporally-changing periods at pH 8 and 9.

Following the desired reaction times (0.25-, 0.5-, 1.0-, 1.5-, 2.0-, 2.5-, 3.0-, 3.5-, and 4.0 hours), waters were analyzed for $NHCl_2$, NH_2Cl, and following quenching of chloramine species, NDMA. DMNO was measured at four hours only. For NDMA and DMNO, ten milliliter aliquots were quenched for chloramines using 0.5 g dry quenching mix (1.8 g ascorbic acid, 1 g KH_2PO_4 and 39 g Na_2HPO_4) and shaken vigorously to ensure complete dissolution within a few seconds, minimizing localized concentration gradients (Schreiber and Mitch, 2006; Le Roux et al., 2011; Padhye et al., 2011; Shen and Andrews, 2013). This quenching mix acted as a pH buffer and salting out agent to improve recoveries of NDMA and DMNO. Next, 1 mL of 100 µg·L^{-1} d_6-NDMA was added and samples immediately extracted with dichloromethane (10:1

water:dichloromethane volume ratio), using a back-and-forth shaker table at high speed for fifteen minutes. Following a five-minute quiescent settling period, dichloromethane was decanted with a Pasteur pipette and stored for NDMA and DMNO analysis.

3.2.2-*N₂O and DO Microelectrode Measurements.*

N_2O and DO were measured using microelectrodes from Unisense which have manufacturer reported response times less than 45 and 10 seconds, respectively, and were calibrated before each experiment. Per the manufacturer's recommendation, N_2O standards were made from dilutions of N_2O saturated solution and had a 1.0 μM-N limit of quantification which produced signal-to-noise ratios greater than 10 for all experiments. DO sensor used a two-point calibration: (i) atmospheric air saturated water and (ii) zero DO condition, achieved by scavenging DO with 0.1 M sodium ascorbate in 0.1 M NaOH.

3.2.3-*Kinetic Parameter Estimation Methodology.*

To estimate parameters and their standard errors, the secant parameter estimation function in AQUASIM (Reichert, 1994) was configured to minimize the weighted residual sum of squares (WRSS) between the measured and simulated results, using the square of the measured value as the weight, resulting in a dimensionless WRSS (Wahman et al., 2014). This procedure was used to prevent greater concentrations from biasing the parameter estimates (Draper and Smith, 1998).

3.3-Results and Discussion

3.3.1-*Preliminary Kinetic Evaluation of UF+SM Model (Pathway A1).*

Pathway A1 was originally developed and validated from end-point (e.g., two-hour reaction) NDMA measurements but was not validated with detailed kinetic measurements (pH 7-10) of reactants (e.g., DO or $NHCl_2$), intermediates (e.g., UDMH-Cl), or products other than

NDMA (Schreiber and Mitch, 2006). If incomplete or not robust, viewing NDMA formation as Pathway A1 may not only limit development of NDMA control strategies but fail to account for production of RNS in chloramine systems and formation of RNS-mediated end products of human health concern (Masuda et al., 2000). The SI (see S2.1 and Figs. s1 and s2) contains a detailed discussion of Pathway A1 kinetics which revealed two results subsequently questioned by the current experimental work: (1) DO consumption during $NHCl_2$ decomposition was nominal and only occurs in the presence of TOTDMA and (2) at pH 9 and 10, NDMA formation continues after complete $NHCl_2$ decomposition.

3.3.2-*Applicability of the UF Model for Chloramine Profiles.*

Under the conditions of the current experiments (decomposition of ca. 800 µeq $Cl_2 \cdot L^{-1}$ $NHCl_2$ at pH 7-10 with and without 10 µM TOTDMA addition), the UF model reactions control chloramine concentrations in Scheme 1. As detailed in the SI (S1.3 and S2.2), the UF model accurately simulated time-course profiles of total chlorine (Figure s3-3), and NH_2Cl and $NHCl_2$ (Figs. s4 and s5c and d). The slight mismatch of NH_2Cl at pH 10 (Figure s3-4d) was not surprising because the original UF model (Jafvert, 1985; Jafvert and Valentine, 1987) was validated at pH 6-9. These results illustrated the applicability of the UF model to simulate chloramine concentrations under the selected conditions in this study.

3.3.3-*Limitations of NDMA Simulations with the UF+SM Model (Pathway A1).*

NDMA formation was measured kinetically in waters containing 10 µM TOTDMA and dosed with ca. 800 µeq $Cl_2 \cdot L^{-1}$ $NHCl_2$ at pH 7-10. Figure s3-6a (see SI, S2.3) shows the measured NDMA profiles at pH 7 and 8 were adequately simulated by the UF+SM model over the four-hour experiment. However, deficiencies in the UF+SM model were apparent at pH 9 and 10 (Figure

s3-6b). At pH 9, the UF+SM model underpredicted the measured NDMA formation throughout the four-hour test by a factor of about 2.5. At pH 10, the UF+SM model underpredicted NDMA formation during the first hour, an indication that the underlying reaction kinetics were not robust. The measured NDMA profile was fully developed by the first sampling point at 0.25 hours whereas the UF+SM model simulated increasing NDMA formation through ca. 2.0 hours. These deficiencies along with the collected experimental data motivated assessment of two additional pathways in Scheme 1 that are subsequently discussed: (1) Pathway B1 and (2) Pathway A2 as a replacement for Pathway A1.

3.3.4-*Proposed Pathways B1 and A2.*

Pathway B1 (see Scheme 1) combines (i) the UF model (Table s3-1), assuming HNO as *I* in U7-U9 and (ii) reactions involving DO, HNO/NO$^-$, and other relevant RNS (Table s3-4, SI S2.4). RNS formation is initiated by NHCl$_2$ hydrolysis to HNO (U7) and NO$^-$ (U7→R2). HNO/NO$^-$ may then either react with (i) NH$_2$Cl or NHCl$_2$ to form nitrogen gas (N$_2$) via U8-U10 which is expected to be the major end product in the UF model (Vikesland et al., 1998), (ii) HNO to form N$_2$O via R1 and/or R2→R3 as a minor end product relative to N$_2$, or (iii) DO to form ONOOH/ONOO$^-$ via R4 and/or R2→R5 which subsequently may react with DMA to form NDMA via R7. Otherwise, ONOOH/ONOO$^-$ decomposition results in NO$_2^-$ and NO$_3^-$ formation (Kirsch et al., 2003) as other minor end products relative to N$_2$. Pathway A2 revises Pathway A1, which included the spin-forbidden incorporation of DO to form NDMA (P8). In the proposed Pathway A2, NDMA is formed through a reaction with ONOOH (R8, see Scheme 1), which is pH-dependent because the pK$_a$ of 6.8 for ONOOH/ONOO$^-$ (see Table s3-3) is relevant between pH 7-10; the pK$_a$ for UDMH-Cl was estimated as 1.5 and thus its concentration is not affected by acid-

base speciation between pH 7-10. Experimental data and associated kinetic modeling were subsequently used to evaluate proposed Pathways B1 and A2.

3.3.5-*N$_2$O Formation from NHCl$_2$ Decomposition.*

To initiate Pathway B1, NHCl$_2$ hydrolysis (Scheme 1, U7) is hypothesized to form HNO. Subsequently, N$_2$O may form from HNO (R1) or NO$^-$ (R2→R3) (Shafirovich and Lymar, 2002). Because N$_2$O is a stable end-product, its detection serves as a HNO/NO$^-$ formation marker and would support Pathway B1.(Irvine et al., 2008) Experiments were conducted with ca. 800 μeq Cl$_2\cdot$L^{-1} NHCl$_2$ and 10 μM TOTDMA at pH 7-10. Figure 3-1 shows N$_2$O formed at pH 7-10 with pH-dependent kinetics and yields and Figure s3-7 (see SI, S2.5) shows these N$_2$O profiles inversely tracked NHCl$_2$ decomposition. The N$_2$O profiles, therefore, qualitatively support HNO/NO$^-$ formation from NHCl$_2$ hydrolysis (Table s3-1, U7) which is required to initiate Pathway B1 (see Scheme 1).

3.3.6-*DO Consumption from NHCl$_2$ Decomposition.*

Once HNO/NO$^-$ forms, DO consumption is required to continue Pathway B1, forming ONOOH (Scheme 1, R5) or ONOO$^-$ (Scheme 1, R4). Therefore, DO should be consumed regardless of DMA presence and serves as an additional ONOOH/ONOO$^-$ (and HNO/NO$^-$) marker. Experiments conducted with ca. 800 μeq Cl$_2\cdot$L^{-1} NHCl$_2$ confirmed DO consumption occurred at pH 7-10 in the absence of DMA (Figure s3-8, SI S2.6). Further, DO profiles tracked with NHCl$_2$ decomposition, indicating DO consumption was linked to NHCl$_2$ decomposition and supported DO consumption in Pathway B1.

3.3.7-_Peroxynitrite Scavenging Decreased NDMA Formation._

To further support Pathway B1 by (i) providing evidence for ONOOH/ONOO$^-$ formation during NHCl$_2$ decomposition and (ii) showing that NDMA formation proceeded through ONOOH/ONOO$^-$, ONOOH/ONOO$^-$ scavenging experiments were conducted with uric acid. To establish the maximum uric acid concentration that could be used, initial control experiments were conducted with uric acid and NHCl$_2$. Figure s3-9 (see SI, S2.7) shows the impact of uric acid during NHCl$_2$ decomposition at pH 8-10. Profiles at pH 7 were not provided because of the aforementioned interference with the indophenol method (see SI, S1.3). At pH 9 (Figure s3-9a and b, SI S2.7), a detailed uric acid control experiment was conducted to establish the upper uric acid dose, and uric acid doses up to and including 160 µM had minimal impact on NHCl$_2$ decomposition.

However, a uric acid dose of 200 µM resulted in greater NHCl$_2$ concentrations that deviated from other data starting at about 0.4 hours (Figure s3-9b). Therefore, a target uric acid dose of about 160 µM was set as the upper limit and was checked at pH 8 and 10. Uric acid doses of 160 and 170 µM did not impact NHCl$_2$ decomposition at pH 8 (Figure s3-9c) and pH 10 (Figure s3-9d), respectively. Therefore, Figure 3-2 shows NDMA yields at uric acid doses of 160 or 170 µM and less.

Figure 3-2 shows uric acid – a ONOOH/ONOO$^-$ scavenger (Hooper et al., 1998) – decreased NDMA formation at pH 7-10. At pH 7, NDMA decreased from about 0.3 µM to below the limit of quantitation (0.05 µM) at uric doses of 140 and 170 µM. This supported that (i) ONOOH/ONOO$^-$ is associated with NHCl$_2$ decomposition and (ii) the vast majority, if not all, of the NDMA formation occurred through a ONOOH/ONOO$^-$ mediated pathway at pH 7. At pH 9, where NDMA formation was maximal, NDMA decreased from about 3.5 to 1.7 µM as the uric

acid dose was increased from 0 to 160 μM. At pH 10, a decrease in NDMA formation was observed only after the uric dose was increased from 140 to 170 μM. On balance, the results in Figure 3-2 implicated ONOOH/ONOO⁻ as (i) a downstream product of $NHCl_2$ decomposition and (ii) the central node in NDMA formation during $NHCl_2$ decomposition, supporting Pathway B1 and contradicting Pathway A1. The pH 7 results (Figure 3-2) support Pathways A2 and B1 over A1 in which all NDMA formation proceeds through ONOOH/ONOO⁻. This contention is further supported in the remaining subsections.

3.3.8-*NDMA and DMNO Yields from NHCl₂ Decomposition.*

Further support for ONOOH/ONOO⁻ formation is NDMA formation concomitantly with DMNO. Experiments conducted with ca. 800 μeq $Cl_2 \cdot L^{-1}$ $NHCl_2$ and 10 μM TOTDMA at pH 7-10 showed NDMA and DMNO formation, with DMNO yields 0.8-1.3% of NDMA regardless of pH (Table s3-5, SI S2.8). Masuda et al. (2000) and Uppu et al. (2000) showed reactions between ONOOH/ONOO⁻ and/or their decomposition products with a secondary amine produced *N*-nitrosamines and *N*-nitramines through nitrosation and nitration pathways, respectively. The presence of carbonate has been shown to alter the prevalence of nitrosation and nitration pathways. A study using the precursor morpholine showed that low levels of carbonate relative to ONOOH/ONOO⁻ could catalyze morpholine nitrosation, but high carbonate levels inhibited nitrosation in favor of *N*-nitramine formation (Uppu et al., 2000). Because carbonate buffer was used only at pH 10 in this work, experiments were conducted at pH 10 with varying amounts (10 to 42 mM) of total carbonate ($TOTCO_3$). Results in Table s3-5 showed that NDMA yields decreased by about a factor of two with increasing $TOTCO_3$. DMNO yields also decreased with increasing $TOTCO_3$, but the percentage of DMNO relative to NDMA remained constant (1.1%). The consistent ratios between DMNO and NDMA at pH 7-10 (0.8-1.3%) further support the

revision and replacement of Pathway A1 with A2 in which all NDMA formation occurs through ONOOH/ONOO$^-$. Further work is needed to elucidate the role of carbonate species and buffer type relative to the fate of ONOOH/ONOO$^-$ decomposition products during NHCl$_2$ decomposition. However, the decreased NDMA and DMNO yields with increased TOTCO$_3$ suggest a common source, and DMNO formation itself directly implicates ONOOH/ONOO$^-$ formation in Pathway B1.

3.3.9-NO$_2^-$ and NO$_3^-$ Formation from NHCl$_2$ Decomposition.

NO$_2^-$ and NO$_3^-$ form rapidly from ONOOH/ONOO$^-$ decomposition (Kirsch et al., 2003) via reaction of radical species and hydrolysis, respectively. Therefore, NO$_2^-$ and NO$_3^-$ are markers for ONOOH/ONOO$^-$ formation. As noted in the SI S1.4 and S2.9, it was only possible to accurately quantify NO$_2^-$ and NO$_3^-$ after NHCl$_2$ had decomposed to less than about 50 μeq Cl$_2$·L^{-1} because of a positive interference produced on NO$_2^-$ by quenching of NHCl$_2$ with thiosulfate. Figure s3-10 shows that quenching 50 μeq Cl$_2$·L^{-1} NHCl$_2$ produced about 1 μM-N NO$_2^-$. Therefore, NO$_2^-$ and NO$_3^-$ are reported in Table s3-6 (SI S2.9) as yields only at pH 8-10 in the absence and presence of 10 μM TOTDMA. Without TOTDMA, NO$_2^-$ production was greater at pH 10 (26 μM) compared to pH 8 and 9 (both 10 μM) and NO$_3^-$ production was similar at all three pH levels (14-16 μM); therefore, the percentage of NO$_2^-$ relative to NO$_2^-$ plus NO$_3^-$ increased with pH, in agreement with the ONOOH/ONOO$^-$ reaction scheme validated by Kirsch et al. (2003) albeit at 37 °C (e.g., internal temperature of the human body). Addition of 10 μM TOTDMA resulted in decreased sums of NO$_2^-$ plus NO$_3^-$ (Table s3-6) by 8 μM at pH 8, 14 μM at pH 9, and 6 μM at pH 10. These decreases are consistent with ONOOH/ONOO$^-$ conversion to other intermediates and minor end-products, including NDMA (see Scheme 1) which is maximal at pH

9 (see Figure 3-1). DO formation from the production of NO_2^- is detailed in the SI (S2.10, see also Table s3-7).

3.3.10-UF+RNS Model Implementation.

To assess the RNS-mediated NDMA formation pathways (see Scheme 1, B1 and A2) and to help interpret the experimental data, a kinetic model (UF+RNS) was implemented in AQUASIM (Reichert, 1994). The UF+RNS included the UF model (Jafvert and Valentine, 1992) (Table s3-1, U1-U14), assuming HNO was I formed by $NHCl_2$ hydrolysis (U7), the two previously described RNS related pathways B1 and A2, and the Kirsch et al. (2003) model for ONOOH/ONOO⁻ decomposition to NO_2^- and NO_3^-. Table s3-8 (see S2.11) shows the current AQUASIM-implementation of the Kirsch et al. (2003) model was within 0.1–3.5% of their digitized NO_2^- and NO_3^- concentrations between pH 7-10. Pathway A2 was included in lieu of Pathway A1 from the UF+SM model. Subsequently, the implemented UF+RNS model was used along with the experimental data (see S2.11, Table s3-9) to estimate revisions to three existing (k_{u7}, k_{u8}, and k_{p5}) and three new (k_{r7A}, k_{r7B}, and k_{r8}) parameters implemented in the UF+RNS model (Table 3-1).

Rate constants for U7-U10 were empirical in the UF model (Jafvert and Valentine, 1992), formulated to match chloramine species concentrations only; therefore, they were initially all considered for re-estimation in the current work. Preliminary analysis indicated k_{u9} and k_{u10} were not sensitive to the conditions of this study (i.e., preformed $NHCl_2$); therefore, k_{u9} and k_{u10} were excluded from the final parameter estimation procedure. Table 3-1 shows the revised rate constants ± one standard error for k_{u7} (from 110 to 186 ± 6 $M^{-1} \cdot s^{-1}$) and k_{u8} (from 2.7×10^4 to $(8.2 \pm 0.8) \times 10^4$ $M^{-1} \cdot s^{-1}$).

R7 was included in the UF+RNS model as a new NDMA-formation reaction between ONOOH and DMA (Scheme 1, Pathway B1), justified by (i) the scavenger results (Figure 3-2) that indicated ONOOH/ONOO$^-$ was a central node in NDMA formation and (ii) the RNS literature that showed ONOOH/ONOO$^-$ and/or their decomposition products (i.e., radicals) reacted with DMA to form NDMA.(Masuda et al., 2000) Figure 3-1 indicated NDMA formation was maximal at pH 9, which is close to the average of the pK_a values listed in Table s3-3 for ONOOH/ONOO$^-$ ($pK_a = 6.8$) and DMA$^+$/DMA (pK_a 10.73). Generally, the reaction rate between an acid of one species and conjugate base of another is maximal at a pH equal to the average of their pK_a values, which is pH 8.8 in this case. The UF+SM model used DMA (i.e., the uncharged base form) in the NDMA formation pathway (Schreiber and Mitch, 2006). Therefore, if a direct reaction occurred involving DMA (base form), ONOOH (acid form) is the likely candidate. The estimated rate constant for R7 (see Table 3-1 and Table s3-11) was determined to be acid catalyzed, $k_{r7} = k_{r7A}\left[\exp\left(-\frac{k_{r7B}}{[H^+]}\right)\right]$ with $k_{r7A} = (2.1 \pm 0.4) \times 10^7 \, \text{M}^{-1} \, \text{s}^{-1}$ and $k_{r7B} = (4.4 \pm 0.3) \times 10^{-10} \, \text{M}$, an empirical formulation that warrants a future research effort to further develop a mechanistic revision of the UF+RNS model.

Although our NDMA data could also be simulated by a UF+RNS model version using only Pathways A1 (e.g., the UF+SM model) and B1, our experimental data did not support Pathway A1 because NDMA formation was shut down at pH 7 in the ONOOH/ONOO$^-$ scavenging experiments (Figure 3-2). Therefore, Pathway A1 was revised and Reaction P8 (UDMH-Cl + DO) was the likely candidate for this revision because it is spin-forbidden and DO consumption was not previously kinetically validated (Schreiber and Mitch, 2006). This prompted assessment of Pathway A2 in which P8 was replaced by R8, the reaction of UDMH-Cl and ONOOH to form NDMA with an estimated rate constant of $(1.3 \pm 0.8) \times 10^7 \, \text{M}^{-1} \cdot \text{s}^{-1}$ (Table 3-1, k_{r8}). The current

implementation of R8 is also empirical because it is not known if it is a direct reaction with ONOOH/ONOO⁻ and/or their decomposition products (Uppu et al., 2000), but it was assumed that either could be simulated based on the ONOOH concentration. Rate constants for reactions P5 and P7 were also initially considered for revision, but P7 proved insensitive and was therefore not re-estimated. The final parameter estimation resulted in a decreased rate constant estimate for P5 from 52 to 28 ± 8 $M^{-1} \cdot s^{-1}$, a logical result given that the UF+SM model did not consider Pathway B1.

3.3.11-*UF+RNS Model Well-Simulated NHCl₂, NH₂Cl, DO, and NDMA at pH 7-10.*

The revised rate constants for U7 and U8 were validated by comparing simulated UF+RNS and UF model free chlorine, NH_2Cl, and $NHCl_2$ concentrations for 20 additional experimental conditions (Exp. 1-15 and 23-27) from Jafvert (1985) that are shown in Figs. s11-s14, s16d, and s17 (see SI, S2.12, Table s3-12 for WRSS and average WRSS (AWRSS) comparisons). In addition, the NH_2Cl and $NHCl_2$ data sets used in parameter estimation (Table s3-9) are also included in Table s3-12. Compared to the UF model, the simulated free chlorine, NH_2Cl, and $NHCl_2$ concentrations with the UF+RNS model had similar or lower summed totals of WRSS and AWRSS (see Table s3-12), indicating the UF+RNS model simulated these data comparable to the UF model. These results showed that revised estimates to the rate constants for U7 and U8 in the UF+RNS model did not compromise the simulations of chloramine species concentrations over a wide range of conditions.

Figure 3-1 shows the UF+RNS model simulations and measured time-course profiles of DO and NDMA at pH 7-10. The kinetics and yields of these measured data were well-simulated by the UF+RNS model at all pH levels tested. Notably, at pH 9 and 10 (Figs. 1c and 1d), the

simulated DO and NDMA profiles matched the measured data in terms of kinetics and yields throughout the 4-hour time-course.

The UF+RNS model was used to determine the relative importance of the two NDMA formation pathways (i.e., Pathways A2 and B1). Figure 3-3 summarizes the percentage of the simulated NDMA that formed via R7 (DMA + ONOOH, Pathway B1) and R8 (UDMH-Cl + ONOOH, Pathway A2) at 0.25 hours (Figure 3-3a) and 4 hours (Figure 3-3b) along with the UF+RNS model simulated and measured NDMA.

At pH 7, R8 was the predominate NDMA formation pathway (70-90%), although the measured NDMA was lower at pH 7 compared to the other pH levels. At pH 8, R8 accounted for 55-59% of the NDMA formation, illustrating Pathways A2 and B1 were both important contributors. At pH 9, where NDMA formation was maximal, R7 was the predominant NDMA formation pathway at 0.25 and 4 hours (81-83%). At pH 10, R7 accounted for 52% of the NDMA formation at 0.25 hours and 4 hours, illustrating the importance of the A2 and B1 pathways. The results in Figure 3-1 and 3-3 support the UF+RNS model because it captured the kinetics and yields of the measured DO and NDMA profiles. Pathway B1 (see Scheme 1) was important at pH 7-10 and, together with Pathway A2, indicated all the measured NDMA could be accounted for through ONOOH/ONOO$^-$, stemming from $NHCl_2$ decomposition.

3.3.12-*Current UF+RNS Model Limitations and Future Research Needs.*

The UF+RNS model Pathways B1 and A2 each currently use an empirical NDMA formation reaction, R7 and R8, respectively. Because of the complexity of the current reaction scheme, the mechanistic determination of R7 and R8 is beyond the scope of the current research and is an avenue of future research. Potential cross interactions remain to be investigated between the chloramine species and known decomposition products of ONOOH/ONOO$^-$, including

hydrogen peroxide and hydroxyl radical (McKay et al., 2013; Gleason et al., 2017). In addition, deviations between the measured NO_2^- and NO_3^- formation and UF+RNS model simulated values (see Table s3-13 in SI S2.13) indicate the need for kinetic N_2, NO_2^-, and NO_3^- data to validate and/or revise the Kirsch et al. (2003) ONOOH/ONOO$^-$ decomposition model for drinking water conditions and temperatures. Finally, the UF+RNS model overpredicted the N_2O data at pH 10 (Figure 3-1d) but underpredicted N_2O at pH 7 to 9 (Figure 3-1a-c), with the corresponding WRSS and AWRSS shown in Table s3-10, illustrating the need to measure N_2, NO_2^-, and NO_3^- kinetically in future work to facilitate further advancement of the UF+RNS model.

3.3.13-*Mechanistic Considerations.*

This study presented multiple lines of evidence to demonstrate that $NHCl_2$ hydrolysis resulted in HNO formation (Scheme 1, U7), the so-called unidentified reactive intermediate (*I*) in the UF model (Jafvert and Valentine, 1992). Per Pathway B1, HNO/NO$^-$ reacts through three competing pathways, which include two minor pathways: (i) N_2O formation (see Figure 3-1) via R1 and/or R2→R3 and (ii) reaction with DO (see Figure 3-1) to form ONOOH/ONOO$^-$ via R5 and/or R2→R4, and one major pathway: (iii) N_2 formation via U8-U10 which was has been previously quantified during NH_2Cl decomposition (Vikesland et al., 1998) and can now be used to investigate nitrogen mass balances during $NHCl_2$ decomposition along with the advancements made in this work.

The two minor pathways are important new additions to $NHCl_2$ decomposition chemistry because they help explain the formation of NO_2^-, NO_3^-, NDMA, and DMNO. Table s3-13 shows the measured values for N_2O, NO_2^-, and NO_3^- account for ca. 4-6% of the nitrogen originally present in $NHCl_2$ and total free ammonia ($NH_3 + NH_4^+$). Although complete nitrogen mass balances have not been tracked during $NHCl_2$ decomposition Saunier (1976), estimated NO_3^-

yields accounted for 8-11% of total nitrogen. Future work should include N_2, NO_2^-, NO_3^-, and total free ammonia kinetic measurements along with the products kinetically measured in this study.

Measurements of $NHCl_2$, NH_2Cl, N_2O, DO, NO_2^-, NO_3^-, NDMA, and DMNO implicate $ONOOH/ONOO^-$ as a proposed unstable intermediate formed during $NHCl_2$ decomposition, which was supported by experiments with uric acid, a $ONOOH/ONOO^-$ scavenger (Hooper et al., 1998). NDMA decreased with increasing uric acid at pH 7-10 (Figure 3-2), and the shutdown of NDMA formation at pH 7 spurred replacement of P8 in the UF+SM model with R8 in the UF+RNS model (Table 3-1), corresponding to replacement of Pathway A1 with A2 in Scheme 1. Together with R7, the UF+RNS model accurately captured the kinetics and yields of DO and NDMA at pH 7-10 (Figure 3-1), indicating all NDMA formation (Figure 3-3) could be accounted for through $ONOOH/ONOO^-$ formation, stemming from $NHCl_2$ decomposition.

3.4-Implications

A logical extension of the current results is that scavenging HNO/NO^- and/or $ONOOH/ONOO^-$ may curb NDMA formation in chloramine systems. $NHCl_2$ does not accumulate to measurable concentrations at pH 9 and greater because its rate of decomposition is greater than its formation (Jafvert and Valentine, 1992), but if total free ammonia is in excess as is the case in chloramine systems, chloramine decomposition occurs through $NHCl_2$; therefore, HNO/NO^- and $ONOOH/ONOO^-$ will form regardless of the pH. Scavenging of these RNS and/or strategies to promote chloramine stability would presumably lead to less NDMA formation.

Future research should extend the UF+RNS model presented here. Specifically, a further mechanistic revision of the UF+RNS model, focusing on U7-U10 (Jafvert and Valentine, 1992), R7, R8, and $ONOOH/ONOO^-$ decomposition chemistry (Kirsch et al., 2003) to well-simulate

measured profiles of the minor products (N_2O, NO_2^-, NO_3^-) and the major products (N_2 and total free ammonia) while maintaining simulations of chloramine species (Figs. s4, s7, s15, and s16), DO (Figure 3-1), and NDMA (Figure 3-1).

Further experimental work should consider additional HNO/NO^- formation pathways independent of $NHCl_2$, including the reaction between NH_2Cl and hydroxylamine (NH_2OH) generated from ammonia-oxidizing bacteria (Wahman et al., 2014; Wahman and Speitel, 2015). The reaction of NH_2Cl with NH_2OH implicated HNO/NO^- and $ONOOH/ONOO^-$ production (Wahman et al., 2014), providing a potential mechanism to evaluate and potentially explain enhanced NDMA formation observed during nitrification episodes (Zeng and Mitch, 2016).

3.5-Associated Content

3.5.1-*Supporting Information*

Chloramine preparation and quantification, nitrite, nitrate, NDMA, and DMNO quantification, kinetic evaluation of Pathway A1, applicability of the unified model for chloramine profiles, dissolved oxygen formation from nitrite production, UF+RNS model rate constants and goodness of fit measures, and impact of uric acid on $NHCl_2$ decomposition.

3.5.2-*Notes*

The authors declare no competing financial interest.

3.5.3-*Acknowledgements*

subject to EPA's quality system requirements. Views expressed are those of the authors and do not necessarily represent views or policies of EPA.

3.6-Tables and Figures

Table 3-1. Revised reactions and rate constants implemented in the UF+RNS model. Estimated rate constants provided with their standard error (SE, n = 528 total data points).

#	Reaction Stoichiometry [a]	Rate Expression [a]	Rate Constant ($M^{-1} \cdot s^{-1}$) Unless Otherwise Noted	
			Published	This work (UF+RNS model) ± SE
U7	$NHCl_2 + H_2O \xrightarrow{k_{u7}} HNO + 2H^+ + 2Cl^-$	$k_{u7}[NHCl_2][OH^-]$	[b] 110	186 ± 6
U8	$HNO + NHCl_2 \xrightarrow{k_{u8}} HOCl + products$ [c]	$k_{u8}[HNO][NHCl_2]$	[d] 2.7×10^4	$(8.2 \pm 0.8) \times 10^4$
P5	$NHCl_2 + (CH_3)_2NH \xrightarrow{k_{p5}} (CH_3)_2NNHCl + H^+ + Cl^-$	$k_{p5}[NHCl_2][(CH_3)_2NH]$	[e] 52	28 ± 8
R7	$ONOOH + (CH_3)_2NH \xrightarrow{k_{r7}} (CH_3)_2NNO + products$ [f]	$k_{r7}[ONOOH][(CH_3)_2NH]$	NA	[g] $k_{r7} = k_{r7A}\left[\exp\left(-\frac{k_{r7B}}{[H^+]}\right)\right]$ $k_{r7A} = (2.1 \pm 0.4) \times 10^7\ M^{-1}\ s^{-1}$ $k_{r7B} = (4.4 \pm 0.3) \times 10^{-10}\ M$
R8	$ONOOH + (CH_3)_2NNHCl \xrightarrow{k_{r8}} (CH_3)_2NNO + products$ [h]	$k_{r8}[ONOOH][(CH_3)_2NNHCl]$	NA	[i] $(1.3 \pm 0.8) \times 10^7$

\# – reaction number corresponding to Scheme 1; Tables s3-1-s3-4 detail published reactions and rate constants

[a] Unidentified intermediate, *I*, of $NHCl_2$ hydrolysis was assumed to be HNO in the UF+RNS model

[b] Jafvert and Valentine (1992)

[c] may include N_2, Cl^-, H^+, and other unidentified reaction products

[d] Jafvert and Valentine (1987)

[e] Schreiber and Mitch (2006)

[f] May include H_2O_2 Kirsch et al., (1998) and other unidentified reaction products

[g] Empirical formulation currently only applicable at pH 7-10, indicating that $ONOOH/ONOO^-$ decomposition products may also react with $(CH_3)_2NH$ to form NDMA

[h] May include H^+, Cl^-, NO_2^-, and other unidentified reaction products

[i] $ONOOH/ONOO^-$ decomposition products may also react with $(CH_3)_2NNHCl$ to form NDMA

NA – not applicable because these reactions are reported for the first time in this work
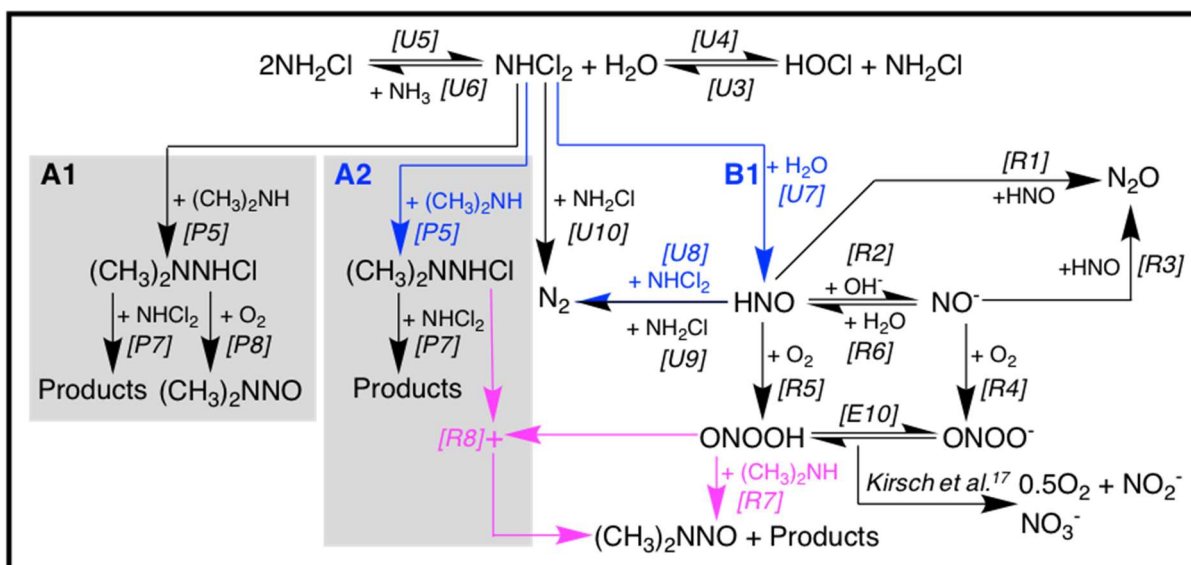
Scheme 3-1 – NDMA formation stemming from NHCl₂ decomposition in the presence of DMA – see Table s3-1 (U1-U14) for UF model reactions. **A1**: currently-accepted NHCl₂-DMA reaction pathway represented by the UF+SM model (Schreiber and Mitch, 2006) – see Table s3-2 for P1-P8 of the UF+SM model (replaced with A2 in the UF+RNS model). **B1**: proposed RNS scheme for NHCl₂ hydrolysis to HNO and subsequent formation of N₂O, ONOOH, and other products – see Tables s3-3 and s4 for the relevant equilibrium reactions and principle RNS model reactions, respectively. In the presence of DMA (R7), ONOOH (shown) and/or radicals formed from ONOOH/ONOO⁻ decomposition (not shown) react with DMA to form NDMA. **A2**: proposed replacement of A1 in which ONOOH (shown) and/or radicals formed from ONOOH/ONOO⁻ decomposition (not shown) react with UDMH-Cl to form NDMA. The UF+RNS model is comprised of A2 and B1, the latter of which includes the 117 reactions in the ONOOH/ONOO⁻ model of Kirsch et al. (2003) with only the principal end-products shown for simplicity. Reaction numbering *[U#]*, *[P#]*, *[E#]*, and *[R#]* corresponds to those listed in Tables s3-1-s3-4, respectively. Blue arrows and text denote the previously-published reactions for which their rate constants were modified to fit the NH₂Cl, NHCl₂, DO, and NDMA kinetic data at pH 7-10 (see Table s3-9) and magenta arrows and text denote the new reactions and rate constants added to the UF+RNS model to fit these same data (see Table 3-1).
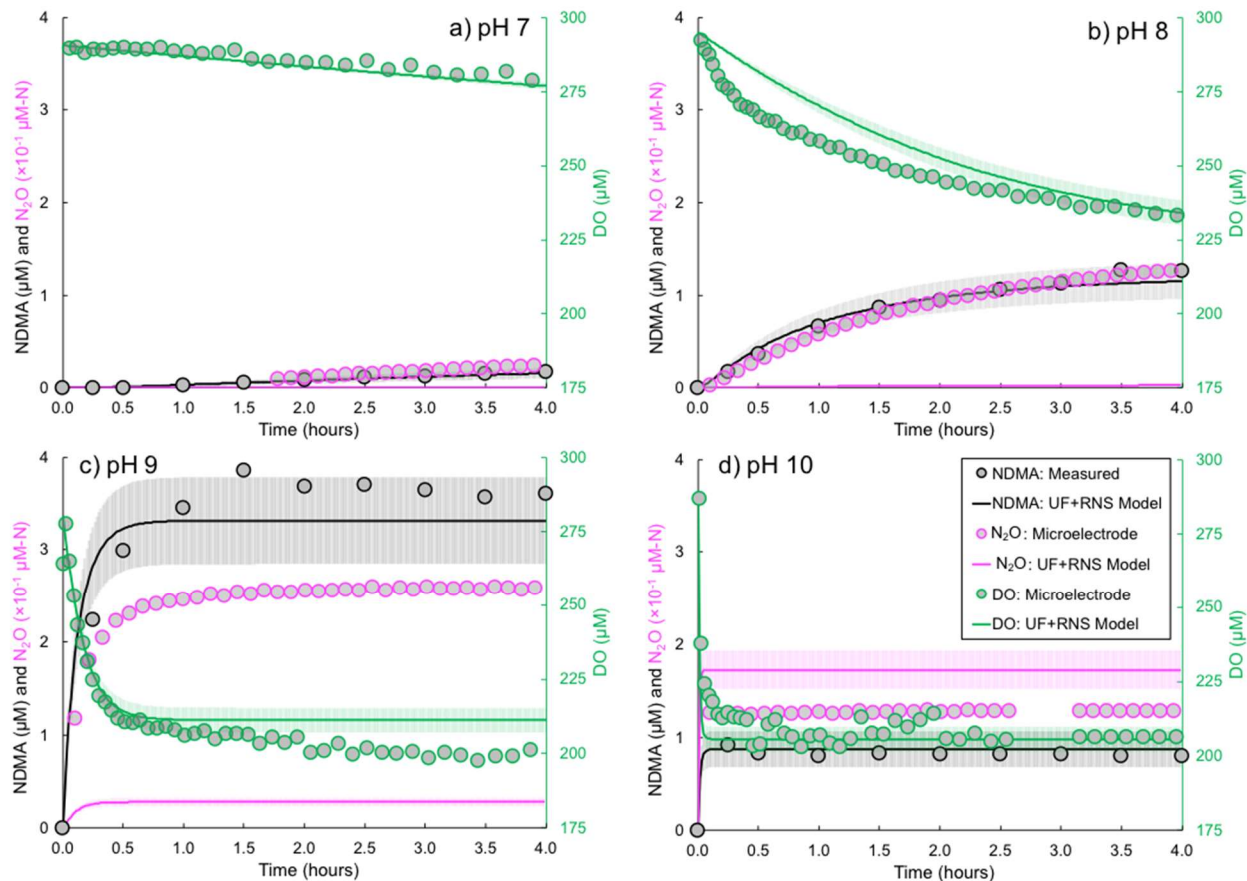
Figure 3-1. NDMA (black, primary y-axis), N_2O (magenta, primary y-axis), and DO (green, secondary y-axis) profiles in waters dosed with ca. 800 μeq $Cl_2 \cdot L^{-1}$ $NHCl_2$ and containing 10 μM TOTDMA buffered at (a) pH 7, (b) pH 8, (c) pH 9, and (d) pH 10. Points are measured values, lines are UF+RNS model simulations, and shaded areas are simulations encompassing one standard error in the estimated parameters (see Table 3-1). Table s3-9 contains the weighted residual sum of squares (WRSS) and the corresponding average weighted residual sum of squares (AWRSS) for data sets used in parameter estimation for the UF+RNS model (e.g., NDMA and DO). In addition, Table s3-10 contains the WRSS and AWRSS for the N_2O data sets to provide an indication of how well the UF+RNS model simulated these data, which were not used during parameter estimation. Notes: N_2O data were divided by ten for scaling purposes (e.g., at pH 10, N_2O stabilized at about 13 μM-N), and the limit of quantitation was 1 μM-N which corresponded to a signal-to-noise ratio greater than ten; at pH 10, the gap in DO and N_2O microelectrode data between 2.6 and 3.2 hours was due to a lost computer connection.
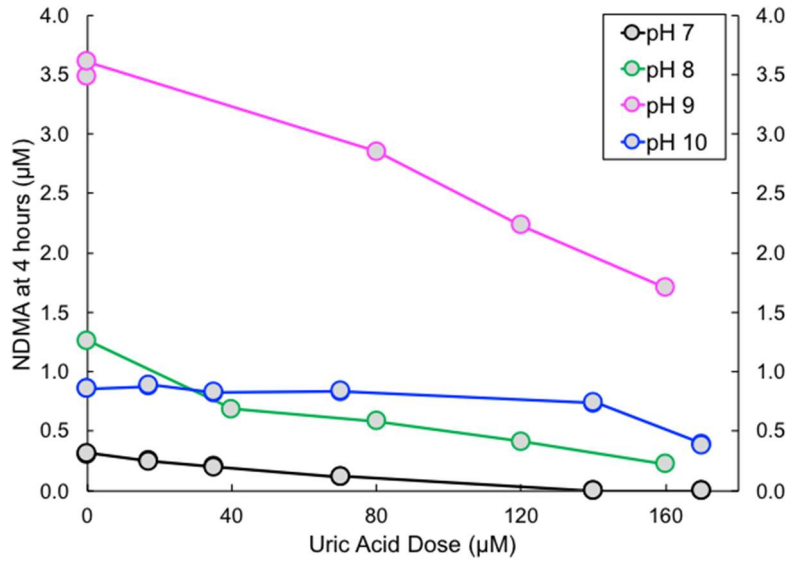
Figure 3-2. NDMA formation at 4 hours versus uric acid dose in waters amended with 10 μM TOTDMA and ca. 800 μeq $Cl_2 \cdot L^{-1}$ $NHCl_2$ at pH 7, 8, 9, and 10. Uric acid is a known $ONOOH/ONOO^-$ scavenger (Hooper et al., 1998).
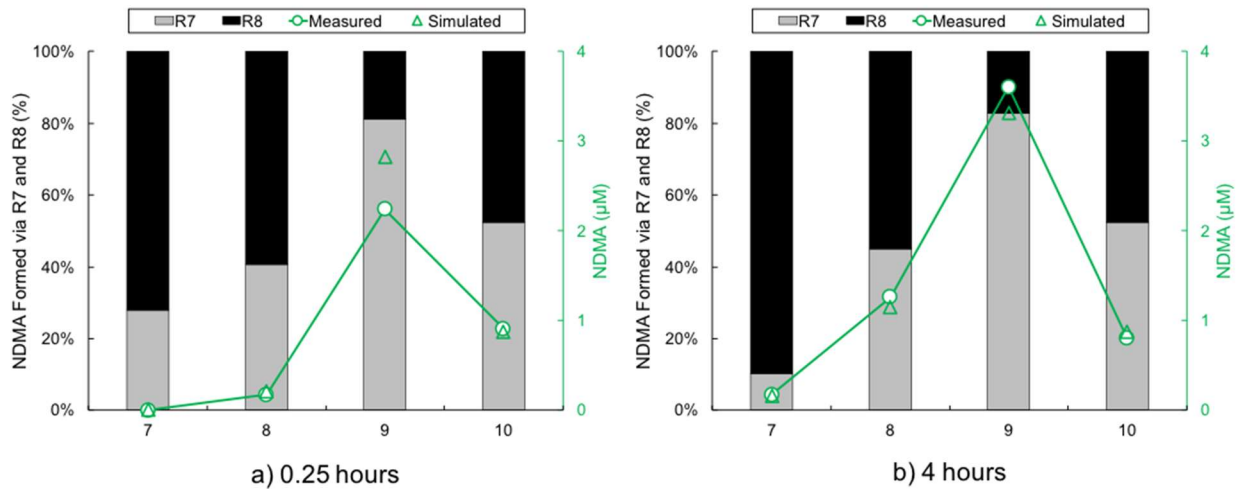
Figure 3-3. Percentage of UF+RNS model simulated NDMA formed via R7 and R8 (primary y-axis) and measured and UF+RNS model simulated NDMA concentrations (secondary y-axis) at pH 7, 8, 9, and 10 at (a) 0.25 hours and (b) 4 hours.

3.7-References

CRC Handbook of Chemistry and Physics, Taylor & Francis, (2010-2011).

Choi, J. and Valentine, R. L., *Water Research*, **36**, 817-824 (2002). 10.1016/S0043-1354(01)00303-7.

Choi, J. and Valentine, R. L., *Water Science and Technology*, **46**, 65-71 (2002). 10.2166/wst.2002.0056.

Cornwell Engineering Group. (2018). 2017 Water Utility Disinfection Survey Report,

Do, T. D., Chimka, J. R. and Fairey, J. L., *Environmental Science & Technology*, **49**, 9858-9865 (2015). 10.1021/acs.est.5b01304.

Draper, N. R. and Smith, H. *Applied Regression Analysis*, John Wiley & Sons, Inc., New York, (1998).

Flowers, R. C. and Singer, P. C., *Environ Sci Technol*, **47**, 7365-7372 (2013). 10.1021/es4003185.

Gleason, J. M., McKay, G., Ishida, K. P. and Mezyk, S. P., *Chemosphere*, **187**, 123-129 (2017). 10.1016/j.chemosphere.2017.08.053.

Hamer, M., Morales Vasquez, M. A. and Doctorovich, F., F. Doctorovich, P. J. Farmer and M. Marti. *The Chemistry and Biology of Nitroxyl (HNO)*. Elsevier. (2016).

Hooper, D. C., Spitsin, S., Kean, R. B., Champion, J. M., Dickson, G. M., Chaudhry, I. and Koprowski, H., *Proceedings of the National Academy of Sciences of the United States of America*, **95**, 675-680 (1998). 10.1073/pnas.95.2.675.

Hrudey, S. E. and Charrois, J. W. A., Eds. *Disinfection By-Products and Human Health*. IWA Publishing and Australian Water Association, London, (2012).

Huang, M. E., Huang, S. and McCurry, D. L., *Environmental Science & Technology Letters*, **5**, 154-159 (2018). 10.1021/acs.estlett.7b00572.

Irvine, J. C., Ritchie, R. H., Favaloro, J. L., Andrews, K. L., Widdop, R. E. and Kemp-Harper, B. K., *Trends in Pharmacological Sciences*, **29**, 601-608 (2008). 10.1016/j.tips.2008.08.005.

Jafvert, C. T. (1985). A Unified Chlorine-Ammonia Speciation and Fate Model. PhD, PhD Dissertation, University of Iowa,

Jafvert, C. T. and Valentine, R. L., *Water Research*, **21**, 967-973 (1987).

Jafvert, C. T. and Valentine, R. L., *Environ Sci Technol*, **26**, 577-586 (1992). Doi 10.1021/Es00027a022.

Kirsch, M., Korth, H. G., Wensing, A., Sustmann, R. and de Groot, H., *Archives of Biochemistry and Biophysics*, **418**, 133-150 (2003). 10.1016/j.abb.2003.07.002.

Kirsch, M., Lomonosova, E. E., Korth, H. G., Sustmann, R. and de Groot, H., *Journal of Biological Chemistry*, **273**, 12716-12724 (1998). 10.1074/jbc.273.21.12716.

Krasner, S. W., Mitch, W. A., McCurry, D. L., Hanigan, D. and Westerhoff, P., *Water Research*, **47**, 4433-4450 (2013). 10.1016/j.watres.2013.04.050.

Le Roux, J., Gallard, H. and Croue, J. P., *Water Research*, **45**, 3164-3174 (2011). 10.1016/j.watres.2011.03.035.

Leavey-Roback, S. L., Krasner, S. W. and Suffet, I. M., *Chemosphere*, **164**, 330-338 (2016). 10.1016/j.chemosphere.2016.08.070.

Masuda, M., Mower, H. F., Pignatelli, B., Celan, I., Friesen, M. D., Nishino, H. and Ohshima, H., *Chemical Research in Toxicology*, **13**, 301-308 (2000). 10.1021/tx990120o.

McKay, G., Sjelin, B., Chagnon, M., Ishida, K. P. and Mezyk, S. P., *Chemosphere*, **92**, 1417-1422 (2013). 10.1016/j.chemosphere.2013.03.045.

Mitch, W. A. and Sedlak, D. L., *Environ Sci Technol*, **36**, 588-595 (2002). 10.1021/es010684q.

Morran, J., Whittle, M., Fabris, R. B., Harris, M., Leach, J. S., Newcombe, G. and Drikas, M., *Journal American Water Works Association*, **103**, 76-+ (2011).

Padhye, L., Luzinova, Y., Cho, M., Mizaikoff, B., Kim, J.-H. and Huang, C.-H., *Environ Sci Technol*, **45**, 4353-4359 (2011). 10.1021/es104255e.

Pliss GB, Z. M., Petrov AS, Khudoley VV., *Arch Geschwulstforsch*, **52**, 629-635 (1982).

Reichert, P., *Water Science and Technology*, **30**, 21-30 (1994).

Russell, C. G., Blute, N. K., Via, S., Wu, X. Y. and Chowdhury, Z., *Journal American Water Works Association*, **104**, 57-58 (2012). 10.5942/jawwa.2012.104.0037.

Saunier, B. M. (1976). Kinetics of Breakpoint Chlorination and Disinfection. Ph.D. Dissertation, University of California, Berkeley, CA.

Schreiber, I. M. and Mitch, W. A., *Environmental Science & Technology*, **39**, 3811-3818 (2005). 10.1021/es0483286.

Schreiber, I. M. and Mitch, W. A., *Environmental Science & Technology*, **40**, 6007-6014 (2006). 10.1021/es060978h.

Selbes, M., Kim, D., Ates, N. and Karanfil, T., *Water Research*, **47**, 945-953 (2013). 10.1016/j.watres.2012.11.014.

Shafirovich, V. and Lymar, S. V., *Proceedings of the National Academy of Sciences of the United States of America*, **99**, 7340-7345 (2002). 10.1073/pnas.112202099.

Shafirovich, V. and Lymar, S. V., *Journal of the American Chemical Society*, **125**, 6547-6552 (2003). 10.1021/ja034378j.

Shen, R. and Andrews, S. A., *Water Research*, **45**, 944-952 (2011). 10.1016/j.watres.2010.09.036.

Shen, R. Q. and Andrews, S. A., *Water Research*, **47**, 802-810 (2013). 10.1016/j.watres.2012.11.004.

Smulik, R., Debski, D., Zielonka, J., Michalowski, B., Adamus, J., Marcinek, A., Kalyanaraman, B. and Sikora, A., *Journal of Biological Chemistry*, **289**, 35570-35581 (2014). 10.1074/jbc.M114.597740.

Spahr, S., Cirpka, O. A., von Gunten, U. and Hofstetter, T. B., *Environmental Science & Technology*, **51**, 280-290 (2017). 10.1021/acs.est.6b04780.

Squadrito, G. L., Cueto, R., Splenser, A. E., Valavanidis, A., Zhang, H., Uppu, R. M. and Pryor, W. A., *Archives of Biochemistry and Biophysics*, **376**, 333-337 (2000). https://doi.org/10.1006/abbi.2000.1721.

Uppu, R. M., Squadrito, G. L., Bolzan, R. M. and Pryor, W. A., *Journal of the American Chemical Society*, **122**, 6911-6916 (2000). 10.1021/ja000270h.

Vikesland, P. J., Ozekin, K. and Valentine, R. L., *Environmental Science & Technology*, **32**, 1409-1416 (1998).

Wahman, D. G. and Speitel, G. E., *Water Research*, **68**, 719-730 (2015). 10.1016/j.watres.2014.10.054.

Wahman, D. G., Speitel, G. E. and Machavaram, M. V., *Water Research*, **60**, 218-227 (2014). 10.1016/j.watres.2014.04.051.

Wei, I. W. (1972). Chlorine-Ammonia Breakpoint Reactions: Kinetics and Mechanism. Ph.D. Dissertation, Harvard University, Cambridge, MA.

Yagil, G. and Anbar, M., *Journal of the American Chemical Society*, **84**, 1797-1803 (1962). 10.1021/ja00869a005.

Zeng, T. and Mitch, W. A., *Environmental Science & Technology*, **50**, 2964-2973 (2016). 10.1021/acs.est.5b05668.

Appendix 1

Supporting Information for

Updated Reaction Pathway for Dichloramine Decomposition: Formation of Reactive

Nitrogen Species and *N*-Nitrosodimethylamine

Contents

The Supporting Information (SI) contains (1) background on uric acid scavenging, (2) methods and materials detailing (i) reagent preparation and washing procedures, (ii) chloramine preparation, (iii) chloramine quantification, (iv) nitrite (NO_2^-) and nitrate (NO_3^-) quantification, and (v) N-nitrosodimethylamine (NDMA) and N-nitrodimethylamine (DMNO) quantification; (3) results and discussion detailing (i) preliminary kinetic evaluation of the unified (UF)(Jafvert and Valentine, 1992) plus Schreiber and Mitch(Schreiber and Mitch, 2006) (SM) model (UF+SM model, Pathway A1), (ii) the applicability of the UF model for chloramine profiles, and (iii) dissolved oxygen (DO) formation from NO_2^- production; (4) thirteen tables; (4) seventeen figures; and (5) references cited in the SI.

S0 Introduction

S0.1 UF+SM model reactions.

Table s3-1. Unified (UF) model of chloramine chemistry (Jafvert and Valentine, 1992)

U#	Reaction Stoichiometry	Rate Expression	Rate Constant	Units
U1	$HOCl + NH_3 \xrightarrow{k_{u1}} NH_2Cl + H_2O$	$k_{u1}[HOCl][NH_3]$	[a] 4.2×10^6	$M^{-1}s^{-1}$
U2	$NH_2Cl + H_2O \xrightarrow{k_{u2}} HOCl + NH_3$	$k_{u2}[NH_2Cl]$	[a] 2.1×10^{-5}	s^{-1}
U3	$HOCl + NH_2Cl \xrightarrow{k_{u3}} NHCl_2 + H_2O$	$k_{u3}[HOCl][NHCl_2]$	[b] 2.8×10^2	$M^{-1}s^{-1}$
U4	$NHCl_2 + H_2O \xrightarrow{k_{u4}} HOCl + NH_2Cl$	$k_{u4}[NHCl_2]$	[b] 6.5×10^{-7}	s^{-1}
U5	$NH_2Cl + NH_2Cl \xrightarrow{k_{u5}} NHCl_2 + NH_3$	$k_{u5}[NH_2Cl]^2$	[c] k_{u5}	$M^{-1}s^{-1}$
U6	$NHCl_2 + NH_3 \xrightarrow{k_{u6}} NH_2Cl + NH_2Cl$	$k_{u6}[NHCl_2][NH_3][H^+]$	[d] 6.0×10^4	$M^{-2}s^{-1}$
U7	$NHCl_2 + H_2O \xrightarrow{k_{u7}} I$ [e]	$k_{u7}[NHCl_2][OH^-]$	[f] 110	$M^{-1}s^{-1}$
U8	I [e] $+ NHCl_2 \xrightarrow{k_{u8}} HOCl + products$[g]	$k_{u8}[I$[e]$][NHCl_2]$	[h] 2.7×10^4	$M^{-1}s^{-1}$
U9	I [e] $+ NH_2Cl \xrightarrow{k_{u9}} products$[g]	$k_{u9}[I$[e]$][NH_2Cl]$	[h] 8.3×10^3	$M^{-1}s^{-1}$
U10	$NH_2Cl + NHCl_2 \xrightarrow{k_{u10}} products$[g]	$k_{u10}[NH_2Cl][NHCl_2]$	[i] 1.5×10^{-2}	$M^{-1}s^{-1}$
U11	$HOCl + NHCl_2 \xrightarrow{k_{u11}} NCl_3 + H_2O$	$k_{u11}[NHCl_2][HOCl]$	[d] k_{u11}	$M^{-1}s^{-1}$
U12	$NHCl_2 + NCl_3 + 2H_2O \xrightarrow{k_{u12}} 2HOCl + products$[g]	$k_{u12}[NHCl_2][NCl_3][OH^-]$	[f] 5.6×10^{10}	$M^{-2}s^{-1}$
U13	$NH_2Cl + NCl_3 + H_2O \xrightarrow{k_{u13}} HOCl + products$[g]	$k_{u13}[NH_2Cl][NCl_3][OH^-]$	[f] 1.4×10^9	$M^{-2}s^{-1}$
U14	$NHCl_2 + 2HOCl + H_2O \xrightarrow{k_{u14}} NO_3^- + 5H^+ + 4Cl^-$	$k_{u14}[NHCl_2][OCl^-]$	[f] 2.3×10^2	$M^{-1}s^{-1}$

U# – reaction number for the unified (UF) model of chloramine chemistry
[a] Morris and Isaac (1983)
[b] Margerum et al. (1978)
[c] Valentine et al. (1988)

$k_{u5} = k_H[H^+] + k_{H_2P}[H_2PO_4^-] + k_{H_3P}[H_3PO_4] + k_{H_2CO_3}[H_2CO_3^*] + k_{HCO_3^-}[HCO_3^-]$

where: $k_H = 6.9 \times 10^3$ $M^{-2}s^{-1}$; $k_{H_2P} = 3.6 \times 10^{-1}$ $M^{-2}s^{-1}$; $k_{H_3P} = 8.9 \times 10^2$ $M^{-2}s^{-1}$

$k_{H_2CO_3} = 7.5 \times 10^{-1}$ $M^{-2}s^{-1}$; $k_{HCO_3^-} = 2.0 \times 10^{-3}$ $M^{-2}s^{-1}$

[d] Hand and Margerum(Hand and Margerum, 1983)

$k_{u11} = k_{OCl^-}[OCl^-] + k_{HP}[HPO_4^{2-}] + k_{OH^-}[OH^-]$

where: $k_{OCl^-} = 9.0 \times 10^4$ $M^{-2}s^{-1}$; $k_{HP} = 1.6 \times 10^4$ $M^{-2}s^{-1}$; $k_{OH^-} = 3.3 \times 10^9$ $M^{-2}s^{-1}$

[e] I is the unidentified intermediate of dichloramine hydrolysis assumed to be nitroxyl (HNO) in this work
[f] Jafvert and Valentine (1992)
[g] may include H_2O, Cl^-, H^+, NO_3^-, N_2, and unidentified species
[h] Jafvert and Valentine (1987)
[i] Leao (1981)

Table s3-2. Reactions (Scheme 1, Pathway A1) added by Schreiber and Mitch (2006) to the unified (UF) model of chloramine chemistry (Table s3-1) to create the UF+SM model

P#	Reaction Stoichiometry	Rate Expression	Rate Constant	Units
P1	$HOCl + (CH_3)_2NH \xrightarrow{k_{p1}} (CH_3)_2NCl + H_2O$	$k_{p1}[HOCl][(CH_3)_2NH]$	6.1×10^7	$M^{-1}s^{-1}$
P2	$(CH_3)_2NH_2^+ + NH_2Cl \xrightarrow{k_{p2}} NH_4^+ + (CH_3)_2NCl$	$k_{p2}[NH_2Cl][(CH_3)_2NH_2^+]$	5.8×10^{-3}	$M^{-1}s^{-1}$
P3	$NH_2Cl + (CH_3)_2NH \xrightarrow{k_{p3}} (CH_3)_2NNH_2 + H^+ + Cl^-$	$k_{p3}[NH_2Cl][(CH_3)_2NH]$	8.1×10^{-2}	$M^{-1}s^{-1}$
P4	$NH_3 + (CH_3)_2NCl \xrightarrow{k_{p4}} (CH_3)_2NNH_2 + H^+ + Cl^-$	$k_{p4}[NH_3][(CH_3)_2NCl]$	4.9×10^{-3}	$M^{-1}s^{-1}$
P5	$NHCl_2 + (CH_3)_2NH \xrightarrow{k_{p5}} (CH_3)_2NNHCl + H^+ + Cl^-$	$k_{p5}[NHCl_2][(CH_3)_2NH]$	52	$M^{-1}s^{-1}$
P6	$NHCl_2 + (CH_3)_2NNH_2 \xrightarrow{k_{p6}} (CH_3)_2NH + products^a$	$k_{p6}[NHCl_2][(CH_3)_2NNH_2]$	4.5	$M^{-1}s^{-1}$
P7	$NHCl_2 + (CH_3)_2NNHCl \xrightarrow{k_{p7}} products^a$	$k_{p7}[NHCl_2][(CH_3)_2NNHCl]$	7.5×10^{-1}	$M^{-1}s^{-1}$
P8	$O_2 + (CH_3)_2NNHCl \xrightarrow{k_{p8}} (CH_3)_2NNO + HOCl$	$k_{p8}[O_2][(CH_3)_2NNHCl]$	1.4	$M^{-1}s^{-1}$

P# – reaction number corresponding to Scheme 1a

[a] may include N_2, Cl^-, H^+, and other unidentified reaction products

Table s3-3. Acid dissociation constants for equilibria relevant to Tables 3-1, s3-1, and s3-2

E#	Equilibrium Expression	pK$_a$
E1	$HOCl \rightleftharpoons H^+ + OCl^-$	7.50 [a]
E2	$NH_4^+ \rightleftharpoons H^+ + NH_3$	9.30 [a]
E3	$H_2CO_3^* \rightleftharpoons H^+ + HCO_3^-$	6.35 [b]
E4	$HCO_3^- \rightleftharpoons H^+ + CO_3^{2-}$	10.33 [b]
E5	$H_3PO_4 \rightleftharpoons H^+ + H_2PO_4^-$	2.16 [b]
E6	$H_2PO_4^- \rightleftharpoons H^+ + HPO_4^{2-}$	7.21 [b]
E7	$HPO_4^{2-} \rightleftharpoons H^+ + PO_4^{3-}$	12.32 [b]
E8	$H_3BO_3 \rightleftharpoons H^+ + H_2BO_3^-$	9.27 [b]
E9	$H_2BO_3^- \rightleftharpoons H^+ + HBO_3^{2-}$	>14 [b]
E10	$ONOOH \rightleftharpoons H^+ + ONOO^-$	6.8 [c]
E11	$(CH_3)_2NH_2^+ \rightleftharpoons H^+ + (CH_3)_2NH$	10.73 [b]
E12	$(CH_3)_2NNH_3^+ \rightleftharpoons H^+ + (CH_3)_2NNH_2$	7.21 [d]

E# – number corresponding to the acid/base equilibrium expression

[a] Snoeyink and Jenkins(1980)

[b] CRC Handbook (2010-2011)

[c] Ferrer–Sueta and Radi (2009)

[d] Hinman (1958)

S0.2 Scavenging Reactions with Uric Acid.

Uric acid is a known scavenger of $ONOOH/ONOO^-$ and/or its decomposition products, but is non-selective and could quench other species too. Stinefelt et al. (2005) also showed that uric acid can scavenge reactive oxygen species (ROS), including hydroxyl ($HO^\bullet$) and superoxide ($O_2^{\bullet-}$) radicals by electron spin resonance, but the kinetic rates are unknown. Importantly, Schreiber and Mitch (2006) ruled out ROS in the formation of NDMA during $NHCl_2$ decomposition. They used superoxide dismutase to scavenge $O_2^{\bullet-}$, $HO^\bullet$, singlet oxygen ($^1O_2$), and peroxyl radical ($ROO^\bullet$) (Rao et al., 1988) and tert-Butanol to scavenge $HO^\bullet$ (Vonpiechowski et al., 1992) but found no impact on NDMA formation. Therefore, uric acid scavenging of ROS likely does not affect NDMA formation.

Many studies have shown that uric acid was an exceptional scavenger of $ONOOH/ONOO^-$ in extracellular fluids (Hooper et al., 1998; Hooper et al., 2000; Kean et al., 2000; Nimse and Pal, 2015). However, the exact reaction pathways remain unknown. The pseudo-first-order rate constant for the reaction between uric acid and $ONOOH/ONOO^-$ in human blood plasma was determined to be 0.05 s^{-1}, which was about 920 times lower than 46 s^{-1} that was measured for CO_2 and $ONOOH/ONOO^-$ (Squadrito et al., 2000). Therefore, uric acid likely does not react directly with $ONOOH/ONOO^-$ but rather the products generated from the reaction of peroxynitrite with CO_2. Intermediate species formed which include $ONOOCO_2^-$ and $O_2NOCO_2^-$ are short-lived and, therefore, uric acid may only directly react with their decomposition products such as $NO_2^\bullet$ and $CO_3^{\bullet-}$. The rate constant for the $NO_2^\bullet$ reaction with uric acid was determined to be $(1.8 \pm 0.2) \times 10^7$ $M^{-1}{\cdot}s^{-1}$ (Simic and Jovanovic, 1989). The rate constant for the reaction of $CO_3^{\bullet-}$ with uric acid is unknown, but it is expected to be greater given that $CO_3^{\bullet-}$ is more reactive than $NO_2^\bullet$ towards reducing agents such as ascorbic acid.

Imaram et al. (2010) studied the direct reaction between uric acid and peroxynitrite. They detected a urate-derived radical which could be an intermediate in the production of the aminocarbonyl radical. At neutral pH, ONOOH and $ONOO^-$ are both present (pK_a = 6.8) along with their decomposition products. Uric acid has a pK_{a1} = 5.8 and a pK_{a2} = 10.3. Therefore, at pH 7 uric acid predominately exists as the mono-ionic urate anion, which is likely to react with uncharged ONOOH or its decomposition radicals ($NO_2^\bullet$, $CO_3^{\bullet-}$, $HO^\bullet$, etc.). At pH 9 and 10, uric acid predominately exists in its dianion form. The direct reaction between the urate dianion and $ONOO^-$ is unfavorable due to the charge repulsion, therefore it likely will react with $ONOO^-$ decomposition radicals.

S1 Methods and Materials

S1.1 Reagent Preparation and Washing Procedures.

High purity water (18.2 MΩ–cm) for batch kinetic experiments was generated using a Millipore Integral 3 purification system and referred to hereinafter as Milli–Q water. All stock chemicals were used as obtained without any further purification, which included: sodium hypochlorite (VWR, ACS grade), ammonium chloride (Amerso, ACS grade), ascorbic acid (Amerso, ACS grade), potassium phosphate monobasic (Anerso, ACS grade), sodium phosphate dibasic (Fisher, ACS grade), dimethylamine (DMA; Sigma, ACS grade), dichloromethane (VWR, HPLC grade), NDMA (AccuStandard, neat), and DMNO (AccuStandard, dissolved in acetonitrile at 100 $\mu g \cdot mL^{-1}$). Glassware and plastic–ware were scrubbed with a mixture of Alconox soap and tap water and triple–rinsed with deionized water and Milli–Q water. Chlorine demand–free glassware was prepared by soaking cleaned glassware in a chlorine bath (at least 100 $mg \cdot L^{-1}$ as Cl_2) for 24 hours, triple–rinsed with deionized followed by Miili–Q water and then baked at 400 °C for at least two hours. PTFE–lined lids were rinsed with acetone and baked at 80 °C for at least one hour.

S1.2 Chloramine Preparation.

$NHCl_2$ stock solutions were made from NH_2Cl stock solutions that were prepared by adding 6.2 mL of 1.0 $mg-N \cdot mL^{-1}$ NH_4Cl and 10 mL of 0.2 M $NaHCO_3$ to a 100 mL volumetric flask containing about 50 mL of Milli-Q water. The solution was placed in the refrigerator at 4 °C for at least 20 minutes to minimize $NHCl_2$ formation during subsequent free chlorine addition. Next, 0.6 mL of 5% NaClO was added followed by Milli-Q water until the total volume was 100 mL. The NH_2Cl concentration (ca. 4 mM) was quantified by UV absorbance measurements at 245 and 295 nm until it was confirmed that only NH_2Cl was present following the spectra

deconvolution (Schreiber and Mitch, 2005). A NH_2Cl stock solution was used to generated $NHCl_2$ stock solutions for spiking in the kinetic experiments.

S1.3 Chloramine Quantification.

The applicability of the UF model was validated against measured profiles of total chlorine, dichloramine ($NHCl_2$), and monochloramine (NH_2Cl) between pH 7–10 and leveraged in experiments to simulate chloramine species concentrations for which these profiles could not be measured simultaneously alongside other target analytes such as N_2O and dissolved oxygen (DO) because of experimental limitations. Total chlorine was quantified by the Hach DPD Method 8167 with a limit of quantification at 0.02 mg$\cdot$L^{-1} as Cl_2. Despite $NHCl_2$ in all samples being below the threshold of 6 mg$\cdot$L^{-1} as Cl_2 established by Hach(2015) following ten-fold dilutions prior to measurement, multiple methods were used to quantify $NHCl_2$ and NH_2Cl in this work. NH_2Cl was quantified using the Hach Indophenol Method 10171 with a limit of quantification at 0.04 mg$\cdot$L^{-1} as Cl_2. However, the Indophenol method raises the pH to ca. 11 which may force $NHCl_2$ to rapidly decompose, a fraction of which is converted to NH_2Cl, potentially producing a positive bias. Therefore, at pH 7 and 8 in particular, where $NHCl_2$ was present throughout the four–hour kinetic experiments, the FAS-DPD titration Method from Standard Methods 4500–Cl F (Eaton et al., 1998) was also used to quantify $NHCl_2$ and NH_2Cl. The potassium permanganate titrant was standardized every two weeks to ensure the accuracy of the titration.

S1.4 NO_2^- and NO_3^- Quantification.

NO_2^- and NO_3^- were quantified using a Metrohm 850 Professional Ion Chromatograph with ultraviolet absorbance detector. 10 mL of the reaction solutions were quenched with 0.4 mM thiosulfate prior to the analysis. A Metrosep A Supp 7 – 250/4.0 column type was used with an oven temperature of 55 °C and a flow rate of 0.7 mL$\cdot$min^{-1} with 3.6 mM Na_2CO_3 eluent. As $NHCl_2$

can react with thiosulfate to form NO_2^- which can be subsequently oxidized to NO_3^-, these data were only considered to be reliable for kinetic experiments in which the $NHCl_2$ had decreased to less 50 µeq $Cl_2 \cdot L^{-1}$. Therefore, it was only possible to determine NO_2^- and NO_3^- yields at pH 8, 9, and 10. This was done in waters with and without 10 µM TOTDMA addition (Table s3-6).

S1.5 NDMA and DMNO Quantification.

NDMA and DMNO were identified and quantified using electrospray ionization gas chromatography–mass spectrometry (GC–MS/EI) using single injections of all blanks, standards, and samples. Blanks and standards were prepared following the same extraction procedure as samples and check standards were run at least every ten samples. Seven–point NDMA standard curves (5 – 500 µg·L^{-1}) and five–point DMNO standard curves (0.10 – 5.0 µg·L^{-1}) were used for quantification and had correlations coefficients greater than 0.995. The limits of quantitation of NDMA and DMNO were 3 and 0.07 µg·L^{-1}, respectively. The Splitless injections of 5 µM were used with an injector temperature at 250 °C. The separation column used was a DB–5 with a length of 30 m, inner diameter 0.25 mm, and a stationary phase film thickness of 0.25 µm. Helium carrier gas was used with constant flow rate at 1.0 mL·min^{-1}. The oven program was 45 °C for three minutes followed by a ramp of 25 °C·min^{-1} to 130 °C and then 12 °C·min^{-1} to 230 °C and held for one minute. For NDMA, the retention time was 6.29 minutes identified at m/z ratios of 74 and 42; for DMNO, the retention time of 7.73 min identified at m/z ratios of 90 and 60.

S2 Results and Discussion

S2.1 Preliminary Kinetic Evaluation of UF+SM Model (Pathway A1).

To conceptually understand Pathway A1, an initial kinetic analysis was conducted. The UF+SM model was implemented in AQUASIM (Reichert, 1994) and then validated, using NDMA data digitized from Figure 3-3a of Schreiber and Mitch (2006) (Figure s3-1) for their conditions (200 μM or 400 μeq $Cl_2 \cdot L^{-1}$ $NHCl_2$; 5 μM TOTDMA; pH 7-10; two-hour reaction). The minor discrepancies (0.3-2.8%) between the digitally captured NDMA concentrations and AQUASIM simulations were attributed to inaccuracies inherent to the digitization process, considering the ordinate is a log-scale.
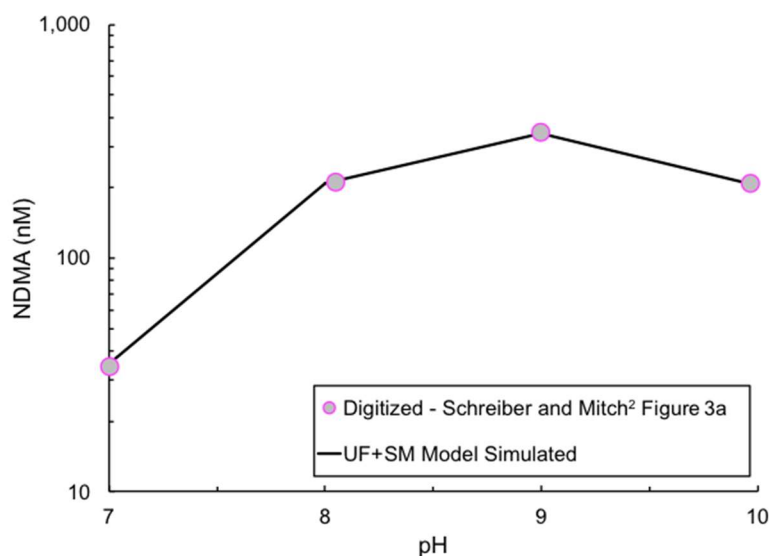
Figure s3-1. Comparison of NDMA formation after two hours from the decomposition of 200 μM $NHCl_2$ (400 μeq $Cl_2 \cdot L^{-1}$) in waters containing 5 μM TOTDMA between pH 7-10 from (i) simulations presented in Figure 3-3a of Schreiber and Mitch(Schreiber and Mitch, 2006) (Digitized) that were captured using GraphClick 3.0.3 and (ii) simulations from an AQUASIM implemented UF+SM model.(Schreiber and Mitch, 2006)

The kinetic profiles of $NHCl_2$, NH_2Cl, UDMH-Cl, DO, DMA, and NDMA were also simulated (Figure s3-2). Because of the relatively small initial TOTDMA (5 μM) versus high initial $NHCl_2$ (400 μeq $Cl_2 \cdot L^{-1}$), $NHCl_2$ and NH_2Cl profiles were controlled by UF model reactions (Table

s3-1) and were unaffected by NDMA-related reactions (Table s3-2). Figure s3-2 shows that as pH increased, so too did $NHCl_2$ decomposition and NH_2Cl formation rates, a well-known result of base-catalyzed $NHCl_2$ hydrolysis (Table s3-1, U4 and U7) and NH_2Cl formation (U4 and U6). Initial DMA concentrations ranged from 0.0009 μM (pH 7) to 0.78 μM (pH 10), and DMA consumption increased with pH (Figure s3-2). UDMH-Cl formation was pH-dependent and maximal at pH 9, owing to its formation via the $NHCl_2$ and DMA reaction (P5).
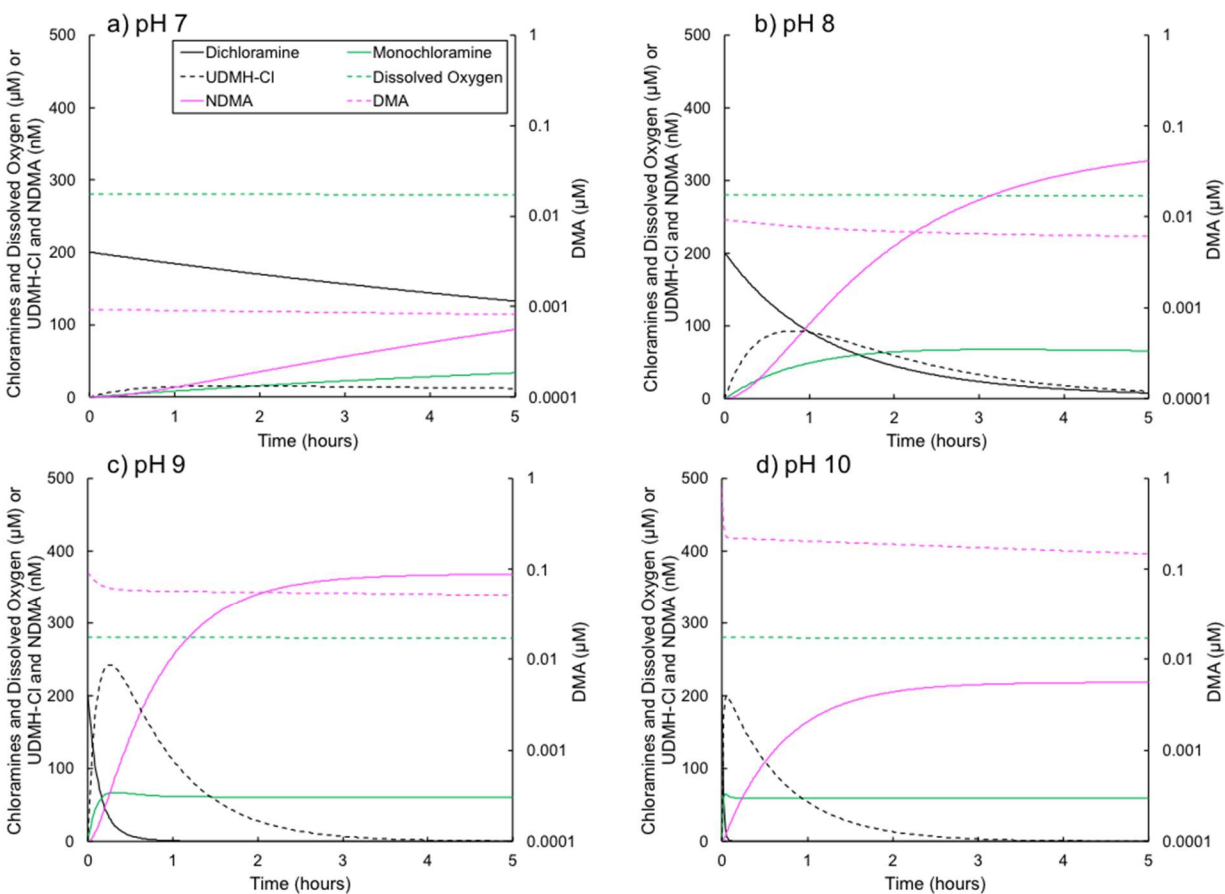
Figure s3-2. UF+SM model simulated concentration profiles for $NHCl_2$, NH_2Cl, UDMH–Cl, DO, DMA, and NDMA at (a) pH 7, (b) pH 8, (c) pH 9, and (d) pH 10. Initial $NHCl_2$ was 200 μM (400 μeq $Cl_2 \cdot L^{-1}$) and TOTDMA was 5 μM. Note: Dimethylammonium cation ($DMAH^+$) and Dimethylamine (DMA) pK_a is 10.73 (Table s3-3, E11).

Over the five-hour simulation, DO consumption via reaction with UDMH-Cl (P8) was only 0.10 μM (pH 7), 0.30 μM (pH 8), 0.40 μM (pH 9), and 0.20 μM (pH 10). Importantly, Schreiber

and Mitch (2006) did not measure DO kinetically during $NHCl_2$ decomposition; therefore, simulated DO profiles have not been experimentally validated. Measured DO profiles during $NHCl_2$ decomposition could serve to support Pathway A1 or provide evidence of another reaction pathway relevant to NDMA formation and/or revise Pathway A1.

Chloramine profiles relative to those of NDMA are also noteworthy, particularly at pH 9 and 10. Figure s3-2c and s2d show simulated NDMA formation continued after complete $NHCl_2$ decomposition. At pH 9, $NHCl_2$ decreased to less than 1 μM (99.5% decomposition) after one hour at which point NDMA was 250 nM or only 68% of its value at 5 hours. At pH 10, $NHCl_2$ decreased to less than 1 μM in 0.1 hours at which point NDMA was 26 nM or only 12% of its value at 5 hours. These observations illustrate the role of UDMH-Cl in Pathway A1 and account for continued NDMA formation even after complete $NHCl_2$ decomposition.

S2.2 Applicability of the UF Model for Chloramine Profiles.

Figure s3-3 shows the decomposition of total chlorine in waters spiked with ca. 800 μeq $Cl_2 \cdot L^{-1}$ $NHCl_2$ (400 μM $NHCl_2$) at pH 7, 7.6, 8, 9, and 10, representing the chloramine conditions studied in the current work. The experimental data at each pH level was compared to simulations from the UF model (Table s3-1) (Jafvert and Valentine, 1992). This was done for waters without TOTDMA (Figure s3-3a and b) and waters with 10 μM TOTDMA (Figure s3-3c and d). The results in Figure s3-3 indicate the UF model adequately captured the pH–dependent decomposition of total chlorine. The addition of 10 μM TOTDMA did not adversely impact the ability of the model to simulate the experimental data, an expected result given the high initial dose of $NHCl_2$ (800 μeq $Cl_2 \cdot L^{-1}$) relative to the low initial dose of TOTDMA (10 μM). At pH 7, 7.6, and 8, the model captured the total chlorine decomposition throughout the four–hour test (Figure s3-3a and c). At pH 9 and 10, the model captured the rate at which total chlorine decomposition occurred

(Figure s3-3b and d) but underpredicted the measured concentrations after one hour by 10–50 μM at pH 9 and 50–95 μM at pH 10. This larger difference at pH 10 may reflect the fact that the UF model of chloramine chemistry was calibrated for pH 7–9 (Jafvert and Valentine, 1987; Jafvert and Valentine, 1992).
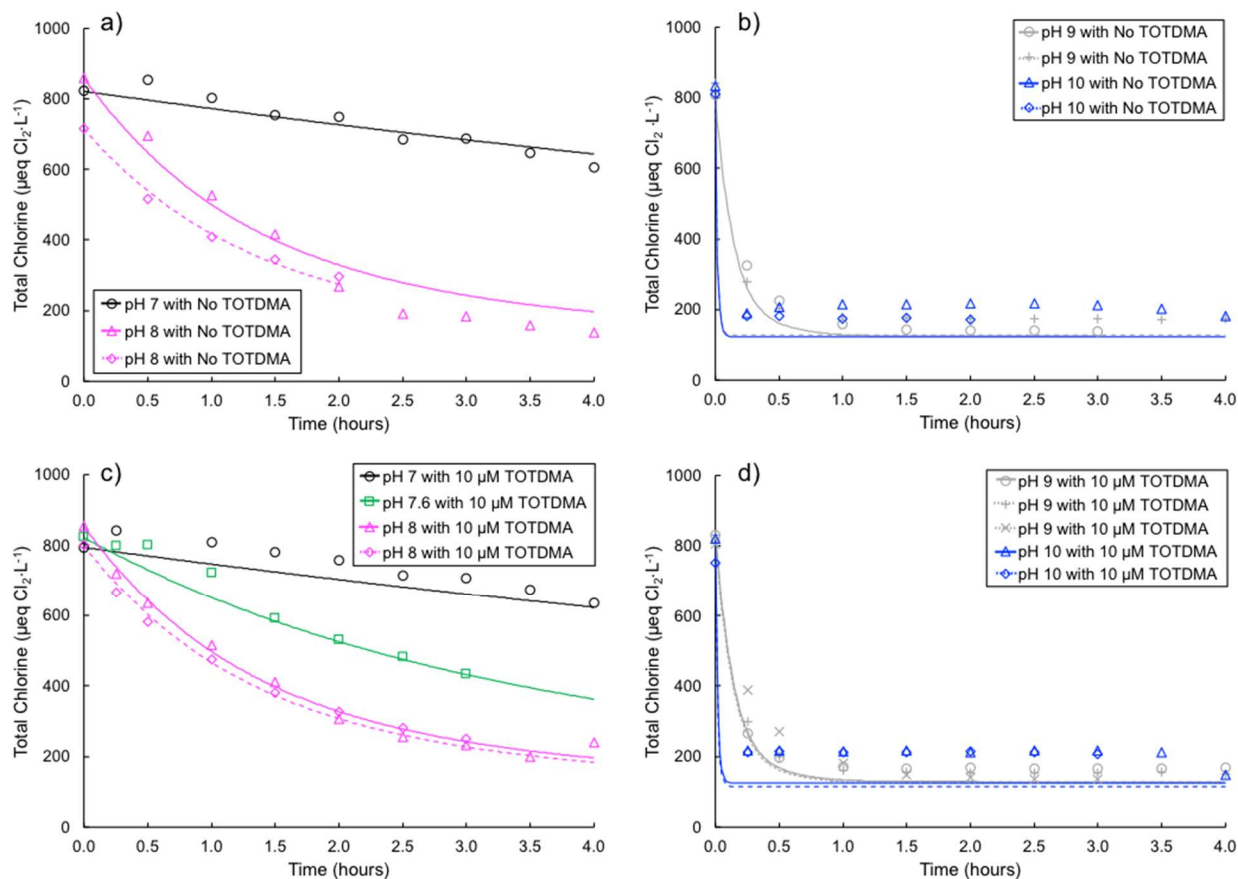
Figure s3-3. Measured total chlorine from ca. 800 μeq $Cl_2 \cdot L^{-1}$ $NHCl_2$ decomposition in waters (a) at pH 7 (black) and pH 8 (magenta) without added TOTDMA, (b) at pH 9 (grey) and pH 10 (blue) without added TOTDMA, (c) at pH 7 (black), pH 7.6 (green), and pH 8 (magenta) with 10 μM TOTDMA, and (d) at pH 9 (grey) and pH 10 (blue) with 10 μM TOTDMA. The points represent experimentally–measured total chlorine concentrations, and the corresponding lines were simulations generated with the unified (UF) model of chloramine chemistry.(Jafvert and Valentine, 1992)

NHCl$_2$ and NH$_2$Cl profiles measured with DPD-FAS titration are shown in Figure s3-4 at pH 7, 8, 9, and 10. Because of the rapid kinetics at pH 9 and 10, the FAS-DPD titration was done at two hours only.
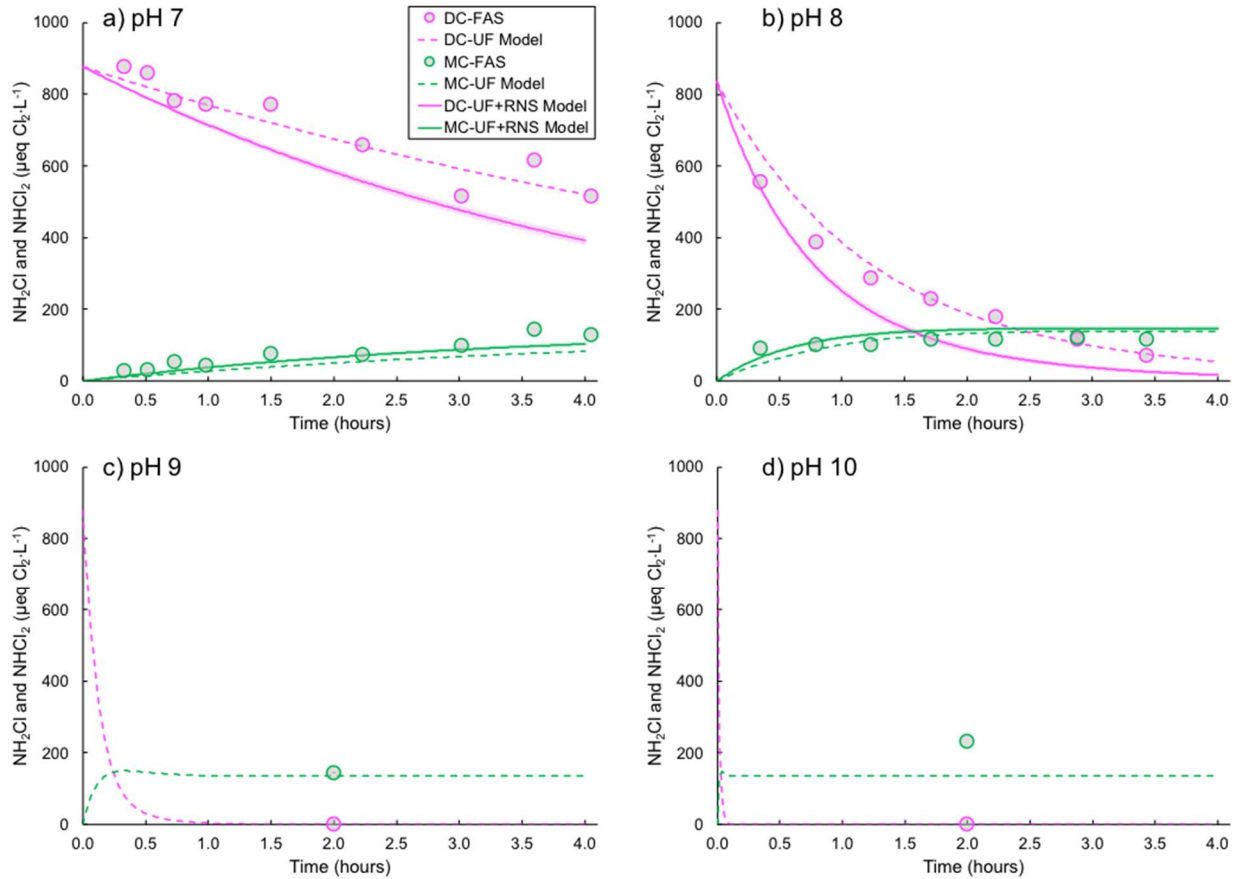
Figure s3-4. FAS-DPD measured NHCl$_2$ and NH$_2$Cl concentrations from ca. 800 μeq Cl$_2$·L^{-1} NHCl$_2$ decomposition in waters at (a) pH 7, (b) pH 8, (c) pH 9, and (d) pH 10. The points represent experimentally–measured NHCl$_2$ and NH$_2$Cl concentrations by FAS-DPD and dashed-lines are UF model simulations (Jafvert and Valentine, 1992). For panels (a) and (b), solid lines are UF+RNS model simulations, and shaded areas are simulations encompassing one standard error in the estimated parameters (see Table 3-1). For panels (a) and (b), Table s3-9 contains the weighted residual sum of squares (WRSS) and the corresponding average weighted residual sum of squares (AWRSS) for the NHCl$_2$ and NH$_2$Cl data sets used in parameter estimation for the UF+RNS model.

A similar mismatch was observed in the NH$_2$Cl concentration at pH 10 (see Figure s3-4d) as was apparent in the total chlorine measurement (see Figure s3-3d). Figure s5 shows another set of NHCl$_2$ and NH$_2$Cl profiles measured with the Hach total chlorine and monochloramine

Indophenol method at pH 7, 8, 9, and 10. Throughout the four-hour profile at pH 7 and during the first hour at pH 8, the UF model underpredicted the measured NH_2Cl, suggesting a positive bias from $NHCl_2$ decomposition.
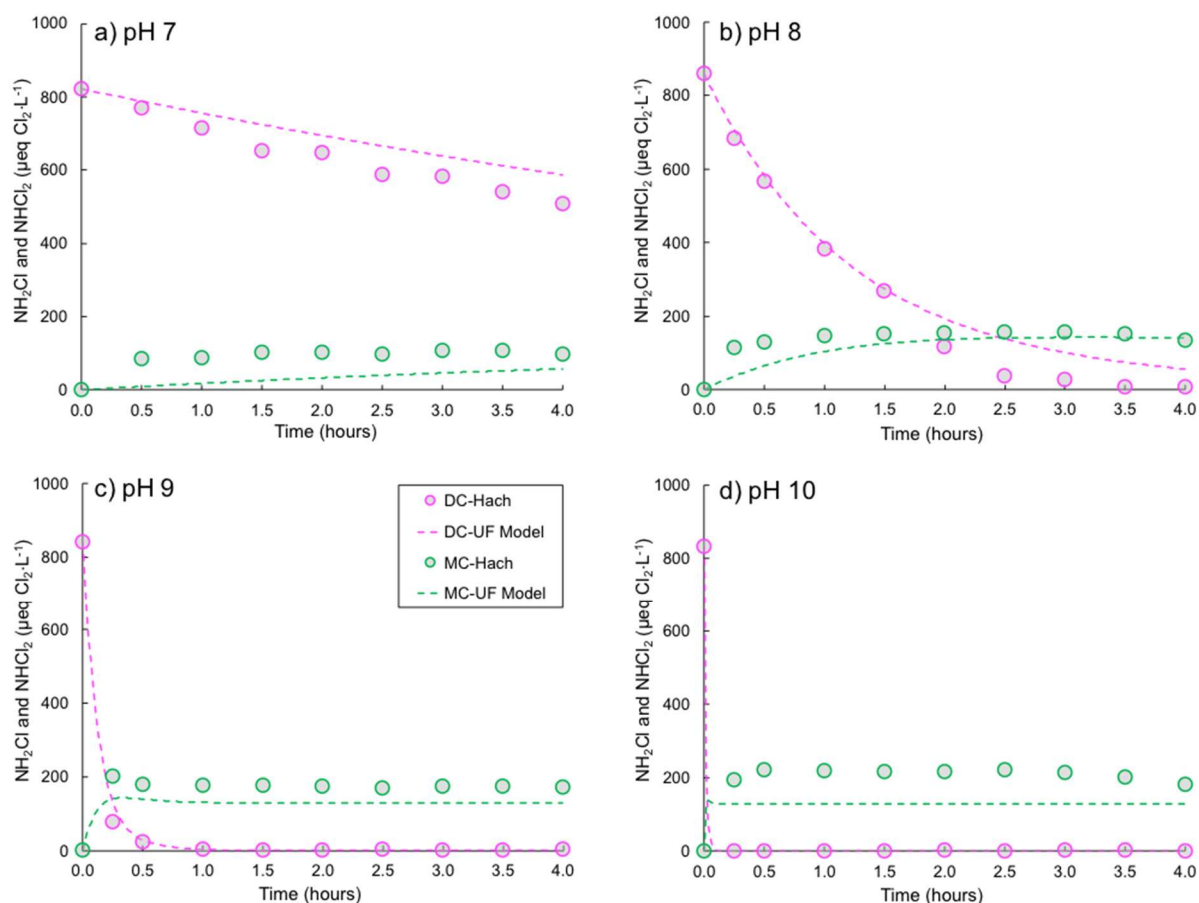
Figure s3-5. NH_2Cl and $NHCl_2$ concentrations from ca. 800 µeq $Cl_2 \cdot L^{-1}$ $NHCl_2$ decomposition in waters at (a) pH 7, (b) pH 8, (c) pH 9, and (d) pH 10. The points represent experimentally–measured Indophenol NH_2Cl or calculated $NHCl_2$ (measured DPD total chlorine minus measured Indophenol NH_2Cl) concentrations and dashed-lines are UF model simulations.(Jafvert and Valentine, 1992)

Regardless, the experimental data and model simulations in Figures s3-s5 indicated that the UF model adequately captured the chloramine species concentrations in waters spiked with $NHCl_2$ at ca. 800 µeq $Cl_2 \cdot L^{-1}$. The UF model was therefore used in Scheme 1 to simulate the NH_2Cl

and NHCl₂ profiles in experiments during which other target analytes were measured to help

validate Scheme 1.

S2.3 Limitations of NDMA Simulations with the UF+SM Model (Pathway A1)
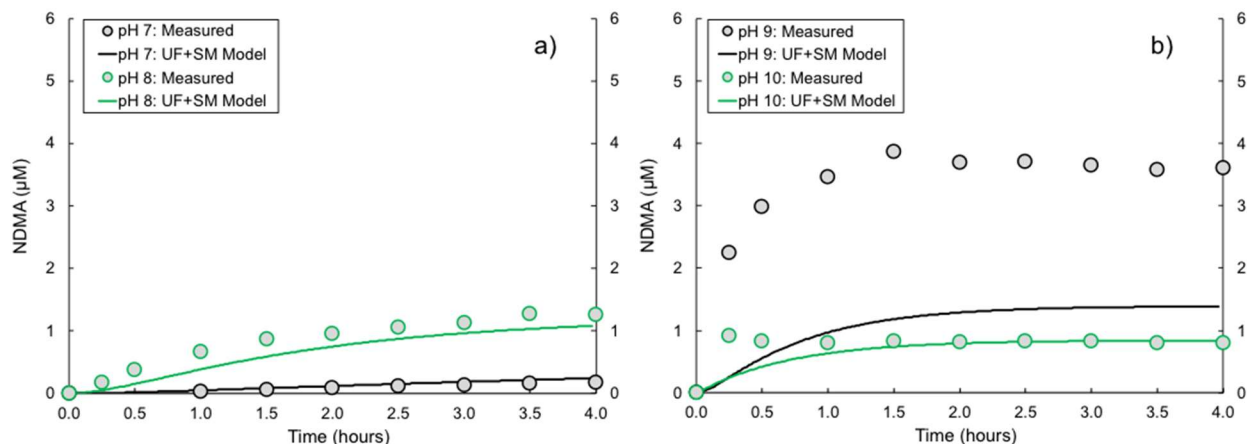
Figure s3-6. NDMA profiles with TOTDMA of 10 µM for ca. 800 µeq $Cl_2 \cdot L^{-1}$ $NHCl_2$ decomposition in waters buffered at (a) pH 7 and 8 and (b) pH 9 and 10. Points are measured values and lines are UF+SM model(Schreiber and Mitch, 2006) simulations.

S2.4 Proposed Pathways B1 and A2.

Table s3-4. HNO/NO⁻ reactions included in the UF+RNS model

R#	Reaction Stoichiometry	Rate Expression	Rate Constant	Units
R1	$HNO + HNO \xrightarrow{k_{r1}} N_2O + H_2O$	$k_{r1}[HNO][HNO]$	[a] 8.0×10^6	$M^{-1}s^{-1}$
R2	$HNO + OH^- \xrightarrow{k_{r2}} NO^- + H_2O$	$k_{r2}[HNO][OH^-]$	[a] 4.9×10^4	$M^{-1}s^{-1}$
R3	$HNO + NO^- \xrightarrow{k_{r3}} N_2O + OH^-$	$k_{r3}[HNO][NO^-]$	[b] 6.6×10^9	$M^{-1}s^{-1}$
R4	$NO^- + O_2 \xrightarrow{k_{r4}} ONOO^-$	$k_{r4}[O_2][NO^-]$	[a] 2.7×10^9	$M^{-1}s^{-1}$
R5	$HNO + O_2 \xrightarrow{k_{r5}} ONOOH$	$k_{r5}[HNO][O_2]$	[c] 1.8×10^4	$M^{-1}s^{-1}$
R6	$NO^- + H_2O \xrightarrow{k_{r6}} HNO + OH^-$	$k_{r6}[NO^-]$	[a] 1.2×10^2	s^{-1}

R# – reaction number corresponding to Scheme 1
[a] Shafirovich and Lymar (2002)
[b] Lymar and Shafirovich (2007)
[c] Smulik et al. (2014)

S2.5 N₂O Formation from NHCl₂ Decomposition.
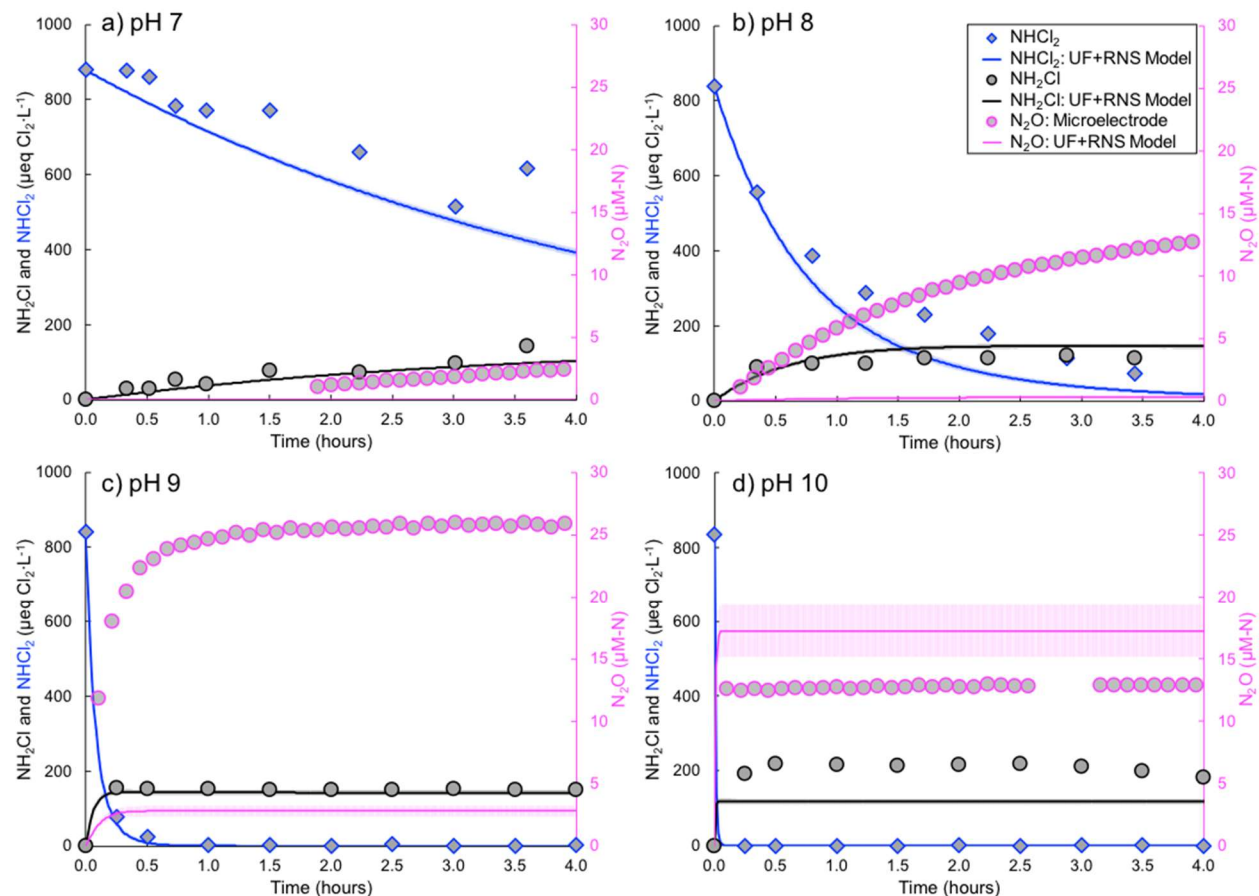
Figure s3-7. NHCl₂ (blue, primary y-axis), NH₂Cl (black, primary y-axis), and N₂O (magenta, secondary y-axis) profiles in waters dosed with ca. 800 μeq Cl₂·L⁻¹ NHCl₂ and containing 10 μM TOTDMA buffered at (a) pH 7, (b) pH 8, (c) pH 9, and (d) pH 10. Points are measured values, lines are UF+RNS model simulations, and shaded areas are simulations encompassing one standard error in the estimated parameters (see Table 3-1). Table s3-9 contains the weighted residual sum of squares (WRSS) and the corresponding average weighted residual sum of squares (AWRSS) for data sets used in parameter estimation for the UF+RNS model (e.g., NHCl₂ and NH₂Cl). In addition, Table s3-10 contains the WRSS and AWRSS for the N₂O data sets to provide an indication of how well the UF+RNS model simulated these data, which were not used during parameter estimation. These data are a summary of other figures as follows: N₂O data were shown in Figure 3-1; pH 7 and 8 NHCl₂ and NH₂Cl were shown in Figure s3-4a-b and measured by DPD-FAS titration; pH 9 and 10 NHCl₂ and NH₂Cl were measured by the Hach DPD and Indophenol methods. Notes: the limit of quantitation for N₂O was 1 μM-N; at pH 10, the gap in the N₂O microelectrode data between 2.6 and 3.2 hours was due to a lost computer connection.

S2.6 DO Consumption from NHCl₂ Decomposition.
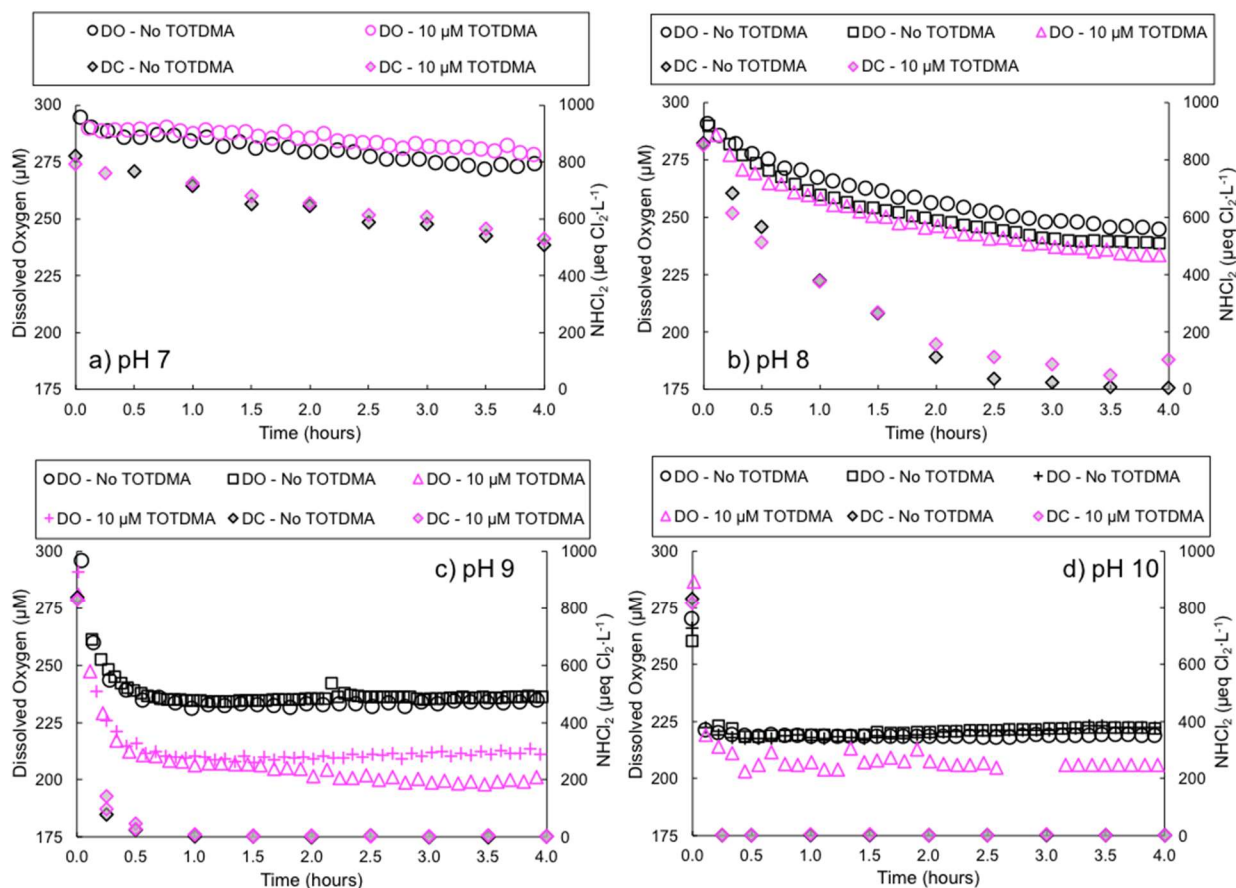
Figure s3-8. Dissolved oxygen (DO) profiles during decomposition of ca. 800 μeq Cl₂·L⁻¹ NHCl₂ (listed as DC in panel legends) for no TOTDMA and 10 μM TOTDMA at (a) pH 7, (b) pH 8, (c) pH 9, and (d) pH 10. DO measurements determined with a DO microelectrode. DC – No TOTDMA (◇) at pH 7-10 presented in Figure s3-5; DC – 10 μM TOTDMA (◆) at pH 9 and 10 presented in Figure s3-7c and d, respectively; DO – 10 μM TOTDMA (△) at pH 8, 9, and 10 presented in Figure 3-1; at pH 10, the gap in DO microelectrode data between 2.6 and 3.2 hours was due to a lost computer connection.

S2.7 Peroxynitrite Scavenger Decreased NDMA Formation.
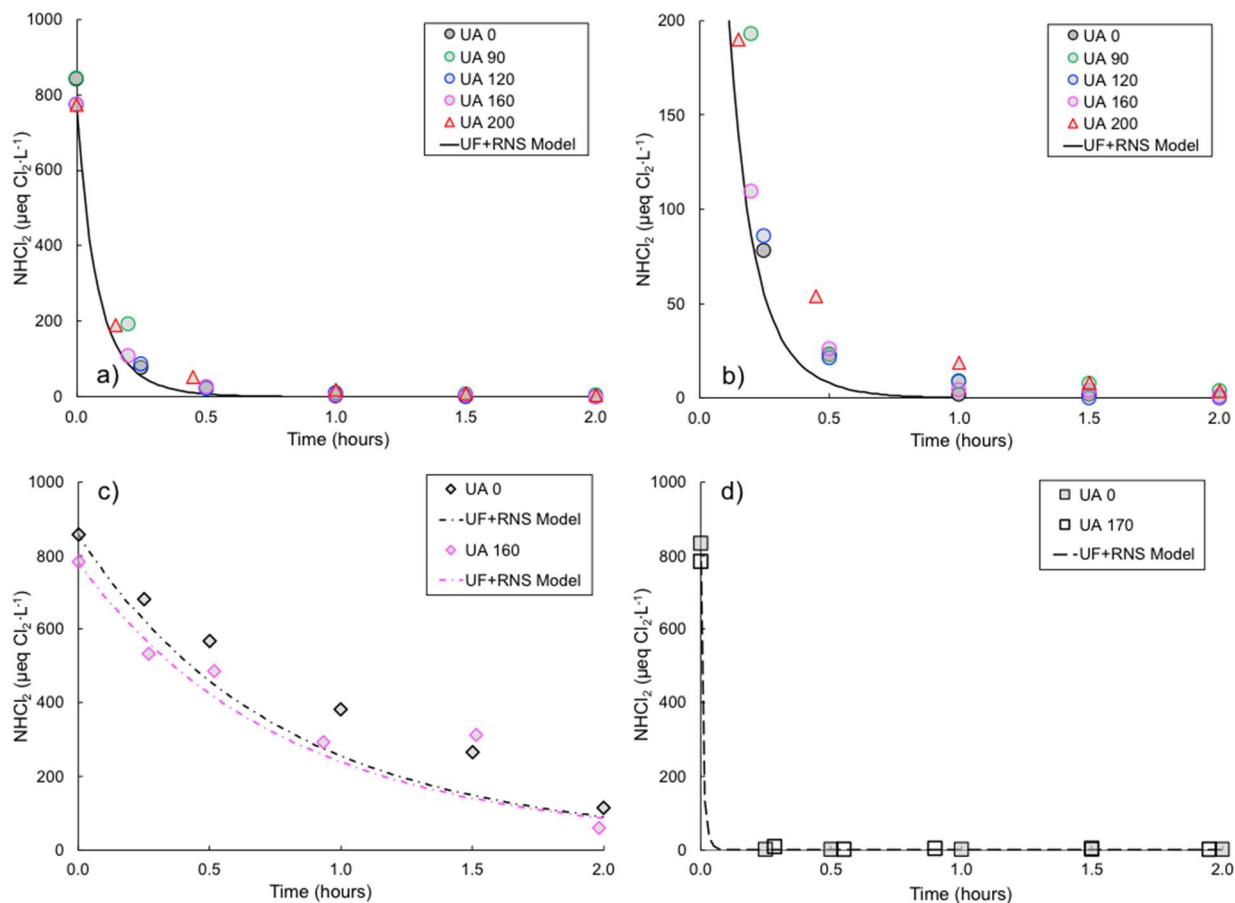
Figure s3-9. Impact of uric acid (UA) on $NHCl_2$ decomposition at (a) pH 9, (b) pH 9 with the y-axis between 0 and 200 μeq $Cl_2 \cdot L^{-1}$, (c) pH 8, and (d) pH 10. Legends indicate the UA dose in μM and UF+RNS model simulations.

S2.8 NDMA and DMNO Yields from NHCl₂ Decomposition.

Table s3-5. NDMA and DMNO yields after a four-hour reaction period with an initial ca. 800 μeq $Cl_2 \cdot L^{-1}$ NHCl₂ dose to 10 μM TOTDMA

pH	[a] TOTCO₃ (mM)	[b] NDMA (nM)	[b] DMNO (nM)	DMNO relative to NDMA (%)
7	2	197 ± 51	2.5 ± 0.9	1.3
8	2	$1,067 \pm 38$	9.4 ± 0.4	0.9
9	2	$3,602 \pm 128$	28 ± 2.9	0.8
10	10	$1,417 \pm 40$	15 ± 0.7	1.1
10	18	890 ± 91	10 ± 1.0	1.1
10	26	760 ± 69	8.7 ± 0.8	1.1
10	34	717 ± 92	8.2 ± 1.0	1.1
10	42	714 ± 82	7.7 ± 0.6	1.1

[a] TOTCO₃ is total carbonate

[b] Average ± standard deviation of quadruplicate measurements (n = 4)

S2.9 NO₂⁻ and NO₃⁻ Formation from NHCl₂ Decomposition.
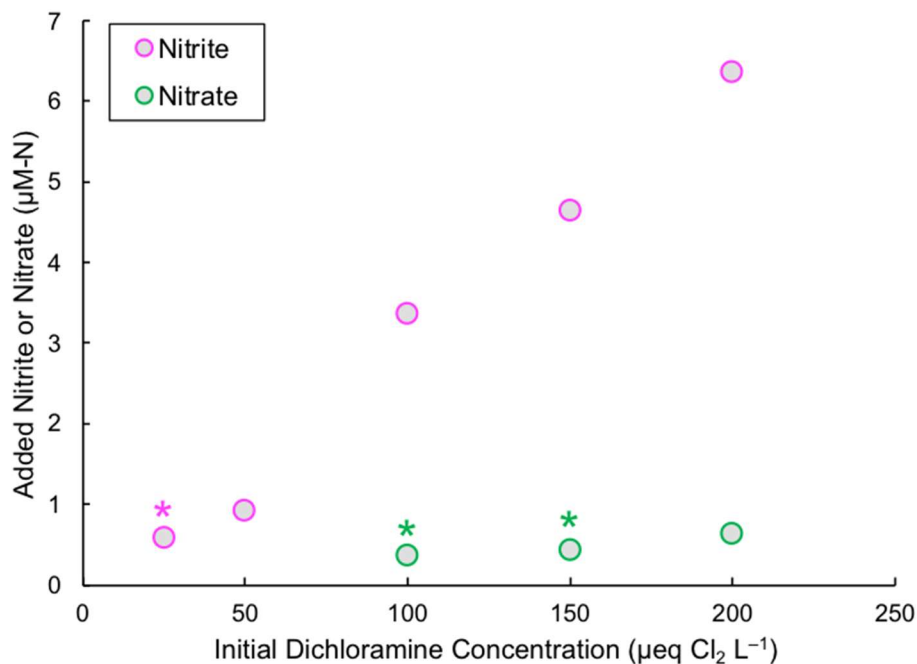
Figure s3-10. Added nitrite or nitrate concentration from quenching of the stated initial dichloramine (NHCl₂) concentration with thiosulfate. Based on these data, a threshold initial NHCl₂ concentration of 50 µeq Cl₂·L⁻¹ was established, which added a positive interference of about 1 µM-N NO₂⁻. The method detection limit (MDL) for NO₂⁻ was 0.9 µM-N and NO₃⁻ was 0.5 µM-N; an asterisk indicates the concentration was below the MDL, color coded to its respective analyte.

Table s3-6. Nitrite (NO₂⁻) and nitrate (NO₃⁻) yields from the decomposition of ca. 800 µeq Cl₂·L⁻¹ dichloramine (NHCl₂) and with and without 10 µM TOTDMA.

pH	No TOTDMA (µM)			10 µM TOTDMA (µM)		
	NO₂⁻	NO₃⁻	NO₂⁻ + NO₃⁻	NO₂⁻	NO₃⁻	NO₂⁻ + NO₃⁻
8	10 (38%)	16 (62%)	26	7.0 (39%)	11 (61%)	18
9	10 (43%)	14 (57%)	24	3.5 (36%)	6.2 (64%)	9.7
10	26 (63%)	15 (37%)	42	26 (73%)	10 (27%)	36

S2.10 DO Formation from NO_2^- Production.

We previously showed the measured DO profiles supported HNO/NO^- and $ONOOH/ONOO^-$ formation from $NHCl_2$ decomposition (Figure s3-8). As shown in Pathway B1, DO consumption can also serve as an estimate of $ONOOH/ONOO^-$ formation, but NO_2^- production must be taken into consideration. As shown in Scheme 1, each mole of NO_2^- produced from $ONOOH/ONOO^-$ decomposition produces one-half mole of DO. Therefore, to determine the total DO consumed after four hours ($\Delta DO_{4hr,TOT}$), the measured microelectrode DO consumptions ($\Delta DO_{4hr,M}$) were adjusted to account for the DO produced concomitantly with NO_2^- ($\Delta DO_{4hr,NO2-P}$, which equals one-half the molar nitrite formed, Table s3-7). Determination of $\Delta DO_{4hr,NO2-P}$ was not possible at pH 7 due to the presence of $NHCl_2$ in excess of 50 μeq $Cl_2 \cdot L^{-1}$ which interfered with the NO_2^- measurement as discussed previously.

Table s3-7 indicates $\Delta DO_{4hr,M}$ was pH-dependent. Without TOTDMA, $\Delta DO_{4hr,M}$ ranged from 12 μM (pH 7) to 64 μM (pH 9). After accounting for DO produced from NO_2^- formation which was only possible at pH 8-10, $\Delta DO_{4hr,TOT}$ ranged from 51-69 μM and was maximal at pH 9. Critically, DO consumption occurred at all pH levels in the absence of TOTDMA, supporting DO incorporation by a $NHCl_2$ decomposition product such as HNO/NO^- as shown in Pathway B1 to form $ONOOH/ONOO^-$. The addition of 10 μM TOTDMA increased $\Delta DO_{4hr,TOT}$ at pH 8, 9, and 10 by average values of 2, 16, and 37 μM, respectively. After correcting for the DO produced from NO_2^- (Table s3-6), $\Delta DO_{4hr,TOT}$ (Table s3-7) at pH 9 (82-84 μM) was less than that at pH 10 (94 μM). It is possible that DMA reacted with $ONOOH/ONOO^-$ decomposition products, resulting in additional DO consumption.

Table s3-7. DO consumption (µM) from four-hour $NHCl_2$ decomposition experiments (see Figure s3-8) with and without 10 µM TOTDMA

pH	No TOTDMA				10 µM TOTDMA				
	Control	$\Delta DO_{4hr,M}$	$\Delta DO_{4hr,NO2-P}$	$\Delta DO_{4hr,TOT}$	Test	$\Delta DO_{4hr,M}$	$\Delta DO_{4hr,NO2-P}$	$\Delta DO_{4hr,TOT}$	$\Delta DO_{4hr,A}$
7	1	12	NE	ND	1	12	NE	ND	ND
	2	20	NE	ND					
8	1	52	5	57	1	52	4	56	2
	2	46	5	51					
9	1	64	5	69	1	82	2	84	16
	2	61	5	66	2	80	2	82	
10	1	38	13	51	1	81	13	94	37
	2	51	13	64					
	3	44	13	57					

NE = not estimated because $NHCl_2$ interfered with measured nitrite (see discussion of Table s3-6 in text)

ND = not determined because $\Delta DO_{4hr,NO2-P}$ could not be estimated

$\Delta DO_{4hr,A}$ = average $\Delta DO_{4hr,TOT}$ increase due to the addition of 10 µM TOTDMA

$\Delta DO_{4hr,M}$ = microelectrode measured DO consumed after four hours

$\Delta DO_{4hr,NO2-P}$ = calculated DO released from measured NO_2^- produced after four hours (see Table s3-6 and Scheme 1)

$\Delta DO_{4hr,TOT}$ = total DO consumed after four hours, sum of $\Delta DO_{4hr,M}$ and $\Delta DO_{4hr,NO2-P}$

S2.11 UF+RNS Model Implementation.

Table s3-8 shows the simulated NO_2^- and NO_3^- formation at pH 7–10 with the UF+RNS model was within 0.1–3.5% of the plot-digitized data of Kirsch et al. (2003) validating the AQUASIM-based implementation of the Kirsch et al. (2003) model.

Table s3-8. Comparison of NO_2^- and NO_3^- (μM-N) from plot-digitized values from Figure 3-1 of Kirsch et al. (2003) compared to the UF+RNS model at discrete reaction times (minutes)

pH	Time	NO_2^-			NO_3^-		
		Kirsch	UF+RNS	[a] % Difference	Kirsch	UF+RNS	[a] % Difference
7	15	416	412	1.0	756	755	0.2
8	15	613	612	0.1	559	556	0.6
9	60	807	816	1.1	354	352	0.6
10	120	826	842	2.0	337	325	3.5

[a] absolute value of the percent difference between Kirsch et al. (2003) and the UF+RNS model

Table s3-9 summarizes the kinetic data used for parameter estimation in AQUASIM to update the reaction rate constants for U7 and U8 along with those for reactions associated with NDMA formation (P5, R7, and R8). The data includes (1) NH_2Cl and $NHCl_2$ data from (a) pH 7 and 8 experiments (see Figure s3-4a and b) measured with the DPD-FAS titration, (b) pH 9 and 10 experiments (see Figure s3-7c and d) measured with the Hach DPD and Indophenol methods, and (c) seven experiments from Jafvert (1985) shown in Figure s3-15 and Figure s3-16a-c used to ensure the revised rate constants did not adversely affect chloramine species simulations over periods of days, (2) DO data from pH 7-10 experiments trimmed to a temporal frequency of 4 minutes such that the number of DO observations was equal to that of NH_2Cl and $NHCl_2$ data combined, and (3) NDMA data from pH 7-10 experiments shown in Figure 3-1. N_2O data was excluded in parameter estimation (see Table s3-10) because N_2 was not measured and NO_2^- and NO_3^- were not able to be kinetically obtained (see SI S1.4).

Table s3-9. Weighted residual sum of squares (WRSS) and average weighted residual sum of squares (AWRSS) summary for experimental data used during UF+RNS model parameter estimation. WRSS and AWRSS are dimensionless. n represents the number of data points in each data set (total n = 528). The n listed may differ from those shown in the associated figure because zero value concentrations would result in an undefined WRSS and AWRSS.

pH	Species	n	WRSS	AWRSS	Location
This work, experiments with 10 μM TOTDMA					
7	DO	58	2.3×10^{-3}	4.0×10^{-5}	Figure 3-1a
7	NDMA	7	7.7×10^{-2}	1.1×10^{-2}	Figure 3-1a
8	DO	58	3.3×10^{-2}	5.8×10^{-4}	Figure 3-1b
8	NDMA	9	1.1×10^{-1}	1.2×10^{-2}	Figure 3-1b
9	NH$_2$Cl	10	1.0	1.0×10^{-1}	Figure s3-7c
9	NHCl$_2$	8	5.1	6.4×10^{-1}	Figure s3-7c
9	DO	58	1.0×10^{-1}	1.7×10^{-3}	Figure 3-1c
9	NDMA	9	1.4×10^{-1}	1.5×10^{-2}	Figure 3-1c
10	NH$_2$Cl	10	2.7	2.7×10^{-1}	Figure s3-7d
10	NHCl$_2$	5	4.0	8.0×10^{-1}	Figure s3-7d
10	DO	54	2.0×10^{-2}	3.7×10^{-4}	Figure 3-1d
10	NDMA	9	4.1×10^{-2}	4.6×10^{-3}	Figure 3-1d
This work, experiments without TOTDMA					
7	NH$_2$Cl	9	8.3×10^{-1}	9.2×10^{-2}	Figure s3-4a
7	NHCl$_2$	10	2.3×10^{-1}	2.3×10^{-2}	Figure s3-4a
8	NH$_2$Cl	8	1.4	1.8×10^{-1}	Figure s3-4b
8	NHCl$_2$	8	1.5	1.9×10^{-1}	Figure s3-4b
Jafvert(Jafvert, 1985)					
6.91	NH$_2$Cl	15	2.1×10^{-2}	1.4×10^{-3}	E16, Figure s3-15a
6.91	NHCl$_2$	15	1.5	1.0×10^{-1}	E16, Figure s3-15a
6.93	NH$_2$Cl	15	5.0×10^{-2}	3.3×10^{-3}	E17, Figure s3-15b
6.93	NHCl$_2$	15	1.1	7.2×10^{-2}	E17, Figure s3-15b
6.95	NH$_2$Cl	15	6.6×10^{-1}	4.4×10^{-2}	E18, Figure s3-15c
6.95	NHCl$_2$	15	7.9×10^{-1}	5.3×10^{-2}	E18, Figure s3-15c
7.43	NH$_2$Cl	15	7.4×10^{-2}	4.9×10^{-3}	E19, Figure s3-15d
7.43	NHCl$_2$	11	3.5	3.2×10^{-1}	E19, Figure s3-15d
7.47	NH$_2$Cl	15	1.0×10^{-2}	7.0×10^{-4}	E20, Figure s3-16a
7.47	NHCl$_2$	10	2.5	2.5×10^{-1}	E20, Figure s3-16a
7.46	NH$_2$Cl	15	4.7×10^{-2}	3.1×10^{-3}	E21, Figure s3-16b
7.46	NHCl$_2$	12	7.1	5.9×10^{-1}	E21, Figure s3-16b
6.46	NH$_2$Cl	15	2.1×10^{-1}	1.4×10^{-2}	E22, Figure s3-16c
6.46	NHCl$_2$	15	1.1	7.3×10^{-2}	E22, Figure s3-16c

Table s3-10. Weighted residual sum of squares (WRSS) and average weighted residual sum of squares (AWRSS) for UF+RNS model simulations compared to the nitrous oxide (N_2O) data. WRSS and AWRSS are dimensionless. n represents the number of data points in each data set. Note: number of data points listed here may differ from those shown in the associated figure because zero value concentrations would result in an undefined WRSS and AWRSS.

pH	n	WRSS	AWRSS	Location
7	125	124	9.9×10^{-1}	Figure 3-1a
8	228	155	6.8×10^{-1}	Figure 3-1b
9	240	128	5.3×10^{-1}	Figure 3-1c
10	240	5.5	2.3×10^{-2}	Figure 3-1d

Table s3-11. Values for k_{r7} for pH 7-10.

pH	k_{r7} (M^{-1} s^{-1})
7	2.1×10^7
8	2.0×10^7
9	1.4×10^7
10	2.6×10^5

S2.12 UF+RNS Model Well-Simulated NHCl₂, NH₂Cl, DO, and NDMA at pH 7-10.
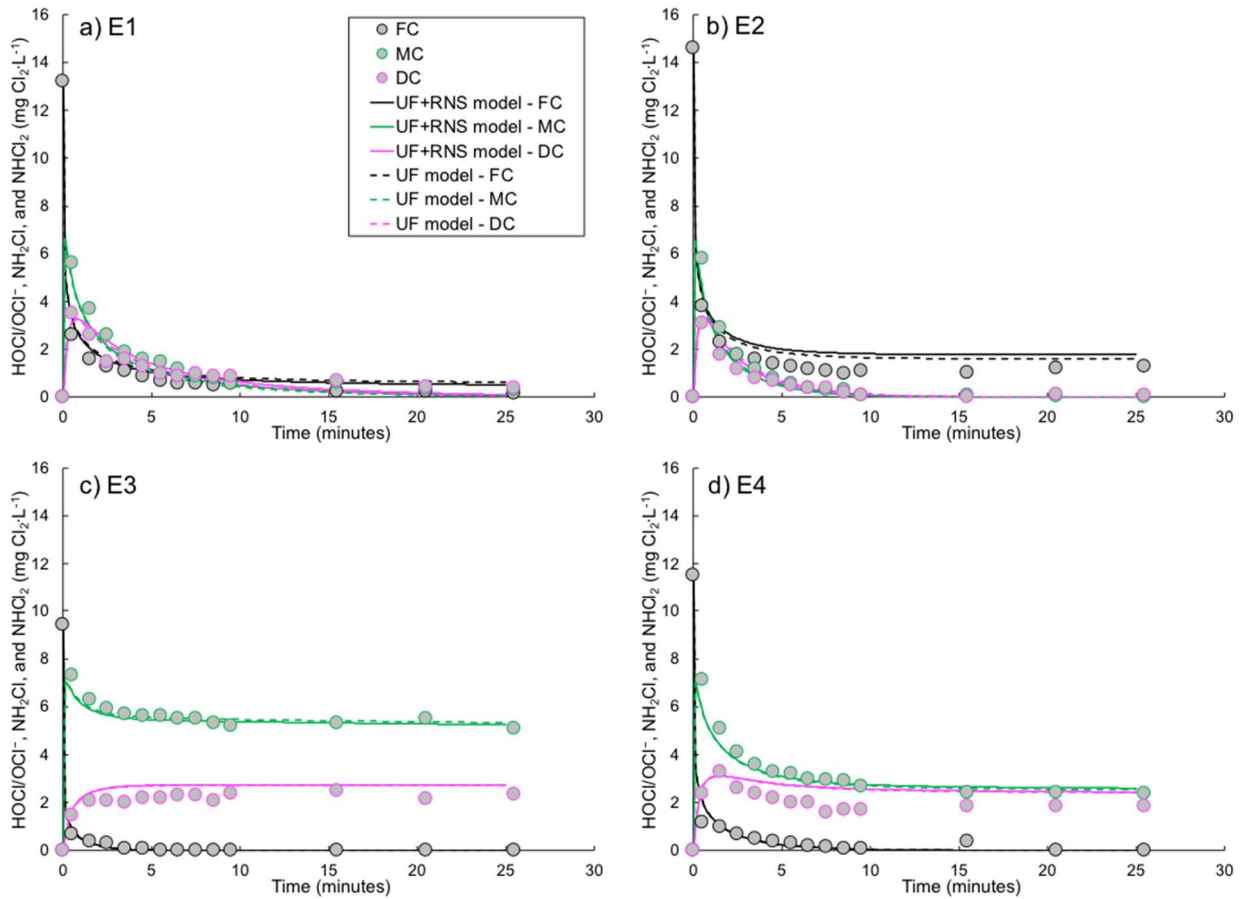
Figure s3-11. Free chlorine (FC, HOCl plus OCl⁻), monochloramine (MC, NH₂Cl), and dichloramine (DC, NHCl₂) time-course profiles from Jafvert (1985). Points are measured values, solid lines are UF+RNS model simulations, and dashed-lines are UF model simulations. E# - Experiment number from Jafvert (1985). Table s3-12 contains the weighted residual sum of squares (WRSS) and the corresponding average weighted residual sum of squares (AWRSS) for FC, NHCl₂, and NH₂Cl data sets resulting from simulations with the UF+RNS and UF models.
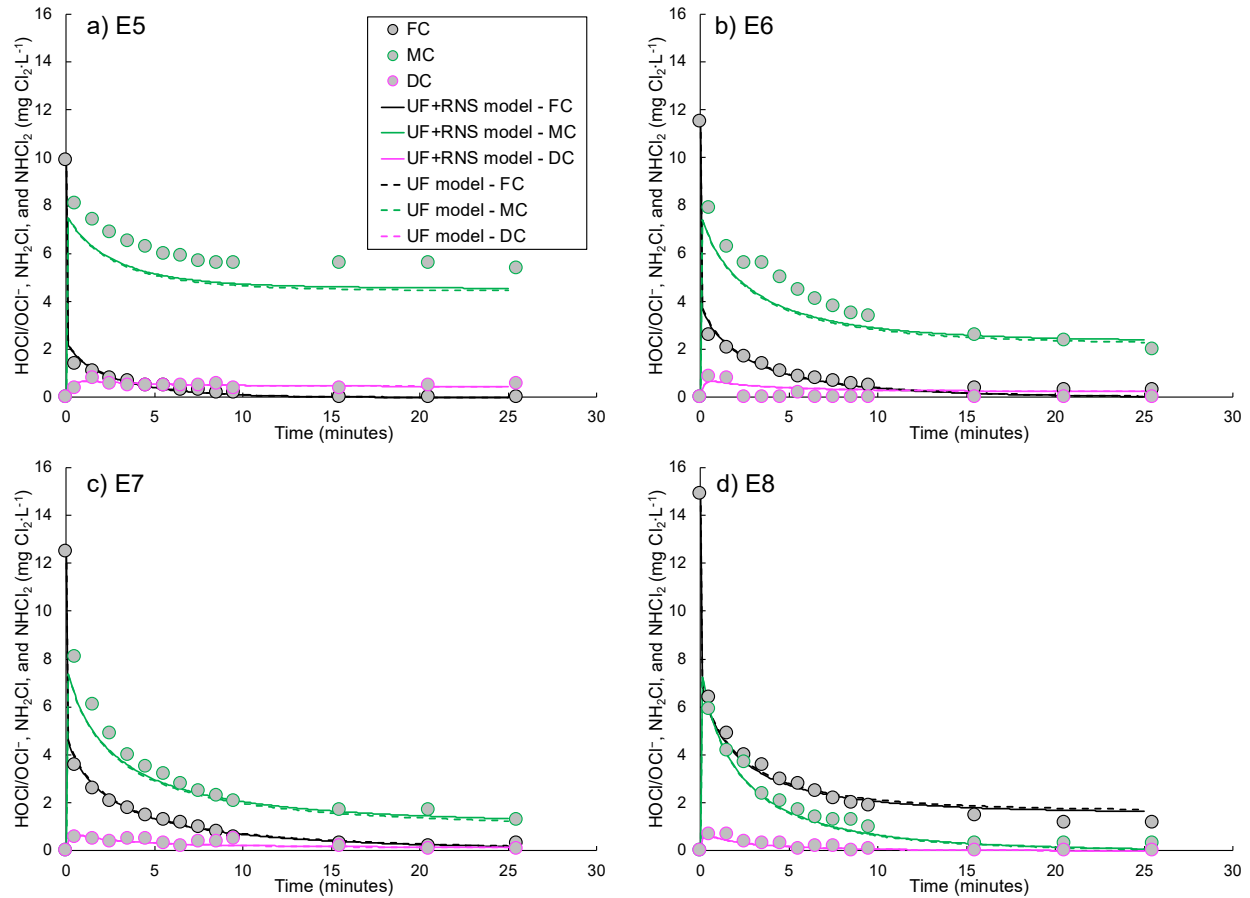
Figure s3-12. Free chlorine (FC, HOCl plus OCl⁻), monochloramine (MC, NH₂Cl), and dichloramine (DC, NHCl₂) time-course profiles from Jafvert (1985). Points are measured values, solid lines are UF+RNS model simulations, and dashed-lines are UF model simulations. E# - Experiment number from Jafvert (1985). Table s3-12 contains the weighted residual sum of squares (WRSS) and the corresponding average weighted residual sum of squares (AWRSS) for FC, NHCl₂, and NH₂Cl data sets resulting from simulations with the UF+RNS and UF models.
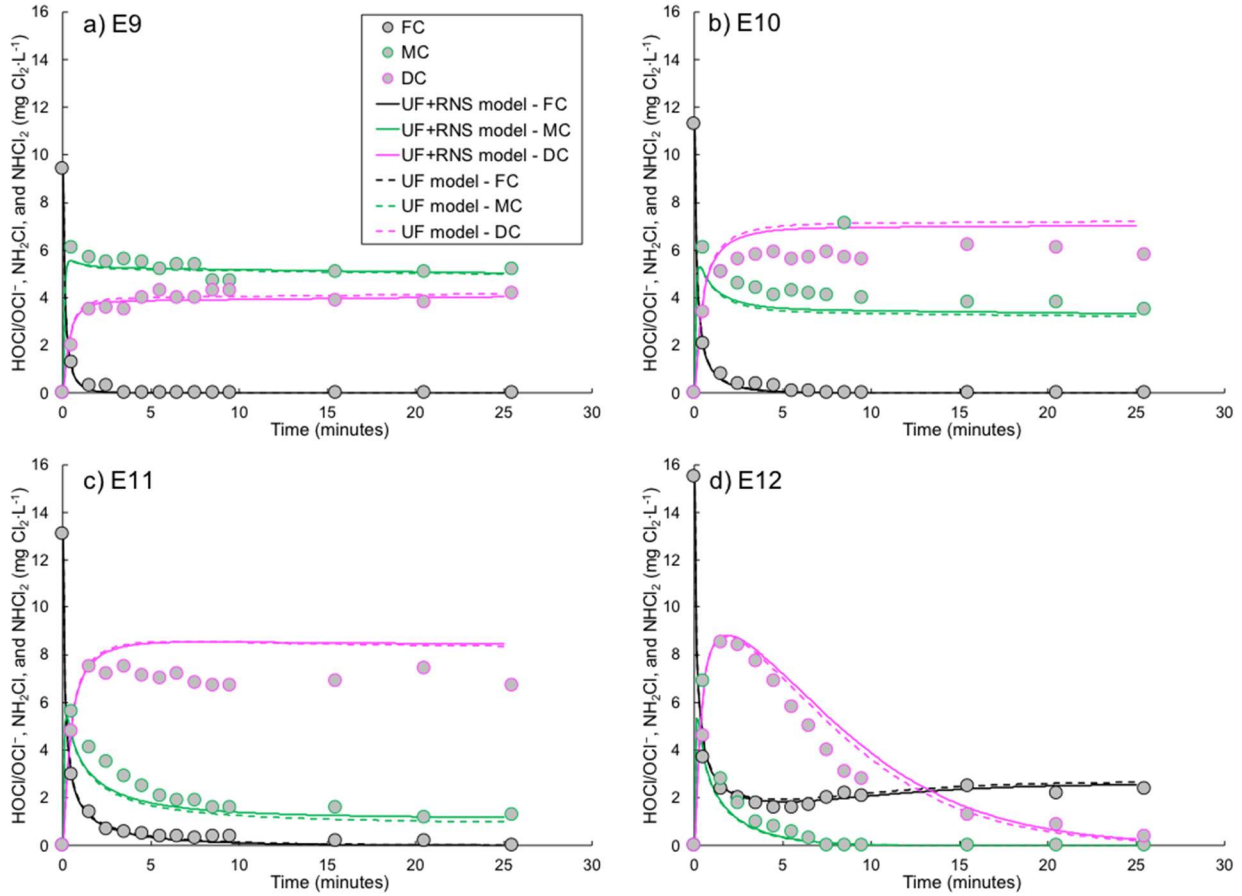
Figure s3-13. Free chlorine (FC, HOCl plus OCl⁻), monochloramine (MC, NH$_2$Cl), and dichloramine (DC, NHCl$_2$) time-course profiles from Jafvert (1985). Points are measured values, solid lines are UF+RNS model simulations, and dashed-lines are UF model simulations. E# - Experiment number from Jafvert (1985). Table s3-12 contains the weighted residual sum of squares (WRSS) and the corresponding average weighted residual sum of squares (AWRSS) for FC, NHCl$_2$, and NH$_2$Cl data sets resulting from simulations with the UF+RNS and UF models.
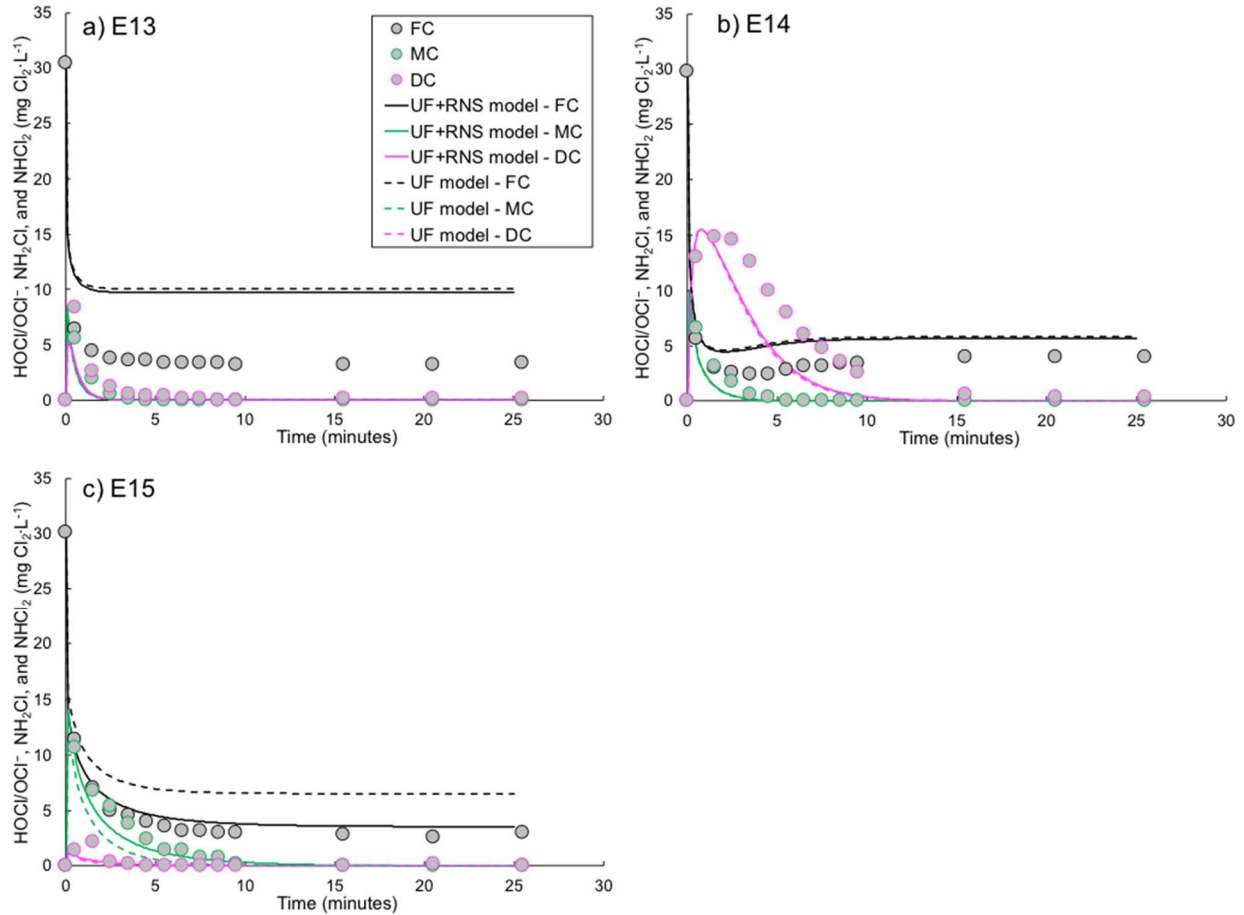
Figure s3-14. Free chlorine (FC, HOCl plus OCl$^-$), monochloramine (MC, NH$_2$Cl), and dichloramine (DC, NHCl$_2$) time-course profiles from Jafvert (1985). Points are measured values, solid lines are UF+RNS model simulations, and dashed-lines are UF model simulations. E# - Experiment number from Jafvert (1985). Table s3-12 contains the weighted residual sum of squares (WRSS) and the corresponding average weighted residual sum of squares (AWRSS) for FC, NHCl$_2$, and NH$_2$Cl data sets resulting from simulations with the UF+RNS and UF models.
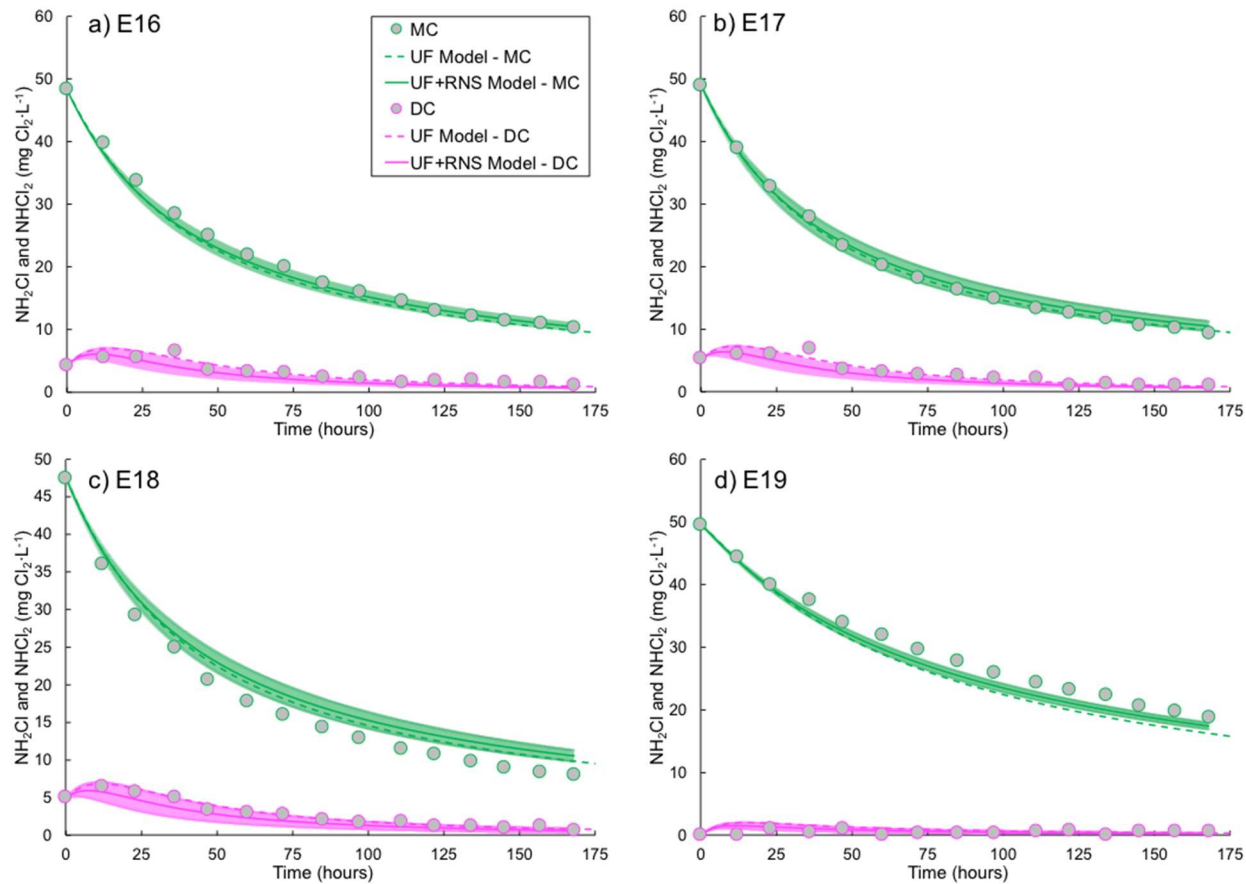
Figure s3-15. Monochloramine (MC, NH$_2$Cl) and dichloramine (DC, NHCl$_2$) time-course profiles from Jafvert (1985). Points are measured values, solid lines are UF+RNS model simulations, dashed-lines are UF model simulations, and shaded areas are UF+RNS simulations encompassing one standard error in the estimated parameters (see Table 3-1). Experiment number from Jafvert (1985). Table s3-9 contains the weighted residual sum of squares (WRSS) and the corresponding average weighted residual sum of squares (AWRSS) for the NHCl$_2$ and NH$_2$Cl data sets used in parameter estimation for the UF+RNS model. Table s3-12 contains the WRSS and AWRSS for simulations with the UF+RNS and UF models.
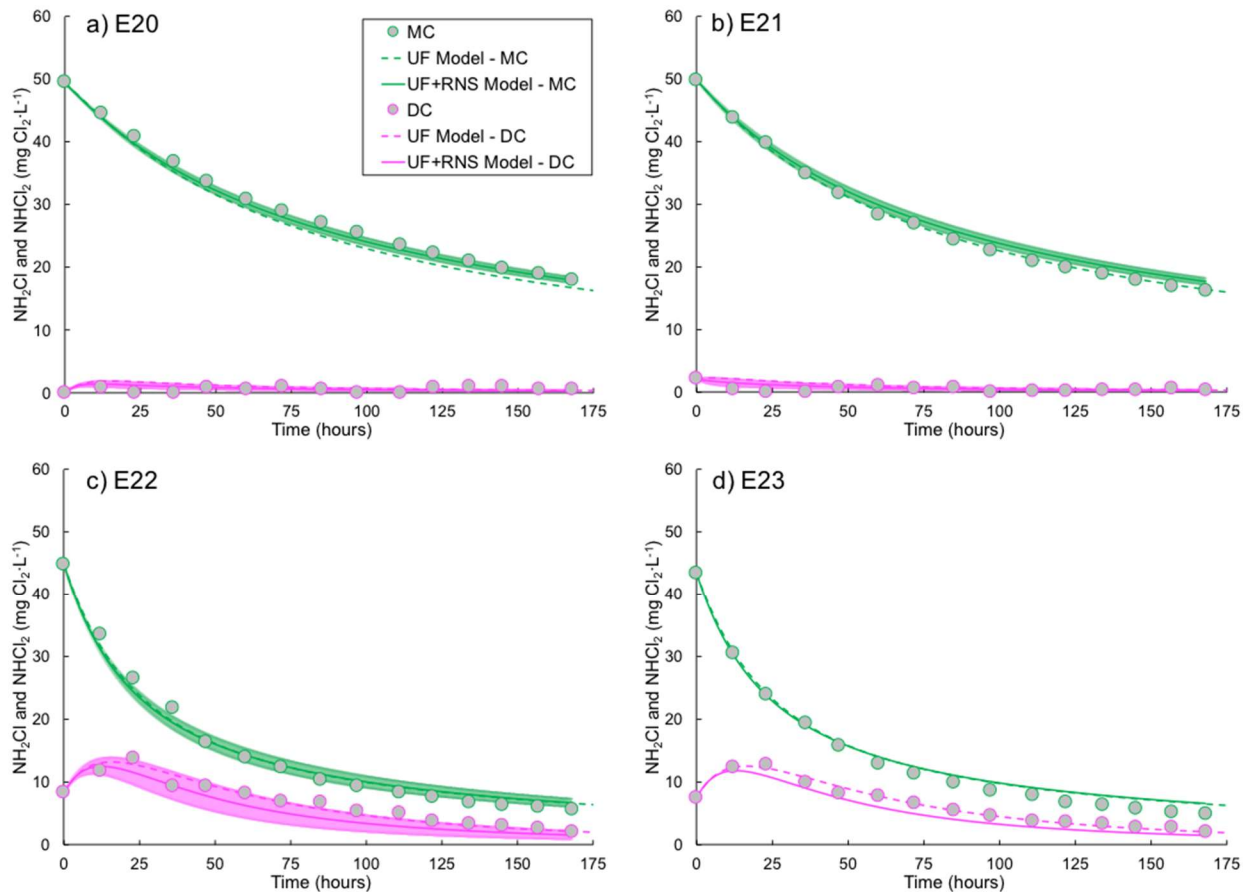
Figure s3-16. Monochloramine (MC, NH_2Cl) and dichloramine (DC, $NHCl_2$) time-course profiles from Jafvert (1985). Points are measured values, solid lines are UF+RNS model simulations, and dashed-lines are UF model simulations. For panels a-c, shaded areas are UF+RNS simulations encompassing one standard error in the estimated parameters (see Table 3-1). Experiment number from Jafvert (1985) For panels a-c, Table s3-9 contains the weighted residual sum of squares (WRSS) and the corresponding average weighted residual sum of squares (AWRSS) for the $NHCl_2$ and NH_2Cl data sets used in parameter estimation for the UF+RNS model. Table s3-12 contains the WRSS and AWRSS for simulations with the UF+RNS and UF models.
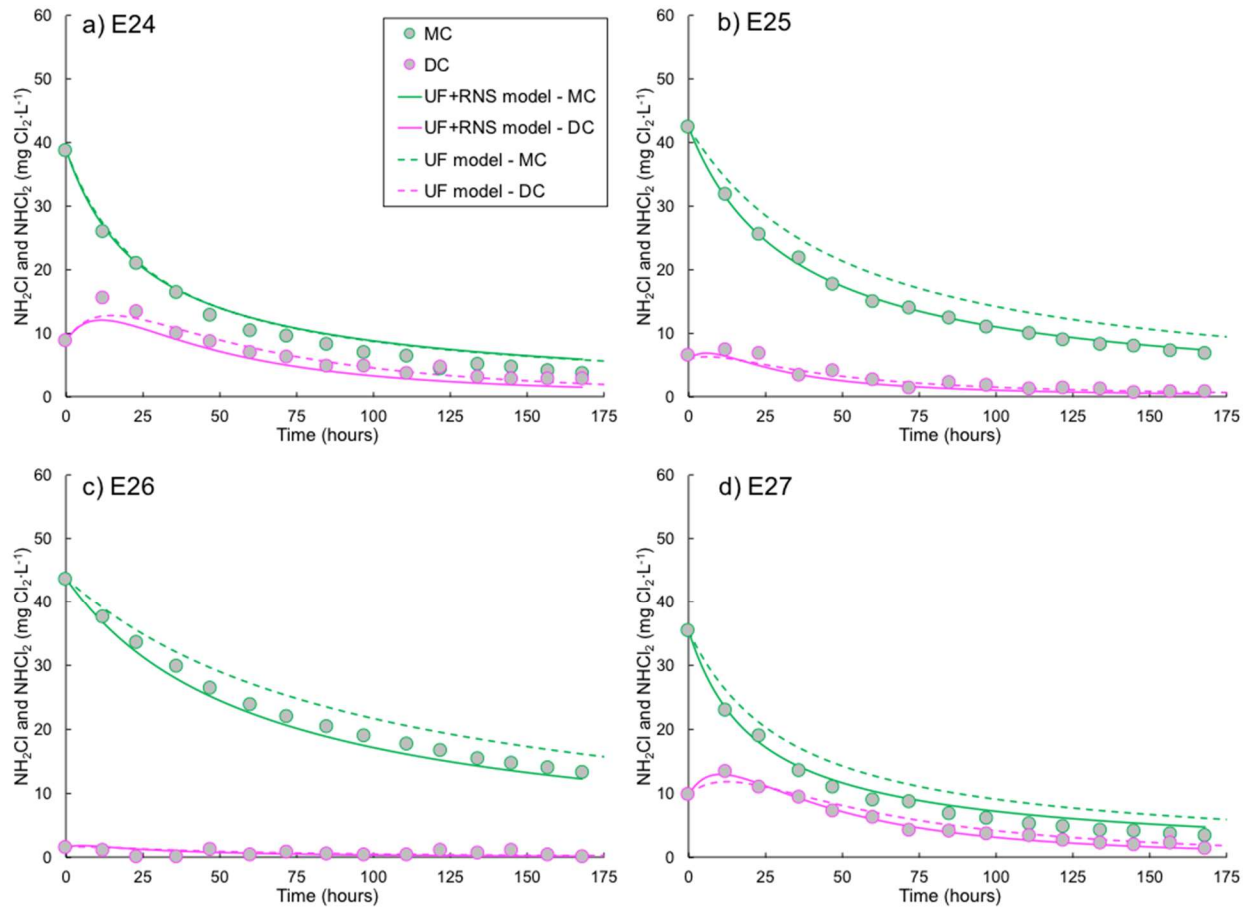
Figure s3-17. Monochloramine (MC, NH_2Cl) and dichloramine (DC, $NHCl_2$) time-course profiles from Jafvert (1985). Points are measured values, solid lines are UF+RNS model simulations, and dashed-lines are UF model simulations. Experiment number from Jafvert (1985). Table s3-12 contains the weighted residual sum of squares (WRSS) and the corresponding average weighted residual sum of squares (AWRSS) for $NHCl_2$ and NH_2Cl data sets resulting from simulations with the UF+RNS and UF models.

Table s3-12. Weighted residual sum of squares (WRSS) and average weighted residual sum of squares (AWRSS) for UF+RNS and UF model simulations compared to Jafvert(Jafvert, 1985) data for free chlorine, monochloramine (NH_2Cl) and dichloramine ($NHCl_2$) (Exp. 1-27) and data shown in Figs. s4a and b and s7c and d. WRSS and AWRSS are dimensionless. Data points may differ from associated figure because zero value concentrations result in undefined WRSS and AWRSS.

| [a] Exp.	UF+RNS Model						UF Model						[b] L
	Free Chlorine		NH_2Cl		$NHCl_2$		Free Chlorine		NH_2Cl		$NHCl_2$		
	WRSS	AWRSS	WRSS	AWRSS	WRSS	AWRSS	WRSS	AWRSS	WRSS	AWRSS	WRSS	AWRSS	
1	6.5	5.0×10^{-1}	7.2×10^{-1}	6.0×10^{-2}	1.6	1.3×10^{-1}	9.2	7.1×10^{-1}	1.7	1.4×10^{-1}	1.5	1.2×10^{-1}	s3-11a
2	4.1	3.1×10^{-1}	1.9	1.6×10^{-1}	2.6	2.4×10^{-1}	2.3	1.8×10^{-1}	2.0	1.7×10^{-1}	2.0	1.8×10^{-1}	s3-11b
3	6.2×10^{-1}	1.0×10^{-1}	1.5×10^{-2}	1.2×10^{-3}	5.5×10^{-1}	4.6×10^{-2}	9.4×10^{-1}	1.6×10^{-1}	1.6×10^{-2}	1.4×10^{-3}	5.7×10^{-1}	4.8×10^{-2}	s3-11c
4	1.8	1.5×10^{-1}	5.3×10^{-2}	4.4×10^{-3}	1.7	1.4×10^{-1}	1.8	1.5×10^{-1}	8.5×10^{-2}	7.1×10^{-3}	1.5	1.3×10^{-1}	s3-11d
5	3.0×10^{-1}	2.7×10^{-2}	2.5×10^{-1}	2.1×10^{-2}	4.0×10^{-1}	3.4×10^{-2}	4.4×10^{-1}	4.0×10^{-2}	3.3×10^{-1}	2.8×10^{-2}	4.6×10^{-1}	3.8×10^{-2}	s3-12a
6	7.8×10^{-1}	6.0×10^{-2}	2.3×10^{-1}	1.9×10^{-2}	1.2	4.0×10^{-1}	8.7×10^{-1}	6.7×10^{-2}	3.7×10^{-1}	3.1×10^{-2}	9.8×10^{-1}	3.3×10^{-1}	s3-12b
7	5.8×10^{-1}	4.5×10^{-2}	9.2×10^{-2}	7.6×10^{-3}	1.3	1.1×10^{-1}	4.4×10^{-1}	3.4×10^{-2}	2.1×10^{-1}	1.8×10^{-2}	1.2	1.0×10^{-1}	s3-12c
8	2.9×10^{-1}	2.2×10^{-2}	3.1×10^{-1}	2.5×10^{-2}	1.0	1.2×10^{-1}	3.6×10^{-1}	2.8×10^{-2}	7.5×10^{-1}	6.2×10^{-2}	1.1	1.2×10^{-1}	s3-12d
9	7.3×10^{-1}	1.8×10^{-1}	4.3×10^{-2}	3.6×10^{-3}	7.9×10^{-2}	6.6×10^{-3}	9.2×10^{-1}	2.3×10^{-1}	4.4×10^{-2}	3.7×10^{-3}	1.8×10^{-1}	1.5×10^{-2}	s3-13a
10	1.4	1.7×10^{-1}	4.8×10^{-1}	4.0×10^{-2}	3.5×10^{-1}	2.9×10^{-2}	1.8	2.2×10^{-1}	6.0×10^{-1}	5.0×10^{-2}	5.3×10^{-1}	4.4×10^{-2}	s3-13b
11	2.1	1.6×10^{-1}	3.3×10^{-1}	2.7×10^{-2}	4.2×10^{-1}	3.5×10^{-2}	1.9	1.4×10^{-1}	7.3×10^{-1}	6.1×10^{-2}	4.4×10^{-1}	3.7×10^{-2}	s3-13c
12	2.4×10^{-1}	1.9×10^{-2}	5.5×10^{-1}	7.8×10^{-2}	1.8	1.5×10^{-1}	2.3×10^{-1}	1.8×10^{-2}	1.3	1.9×10^{-1}	8.5×10^{-1}	7.1×10^{-2}	s3-13d
13	$3.7\times10^{+1}$	2.9	2.0	5.0×10^{-1}	8.4	8.4×10^{-1}	$4.1\times10^{+1}$	3.1	2.6	6.5×10^{-1}	8.8	8.8×10^{-1}	s3-14a
14	5.5	4.2×10^{-1}	1.5	2.9×10^{-1}	3.8	3.2×10^{-1}	6.7	5.2×10^{-1}	2.3	4.5×10^{-1}	5.2	4.3×10^{-1}	s3-14b
15	8.7×10^{-1}	6.7×10^{-2}	2.5	2.5×10^{-1}	1.7	3.3×10^{-1}	$1.2\times10^{+1}$	8.9×10^{-1}	4.4	4.4×10^{-1}	2.3	4.5×10^{-1}	s3-14c
23			5.1×10^{-1}	3.4×10^{-2}	9.2×10^{-1}	6.1			4.6×10^{-1}	3.1×10^{-2}	7.5×10^{-2}	5.0×10^{-3}	s3-16d
24			1.9	1.3×10^{-1}	1.0	7.0			1.8	1.2×10^{-1}	2.5×10^{-1}	1.7×10^{-2}	s3-17a
25			3.1×10^{-2}	2.1×10^{-3}	1.3	8.6			1.4	9.0×10^{-2}	9.5×10^{-1}	6.4×10^{-2}	s3-17b
26			6.5×10^{-2}	4.4×10^{-3}	2.7	2.2×10^{-1}			3.5×10^{-1}	2.3×10^{-2}	2.8	2.3×10^{-1}	s3-17c
27			9.7×10^{-1}	6.1×10^{-2}	2.0×10^{-1}	1.3			4.3	2.9×10^{-1}	7.9×10^{-1}	5.2×10^{-2}	s3-17d

Note: Table s3-12 is continued on the following page.

113

Table s3-12, continued.

| | UF+RNS Model | | | | | | | UF Model | | | | | | |
| | Free Chlorine | | NH$_2$Cl | | NHCl$_2$ | | | Free Chlorine | | NH$_2$Cl | | NHCl$_2$ | | |
[a] Exp.	WRSS	AWRSS	WRSS	AWRSS	WRSS	AWRSS		WRSS	AWRSS	WRSS	AWRSS	WRSS	AWRSS	[b] L
16			2.1×10^{-2}	1.4×10^{-3}	1.5	1.0×10^{-1}				4.8×10^{-2}	3.2×10^{-3}	5.9×10^{-1}	3.9×10^{-2}	s3-15a
17			5.0×10^{-2}	3.3×10^{-3}	1.1	7.2×10^{-2}				6.8×10^{-3}	4.5×10^{-4}	5.0×10^{-1}	3.3×10^{-2}	s3-15b
18			6.6×10^{-1}	4.4×10^{-2}	7.9×10^{-1}	5.3×10^{-2}				3.7×10^{-1}	2.5×10^{-2}	3.4×10^{-1}	2.3×10^{-2}	s3-15c
19			7.4×10^{-2}	4.9×10^{-3}	3.5	3.2×10^{-1}				1.7×10^{-1}	1.2×10^{-2}	$1.1\times10^{+1}$	9.7×10^{-1}	s3-15d
20			1.0×10^{-2}	7.0×10^{-4}	2.5	2.5×10^{-1}				6.1×10^{-2}	4.0×10^{-3}	3.6	3.6×10^{-1}	s3-16a
21			4.7×10^{-2}	3.1×10^{-3}	7.1	5.9×10^{-1}				1.6×10^{-3}	1.1×10^{-4}	$1.9\times10^{+1}$	1.6	s3-16b
22			2.1×10^{-1}	1.4×10^{-2}	1.1	7.3×10^{-2}				1.8×10^{-1}	1.2×10^{-2}	1.6×10^{-1}	1.1×10^{-2}	s3-16c
pH 7			8.3×10^{-1}	9.2×10^{-2}	2.3×10^{-1}	2.3×10^{-2}				1.9	2.1×10^{-1}	4.2×10^{-2}	4.2×10^{-3}	s3-4a
pH 8			1.4	1.8×10^{-1}	1.5	1.9×10^{-1}				1.4	1.7×10^{-1}	8.6×10^{-2}	1.1×10^{-2}	s3-4b
pH 9			1.0	1.0×10^{-1}	5.1	6.4×10^{-1}				1.2	1.2×10^{-1}	4.4	5.4×10^{-1}	s3-7c
pH 10			2.7	2.7×10^{-1}	4.0	8.0×10^{-1}				2.4	2.4×10^{-1}	4.0	8.0×10^{-1}	s3-7d
[c] $\sum$Exp	63.0	5.1	14.3	1.7	33.0	3.4		80.4	6.5	25.6	2.8	32.5	3.4	
[d] $\sum$Exp	63.0	5.1	21.4	2.4	61.4	6.5		80.4	6.5	33.3	3.6	75.5	7.7	

[a] Experiment number corresponding to the data and model simulations shown in Figure s3-11-s3-17 from Jafvert (1985) or pH 7-10 from the current study (Figures s3-4a and b and s3-7c and d)

[b] Location of corresponding figure

[c] Sum of WRSS or AWRSS for Experiments 1 through 15 and 23 through 27 from Jafvert (1985) (these data sets were not used during parameter estimation)

[d] Sum of WRSS or AWRSS for Experiments 1 through 27 from Jafvert (1985) and pH 7-10 from the current study

Yellow-highlighted values were also shown in Table s9 and shown here for comparison purposes to the UF model

3.8-S2.13 Current UF+RNS Model Limitations and Future Research Needs

Table s3-13. Nitrogen mass balance for the batch kinetic experiments at pH 8, 9, and 10[a]

	pH 8			pH 9			pH 10		
	Concentration (μM N)		[c] Percent of Total Nitrogen	Concentration (μM N)		[c] Percent of Total Nitrogen	Concentration (μM N)		[c] Percent of Total Nitrogen
Species	[b] Simulated	Measured		[b] Simulated	Measured		[b] Simulated	Measured	
Batch Experiment Concentrations at Time Zero									
$NHCl_2$	429	429	47	420	420	46	416	416	47
$NH_3 + NH_4^+$	491	NM	53	490	NM	54	478	NM	53
[d] Total Nitrogen	920		100	910		100	894		100
End of Batch Experiment Concentrations at 4 hours									
$NHCl_2$	8.9	NM	1.0	0	NM	0	0	NM	0
NH_2Cl	152.1	NM	16.5	147.5	NM	16.2	127.2	NM	14.2
N_2O	0.3	12.6	1.4	2.8	25.4	2.8	17.4	14.5	1.6
NO_2^-	1.4	9.8	1.1	12.9	10.2	1.1	54.5	26.1	2.9
NO_3^-	66.9	16.2	1.8	62.8	13.7	1.5	55.4	15.4	1.7
$NH_3 + NH_4^+$	323.1	NM	35.1	327.7	NM	36.0	341.6	NM	38.2
[e] N_2	363.2		43.2	352.4		42.4	284.4		41.3

[a] Mass balance at pH 7 was not possible because $NHCl_2$-based interference with measurements of NO_2^- and NO_3^- at 4 hours – see text

[b] Simulated concentrations with UF+RNS model

[c] Percent of total nitrogen was calculated as follows:
- Time Zero: yellow shaded values were divided by the total nitrogen concentration for each pH level
- Time 4 hours: grey shaded values divided by the total nitrogen concentration for each pH level

[d] Total nitrogen was calculated using the time zero values for $NHCl_2$ and $NH_3 + NH_4^+$ with yellow shading for each pH level

[e] Nitrogen gas concentrations at 4 hours were calculated by difference to complete the total nitrogen mass balance at 4 hours for each pH level

NM – Not Measured

References Cited in the Supporting Information

CRC Handbook of Chemistry and Physics, Taylor & Francis, (2010-2011).

Eaton, A. D., Clesceri, L. S., Greenberg, A. E. and Franson, M. A. H. *Standard methods for the examination of water and wastewater*, American Public Health Association, Washington, DC, (1998).

Ferrer-Sueta, G. and Radi, R., *ACS Chemical Biology*, **4**, 161-177 (2009). 10.1021/cb800279q.

Hach Company (2015). Methos 10171, Chloramine (Mono). Indophenol Method, 0.04 to 4.50 mg Cl_2/L (LR), Hach Company: Loveland, Colorado.

Hand, V. C. and Margerum, D. W., *Inorganic Chemistry*, **22**, 1449-1456 (1983). Doi 10.1021/Ic00152a007.

Hinman, R. L., *Journal of Organic Chemistry*, **23**, 1587-1588 (1958). 10.1021/jo01104a629.

Hooper, D. C., Scott, G. S., Zborek, A., Mikheeva, T., Kean, R. B., Koprowski, H. and Spitsin, S. V., *The FASEB Journal*, **14**, 691-698 (2000). https://doi.org/10.1096/fasebj.14.5.691.

Hooper, D. C., Spitsin, S., Kean, R. B., Champion, J. M., Dickson, G. M., Chaudhry, I. and Koprowski, H., *Proceedings of the National Academy of Sciences of the United States of America*, **95**, 675-680 (1998). 10.1073/pnas.95.2.675.

Imaram, W., Gersch, C., Kim, K. M., Johnson, R. J., Henderson, G. N. and Angerhofer, A., *Free Radical Biology and Medicine*, **49**, 275-281 (2010). 10.1016/j.freeradbiomed.2010.04.010.

Jafvert, C. T. (1985). A Unified Chlorine-Ammonia Speciation and Fate Model. PhD, PhD Dissertation, University of Iowa,

Jafvert, C. T. and Valentine, R. L., *Water Research*, **21**, 967-973 (1987).

Jafvert, C. T. and Valentine, R. L., *Environ Sci Technol*, **26**, 577-586 (1992). Doi 10.1021/Es00027a022.

Kean, R. B., Spitsin, S. V., Mikheeva, T., Scott, G. S. and Hooper, D. C., *The Journal of Immunology*, **165**, 6511 (2000). 10.4049/jimmunol.165.11.6511.

Kirsch, M., Korth, H. G., Wensing, A., Sustmann, R. and de Groot, H., *Archives of Biochemistry and Biophysics*, **418**, 133-150 (2003). 10.1016/j.abb.2003.07.002.

Leao, S. F. (1981). Kinetics of Combined Chlorine: Reaction of Substitution and Redox. Ph.D. Dissertation, University of California, Berkeley,

Lymar, S. V. and Shafirovich, V., *Journal of Physical Chemistry B*, **111**, 6861-6867 (2007). 10.1021/jp070959+.

Margerum, D. W., Gray, E. T. and Jr.; Huffman, R. P., F. E. Brinckman and J. M. Bellama. *Organometals and Organometalloids; Occurrence and Fate in the Environment;*. American Chemical Society. Washington, DC**:** 278-291 (1978).

Morris, J. C. and Isaac, R. A. *Water Chlorination Enviromental Impact and Health Effects*, Ann Arbor Science Publishers, Ann Arbor, (1983).

Nimse, S. B. and Pal, D., *RSC Advances*, **5**, 27986-28006 (2015). 10.1039/C4RA13315C.

Rao, P. S., Luber, J. M., Milinowicz, J., Lalezari, P. and Mueller, H. S., *Biochemical and Biophysical Research Communications*, **150**, 39-44 (1988). 10.1016/0006-291x(88)90483-4.

Reichert, P., *Water Science and Technology*, **30**, 21-30 (1994).

Schreiber, I. M. and Mitch, W. A., *Environmental Science & Technology*, **39**, 3811-3818 (2005). 10.1021/es0483286.

Schreiber, I. M. and Mitch, W. A., *Environmental Science & Technology*, **40**, 6007-6014 (2006). 10.1021/es060978h.

Shafirovich, V. and Lymar, S. V., *Proceedings of the National Academy of Sciences of the United States of America*, **99**, 7340-7345 (2002). 10.1073/pnas.112202099.

Simic, M. G. and Jovanovic, S. V., *Journal of the American Chemical Society*, **111**, 5778-5782 (1989). 10.1021/ja00197a042.

Smulik, R., Debski, D., Zielonka, J., Michalowski, B., Adamus, J., Marcinek, A., Kalyanaraman, B. and Sikora, A., *Journal of Biological Chemistry*, **289**, 35570-35581 (2014). 10.1074/jbc.M114.597740.

Snoeyink, V. L. and Jenkins, D. *Water Chemistry*, John, Wiley & Sons, Inc.,, (1980).

Squadrito, G. L., Cueto, R., Splenser, A. E., Valavanidis, A., Zhang, H., Uppu, R. M. and Pryor, W. A., *Archives of Biochemistry and Biophysics*, **376**, 333-337 (2000). https://doi.org/10.1006/abbi.2000.1721.

Stinefelt, B., Leonard, S. S., Blemings, K. P., Shi, X. and Klandorf, H., *Annals of Clinical & Laboratory Science*, **35**, 37-45 (2005).

Valentine, R. L., Jafvert, C. T. and Leung, S. W., *Water Research*, **22**, 1147-1153 (1988).

Vonpiechowski, M., Thelen, M. A., Hoigne, J. and Buhler, R. E., *Berichte Der Bunsen-Gesellschaft-Physical Chemistry Chemical Physics*, **96**, 1448-1454 (1992).

Chapter 4

Effect of Dissolved Oxygen and Dimethylamine on Dichloramine Decomposition Products:

Evidence of Additional Reaction Pathways Revealed by Nitrogen Mass Balances

Abstract

Nitroxyl (HNO) was recently shown to be the long-standing unidentified intermediate formed by dichloramine ($NHCl_2$) hydrolysis. This prior work revealed that HNO and nitroxyl anion (NO^-) subsequently reacted with dissolved oxygen (DO) to form peroxynitrous acid/peroxynitrite anion ($ONOOH/ONOO^-$), which in the presence of total dimethylamine (TOTDMA), reacted to form *N*-nitrosodimethylamine (NDMA). Here, the role of DO in this reaction scheme was examined at pH 9 by assessing kinetic profiles of $NHCl_2$ and NDMA and nitrogen mass balances under ambient DO (~280 μM) and low-DO (< 20 μM) conditions in the presence and absence of 10 μM TOTDMA. Uric acid, an $ONOOH/ONOO^-$ scavenger, completely shut down NDMA formation under the low-DO condition, validating $ONOOH/ONOO^-$ as the central node in NDMA formation. Yield experiments with initial $NHCl_2$ of 200-, 400-, and 800 μeq $Cl_2 \cdot L^{-1}$ tracked the formation of NH_3/NH_4^+, NH_2Cl, N_2O, N_2, NO_2^-, and NO_3^-. NH_3/NH_4^+ yields were 20–40% greater under the low-DO condition, implying a reaction occurred between NH_3/NH_4^+ and $ONOOH/ONOO^-$ or its decomposition products. NH_2Cl yields were 16–20% lower under the low-DO condition, revealing a previously unknown NH_2Cl formation reaction. Under ambient DO conditions, about 80% of the nitrogen was accounted for compared to the low-DO conditions in which nitrogen recoveries were 90- and 100% in the absence and presence of 10 μM TOTDMA, respectively. An existing mechanistic model accurately predicted NH_3/NH_4^+, NH_2Cl, and N_2 under ambient conditions but underpredicted N_2O and overpredicted NO_2^- and NO_3^-. The results provide a framework to guide future experiments with $ONOOH/ONOO^-$ generators and revise the mechanistic model to better capture the nitrogenous end-products.

4.1-Introduction

Chloramines are commonly used drinking water disinfectants in the United States (Cornwell Engineering Group., 2018). Chloramines generally have lower reactivity compared with free chlorine, allowing drinking water distribution system residuals to be more easily maintained while forming fewer regulated disinfection byproducts (Ratnayaka et al., 2009). Several reaction schemes have been proposed to capture the fate of free chlorine and chloramine species under various drinking water conditions (Wei, 1972; Leao, 1981; Jafvert and Valentine, 1987). The unified (UF) model of chloramine chemistry developed by Jafvert and Valentine (1992) has been validated experimentally and captures chloramine speciation and stability under typical drinking water conditions. The fourteen reactions in the UF model shown in Table s3-1 can be divided into four subparts, which include (1) hypochlorous acid (HOCl) reacting with ammonia (NH_3) to form monochloramine (NH_2Cl, U1) and its corresponding hydrolysis reaction (U2), and HOCl reacting with NH_2Cl to form dichloramine ($NHCl_2$, U3) and its corresponding hydrolysis reaction (U4), (2) NH_2Cl disproportionation to form $NHCl_2$ (U5) and its reverse reaction (U6), (3) redox reactions that occur in the absence of HOCl (U7–U10), and (4) redox reactions that occur when HOCl is present at Cl_2:N ratios near the breakpoint or greater (U11–U14).(Saunier, 1976) Despite the proven utility of the UF model for capturing chloramine speciation and decay, U7–U10 have not been experimentally validated due to, at least in part, the long-standing unidentified intermediate, *I*, that forms by $NHCl_2$ decomposition (U7). The UF model can predict the fate of chloramine species but does not provide any information about other potential nitrogen the end products such as NO_2^-, NO_3^- and N_2 or their underlying reaction pathways.

Our previous study (Pham et al., 2021) indicated that I was the reactive nitrogen species (RNS) nitroxyl (HNO) as the product of U7, shown in Scheme 1. This reaction scheme comprised

the UF+RNS model. and shows the proposed reactions for $NHCl_2$ decomposition under ambient dissolved oxygen (DO) (Pathways A and B) and low-DO conditions (Pathway A only) along with the proposed NDMA formation pathways in the presence of dimethylamine (DMA, Pathways C and D).

Due to the spin-forbidden oxygen transition from the singlet state in HNO to the triplet state in nitroxyl anion (NO^-) (Shafirovich and Lymar, 2002), HNO and NO^- exist in a slow equilibrium as shown in R2 and R6 of Scheme 1. HNO/NO^- are short-lived molecules that can react with (i) HNO to form nitrous oxide (N_2O) by R1 and R3, (ii) $NHCl_2$ and NH_2Cl to produce products that include nitrogen gas, N_2, by U8 and U9, respectively, and (iii) DO to form peroxynitrous acid/peroxynitrite anion ($ONOOH/ONOO^-$) through R5 and R4, which initiates Pathway B in Scheme 1. $ONOOH/ONOO^-$ is unstable and decomposes through 117 reactions to nitrite (NO_2^-) and nitrate (NO_3^-) as end products (Kirsch et al., 2003) With the addition of DMA, $ONOOH/ONOO^-$ was previously shown (Pham et al., 2021) to react with (i) DMA through Pathway D to form *N*-nitrosodimethylamine (NDMA) and its companion *N*-nitramine, *N*-nitrodimethylamine (DMNO) by R7 or (ii) chlorinated unsymmetrical dimethylhydrazine (UDMH-Cl), the product of the direct reaction between DMA and $NHCl_2$ (P5), to form NDMA only by R8.

All previously reported $NHCl_2$ decomposition studies were completed under an ambient atmosphere in which DO was near saturation concentrations (Wei, 1972; Saunier, 1976; Leao, 1981; Hand, 1982; Jafvert, 1985). Given our previous study showed HNO/NO^- formed from $NHCl_2$ hydrolysis (U7) and can react with DO to form $ONOOH/ONOO^-$ (Pham et al., 2021), potential cross reactions exist between these RNS and/or their decomposition products and species such as NH_2Cl, $NHCl_2$, and NH_3/NH_4^+. To challenge the robustness of the Scheme 1 and identify

relevant cross reactions, $NHCl_2$ decomposition was assessed under ambient and low-DO conditions in the absence and presence of TOTDMA.

Without TOTDMA addition and under the current UF+RNS model, Pathways A and B of Scheme 1 describe $NHCl_2$ decomposition under ambient DO conditions while Pathway A alone predominates under low-DO conditions. In this case, only nominal DO is available to react with HNO/NO^-, decreasing $ONOOH/ONOO^-$ formation and in turn NO_2^- and NO_3^-. Less HNO/NO^- feeding into Pathway B under low-DO conditions means more HNO/NO^- should proceed to the other reaction pathways which include (i) R1 and R3 to form more N_2O, (ii) U8 and U9 to produce higher N_2 yields, and/or (iii) U8 to form more $HOCl$ which subsequently reacts with NH_3 by U1 to increase NH_2Cl yields.

With TOTDMA addition under ambient DO conditions, Pathways A–D of Scheme 1 are all relevant. Pathway C is initiated by the direct reaction of DMA and $NHCl_2$ to produce UDMH-Cl by P5 (Schreiber and Mitch, 2006), which can then react with $NHCl_2$ to form other products by P7 or proceed to Pathway D and react with ONOOH to form NDMA by R8 (Pham et al., 2021). In Pathway D, NDMA is also produced by the reaction between DMA and ONOOH by R7. Under low-DO conditions, Pathways A and C should predominate and result in lower NDMA yields because Pathways B and D are initiated by the formation of $ONOOH/ONOO^-$.

Other researchers used nitrogen mass balances to assess products of NH_2Cl decomposition under an ambient atmosphere (Vikesland et al., 1998). Nitrogen in chloramine species is preferentially oxidized to N_2 along with small quantities of NO_3^-, and possibly one or more minor unidentified products (Valentine et al., 1986; Valentine and G.G, 1990; Leung and Valentine, 1994). These prior studies used initial NH_2Cl concentrations of 50-, 250-, and 900 µeq $Cl_2 \cdot L^{-1}$ with Cl/N molar ratio of 0.7 at pH 6.5 and 7.5 in 4 mM carbonate buffer (Vikesland et al., 1998).

The yields of N_2, $TOTNH_3$, NO_2^- and NO_3^- were measured after 4-, 9-, and 15 days and the average total nitrogen recovery was $90 \pm 7.0\%$. The primary nitrogen-containing products were $TOTNH_3$ at $47 \pm 3.4\%$ and N_2 at $43 \pm 7.9\%$. Small amounts of NO_3^- were formed with an average level of $1.2 \pm 0.7\%$, but no NO_2^- was detected.

Nitrogen mass balances have not been performed during $NHCl_2$ decomposition under ambient- or low-DO conditions. Nor has N_2O been considered, which is now relevant based on our prior work that showed its kinetics and yields tracked inversely with $NHCl_2$ decay (Pham et al., 2021). As NH_2Cl decays through $NHCl_2$ in the presence of excess free ammonia (Jafvert and Valentine, 1992), which is typical in drinking water systems, $TOTNH_3$ and N_2 should be the primary nitrogen-containing end products for $NHCl_2$ decomposition. Other expected nitrogen-containing end products include NH_2Cl, N_2O, NO_2^-, NO_3^- and, with the addition of TOTDMA, NDMA and DMNO. Yields of these compounds can be used to assess nitrogen mass balances during $NHCl_2$ decomposition and the existence of potential cross reactions between $ONOOH/ONOO^-$ and/or its decay products and species such as $NHCl_2$, NH_2Cl, and $TOTNH_3$. The nitrogen mass balance for $NHCl_2$ decomposition under the ambient atmosphere is expected to be less than about 95% because of the formation of the so-called unidentified product (Leung and Valentine, 1994), which cannot be more than a few percent of the total initial $NHCl_2$. However, the impact of DO on the nitrogen mass balance and the formation of the unidentified product during $NHCl_2$ decomposition is unknown.

The objective of the current study was to challenge the robustness of Scheme 1 and assess potential cross reactions between $ONOOH/ONOO^-$ and/or its decay products and species such as $NHCl_2$, NH_2Cl, and $TOTNH_3$. Experiments at pH 9 were completed in the presence and absence of 10 µM TOTDMA at initial $NHCl_2$ concentrations of 200-, 400-, and 800 µeq $Cl_2 \cdot L^{-1}$ under an

ambient atmosphere (~280 μM DO) and in a controlled-atmosphere glovebox in which DO was ≤ 20 μM. To perform the nitrogen mass balances, yields of NH_2Cl, $NHCl_2$, $TOTNH_3$, N_2O, NO_2^-, NO_3^-, N_2, NDMA and DMNO were measured following completed $NHCl_2$ decomposition. Differences in the yields of these compounds based on DO level and DMA addition allowed further interrogation of Scheme 1 and assessment of the aforementioned cross reactions. Additional experiments with uric acid, an $ONOOH/ONOO^-$ scavenger (Hooper et al., 1998; Hooper et al., 2000; Kean et al., 2000), were completed under low-DO conditions to further assess $ONOOH/ONOO^-$ as a central node in the NDMA formation pathway.

4.2-Materials and Methods

Pham et al. (2021) detailed select methods used in this present work, including the NH_2Cl and $NHCl_2$ preparation and quantification, $NHCl_2$ decay kinetic experiments, analytical techniques used for quantifying NH_2Cl, $NHCl_2$, N_2O, NO_2^-, NO_3^-, NDMA, and DMNO, and AQUASIM simulations for the UF+RNS model. This section's remainder details the $NHCl_2$ decay yield experiments under ambient DO and low-DO conditions and quantification of N_2 and $TOTNH_3$, which were needed along with the aforementioned N-containing species to interpret the mass balances.

Ambient and Low DO Experiments. The ambient DO experiments were prepared in triplicate in 40 mL headspace-free amber glass vials buffered at pH 9 with 40 mM total borate ($TOTBO_3$) at target initial $NHCl_2$ concentrations of 200-, 400-, and 800 μeq $Cl_2 \cdot L^{-1}$. Borate buffer was used because it has a pK_a of 9.24 and, unlike carbonate and phosphate, does not impact chloramine species (Valentine and Jafvert, 1988; Valentine et al., 1988). The $TOTCO_3$ can also decrease NDMA formation as shown in our previous work (Pham et al., 2021) and, therefore, only $TOTBO_3$ was used in this study to prevent complications associated with the buffer itself. One set

of experiments was completed with no added TOTDMA and another set with 10 μM TOTDMA. After 24 hours (i.e., following complete $NHCl_2$ decay), the solutions were analyzed for pH, NH_2Cl, $NHCl_2$, N_2O, $TOTNH_3$, NO_2^-, NO_3^-. For the experiments in which 10 μM TOTDMA was added, NDMA and DMNO were also measured to help close the N mass balances.

Each nitrogen yield experiment was prepared in triplicate in 40 mL headspace-free amber glass vials at pH 9 in 40 mM $TOTBO_3$ with target initial $NHCl_2$ concentrations of 200-, 400-, and 800 μeq $Cl_2 \cdot L^{-1}$, each in the absence and presence of 10 μM TOTDMA. Additionally, for the 800 μeq $Cl_2 \cdot L^{-1}$ $NHCl_2$ dose only, uric acid was added at 20-, 40-, 80-, 120- and 160 μM to quench $ONOOH/ONOO^-$ while not impacting chloramine species concentrations (Pham et al., 2021). After 24 hours (i.e., following complete $NHCl_2$ decomposition), N_2O was measured for 7–10 minutes per sample inside the glovebox using a N_2O-NP microelectrode (Unisense) which was calibrated using methods described in Pham et al. (2021) with a range of 2–80 μM-N. All remaining sample vials were removed from the glovebox for measurement of pH, $TOTNH_3$, NH_2Cl, $NHCl_2$, NO_2^-, NO_3^-. Total chlorine and NH_2Cl measurements using Hach methods were detailed in Pham et al. (2021) and were completed within 10 minutes after the vial was opened to minimize any possible interference with DO. When TOTDMA was present, NDMA and DMNO were also measured using methods detailed previously (Pham et al., 2021).

For the experiment under low-DO condition, the process is exactly the same with addition to the preparation step as follow. $NHCl_2$ decay and nitrogen end-product formation were studied under low-DO conditions in a glovebox (Labconco, Model 50700-00) in waters with and without 10 μM TOTDMA. Milli-Q water was used to prepare the following stock solutions for the low-DO experiments: NH_4Cl (71 mM or 1 g-N·L^{-1}), $^{15}NH_4Cl$ (71 mM or 1g-N·L^{-1}), TOTDMA (25 μM), H_2SO_4 (2 M), NaOH (1 M), $TOTBO_3$ (200 mM), and uric acid (360 μM) buffered at pH 9

with 200 mM TOTBO$_3$. All stock solutions were covered with parafilm and a 1 mL syringe needle was used to make 20–30 holes prior to purging with ultra-high purity (UHP) N$_2$ gas for about 30 minutes under an ambient atmosphere. The bottle headspace was also purged with UHP N$_2$ gas for 30 seconds before being tightly capped. Next, these solutions were placed inside the transfer chamber of a glovebox which was evacuated three times down to 635 mm-Hg and refilled with UHP N$_2$ prior to moving the uncapped empty vials and capped bottles with stock solutions inside the glovebox. NH$_2$Cl was then prepared following the same procedure used for the ambient DO experiments (Pham et al., 2021). Approximately 1.5 mL of the NH$_2$Cl was transferred into a screw cap cuvette and taken outside for quantification using the UV-Vis spectrophotometer. If the NH$_2$Cl prepared inside the glovebox was within ± 5% of the yield in comparison with that prepared under ambient conditions, then the stock solution was used for further experiments. Prior to each experiment, all stock solutions and Milli-Q water were checked to ensure the DO was $\leq$ 20 μM, using an OX-NP microsensor (Unisense) customized for low range measurement with a manufacturer-determined detection limit of 0.050 μM. The stock 5% NaOCl solution was not purged with UHP N$_2$ gas due to safety concerns, but only 0.6 mL of this reagent was added per 100 mL of the final stock NH$_2$Cl, which added about 2 μM DO. NHCl$_2$ was then prepared inside the glovebox, following the methods detailed in Pham et al. (2021) for preparation under an ambient atmosphere. Next, 10 mL of NH$_2$Cl (pH > 9) and NHCl$_2$ (pH 3.4–4.0) stock solutions were transferred into 25 mL amber glass vials and removed from the glovebox for UV measurement at 245- and 295 nm to quantify chloramine species following spectral deconvolution (Schreiber and Mitch, 2006) to determine their initial concentrations. This process took about 30 minutes during which the NH$_2$Cl and NHCl$_2$ stock solutions were known to be stable (Hand and Margerum, 1983). For kinetic measurement for NHCl$_2$ decomposition, NHCl$_2$ was quantified

inside the glovebox following the same spectral deconvolution method (Schreiber and Mitch, 2006) measured using a Jenway 7615 UV/Vis spectrometer instead of the Hach monochloramine and total chlorine method.

Nitrogen gas quantification. Mass labeled $^{15}NH_4Cl$ was used to make $^{15}NHCl_2$ and mixed with $^{14}NHCl_2$ at 5-, 10-, 15- and 20% v/v (n = 1) for each initial target $NHCl_2$ concentration (i.e., 100-, 200-, 400-, 800-, and 1600 µeq $Cl_2·L^{-1}$). Solutions were buffered at pH 9 with 40 mM $TOTBO_3$ under ambient DO and low-DO conditions, each in the absence and presence of 10 µM TOTDMA, to make 12.5 mL solutions in 20 mL nominal crimp seal vials. After 24 hours, the vials were agitated in a back-and-forth shaker table at high speed for 15 minutes. Next, 500 µL of headspace gas from each vial was manually injected to a Thermo Fisher Scientific GC IsoLink system coupled with a ConFlo IV universal continuous flow interface and a Delta V plus Isotope Ratio Mass Spectrometer for measurement of the $\delta^{15}N$ stable isotope. Equation 1 shows the relationship between the percentage of mass labeled ^{15}N with the measured $\delta^{15}N$ stable isotope value.

$$\delta 15N \approx \frac{n_{N_2\ formed}}{n_{15N_2,air}} \times Ratio_{15N/14N} \times 1000\ ‰ \quad \text{Equation 1}$$

The slope of the plot between v/v percentages of $^{15}N/^{14}N$ versus $\delta^{15}N$ was used to calculate the moles of N_2 gas formed during the $NHCl_2$ decay experiments.

TOTNH₃ quantification. $TOTNH_3$ was measured using an Orion High Performance Ammonia Electrode manufactured by Thermo Scientific. The electrode was calibrated weekly with an eight-point calibration curve between 15–1,500 µM-N.

4.3-Results and Discussion

Correction of DO profiles and UF+RNS model. Preliminary data collected inside the glovebox showed that NH_2Cl and $NHCl_2$ produced positive interferences on the DO microelectrode (Figure s4-1). This finding indicated that the DO consumption was overestimated in our previous paper (Pham et al., 2021) in which the UF+RNS model was developed. Given the DO consumption profiles were used to estimate the rate constants for reactions U7, U8, P5, R7 and R8 (see Scheme 1), these profiles were corrected for the NH_2Cl and $NHCl_2$ interferences (Figure s4-2), and model parameters were refit (Table s3-2). Overall, the revised reaction rates did not change the fits for NH_2Cl, $NHCl_2$, and NDMA (Table s3-3). Additional discussion of the DO microelectrode corrections for the NH_2Cl and $NHCl_2$ interferences along with the revision of the UF+RNS model are contained in the Supporting Information, Section S2.1.

Impact of Buffer Strength. $TOTBO_3$ was assessed for possible impacts in the UF+RNS reaction scheme (Pham et al., 2021). Experiments were conducted in triplicate with 800 μeq $Cl_2 \cdot L^{-1}$ $NHCl_2$ and 10 μM TOTDMA at pH 9 with $TOTBO_3$ at 10-, 20-, 30-, and 40 mM. After 24 hours, the solutions were analyzed for NH_2Cl, $NHCl_2$, N_2O, and NDMA as shown in Table s3-4 with the exception of $NHCl_2$ which was below detection, an expected result (Pham et al., 2021). Analysis of variance (ANOVA) (Montgomery, 2013) was used to determine if there was a difference in NH_2Cl, N_2O and NDMA yields with changing the buffer strength at 20-, 30-, and 40 mM $TOTBO_3$. The 10 mM $TOTBO_3$ condition was excluded from further analysis because the final pH was 8.77, indicating a drift greater than 0.10 log units. The ANOVA tables for NH_2Cl (Table s3-5), N_2O (Table s3-6) and NDMA (Table s3-7) showed the p-values were greater than 0.05, indicating there were no significant differences in these yields for the $TOTBO_3$ concentrations tested at the $\alpha = 0.05$ level of significance. Given the NH_2Cl concentrations were similar for all three buffer

concentrations (Tables s3-4 and s3-5), borate did not significantly impact the yields of NH_2Cl during dichloramine hydrolysis reactions in the UF+RNS model shown in U7, U8, U4 and U3 of Scheme 1. Similarly, the N_2O yields were not affected by the change in $TOTBO_3$, indicating reactions R1, R2 and R3 were independent of borate. Lastly, as the NDMA concentration was unchanged, borate did not interfere with the peroxynitrite reactivity, shown in reactions R7 and R8. Overall, the borate buffer strength did not impact the UF+RNS model reaction scheme and was therefore used as the buffer for all experiments in this study.

Impact of DO on $NHCl_2$ Decomposition and NDMA Formation Kinetics. Figure 4-1 shows the kinetic profiles of 800 µeq $Cl_2 \cdot L^{-1}$ $NHCl_2$ spiked into waters in the presence and absence of 10 µM TOTDMA addition under ambient DO (~280 µM) and low-DO (~20 µM) conditions. The UF+RNS model underpredicted the measured $NHCl_2$ profiles between about 0.2–0.6 hours. Given the restricted space available for measurements inside the glovebox, $NHCl_2$ was quantified by direct UV-Vis spectrometry, which is subject to a known interference from the so-called unidentified product of chloramine chemistry that has a UV absorbance spectrum between 200–300 nm and is maximal around 245 nm (Leung and Valentine, 1994). As such, the UF+RNS model predictions are likely more accurate than the measured $NHCl_2$ profiles in Figure 4-1. A photodecomposition study of NH_2Cl (pH 7–10) and $NHCl_2$ (pH 3.7) (De Laat et al., 2010) showed that under a low DO condition NH_2Cl decomposition doubled but $NHCl_2$ remained unchanged. As expected, based on Scheme 1, the measured $NHCl_2$ profiles were not affected by 10 µM TOTDMA addition or the initial DO. TOTDMA was added at a lower concentration (i.e., ~40 times on a molar basis) than $NHCl_2$, and DO reacts with an intermediate downstream of $NHCl_2$ decomposition.

Figure 4-1 also shows the NDMA kinetics profiles for the ambient atmosphere collected in our previous study (Pham et al., 2021) compared to that from the low-DO condition. The shape of the NDMA profiles were similar, reaching a near-constant level at about 1 hour. However, the NDMA yield was about 3.5 μM in the ambient DO condition compared to 1.3 μM in the low-DO condition, similar to observations reported by Schreiber and Mitch (2006) and Yang et al. (2009) Following Scheme 1, the production of ONOOH/ONOO⁻ is limited by reactions R4 and R5 in the low-DO condition which leads to decreased NDMA formation. However, this observation alone does not only support the UF+RNS model reaction scheme as the NDMA formation pathway proposed by Schreiber and Mitch (2006) also accounts for the importance of DO through a direct reaction between DO and UDMH-Cl to form NDMA.

Peroxynitrite Scavenging Shutdown NDMA Formation. To further assess the robustness of the UF+RNS model, NDMA yields were measured under the low-DO condition in waters spiked with uric acid, a known peroxynitrite scavenger (Hooper et al., 1998; Hooper et al., 2000; Stinefelt et al., 2005). The maximum concentration of uric acid that can be added to 800 μeq $Cl_2 \cdot L^{-1}$ $NHCl_2$ without substantially altering the NH_2Cl and $NHCl_2$ kinetic profiles was previously determined to be 160 μM (Pham et al., 2021). Figure 4-2 shows NDMA yields at pH 9 at uric acid doses between 0–160 μM. Under ambient DO conditions, NDMA decreased from about 3.5- to 1.7 μM as the uric acid dose increased from 0 to 160 μM. There are two possible explanations for this decrease in NDMA, which are (i) there is another NDMA formation pathway that is not associated with ONOOH/ONOO⁻ and/or (ii) 160 μM uric acid did not quench all the ONOOH/ONOO⁻ formed, leaving some to react with TOTDMA in R7 and R8.

In low-DO condition, Figure 4-2 shows NDMA decreased from about 1.2 μM to below the limit of quantitation (0.05 μM) at uric acid doses of 80 μM and greater. This observation indicates

that all NDMA formation occurred through ONOOH/ONOO$^-$ as described by the UF+RNS model (*Scheme 1*). Less ONOOH/ONOO$^-$ forms under the low-DO condition, which resulted in decreased of NDMA formation for a given uric acid dose. Additionally, less ONOOH/ONOO$^-$ also means less uric acid is needed to quench the ONOOH/ONOO$^-$.

Impact of DO and DMA on Yields of N-containing Species during NHCl$_2$ Decomposition. Scheme 1 was used to assess the fate of other ends products such as N$_2$, N$_2$O, NO$_2^-$, NO$_3^-$, and NDMA under ambient and low-DO conditions. According to the UF+RNS model (Pham et al., 2021)*,* HNO is the product of NHCl$_2$ hydrolysis by U7. Subsequently, HNO may react with (1) HNO and/or NO$^-$ to form N$_2$O by R1 or R2 followed by R3, (2) NHCl$_2$ and/or NH$_2$Cl to form N$_2$ through U8 and U9, respectively, and (3) DO to form ONOOH/ONOO$^-$ through R4 and R5. ONOOH/ONOO$^-$ rapidly decays to NO$_2^-$, NO$_3^-$, and, in the presence of TOTDMA, reacts to form NDMA and DMNO by R7 and R8. If the UF+RNS model is robust, under the low-DO condition, less ONOOH/ONOO$^-$ will form, resulting in decreased NO$_2^-$ and NO$_3^-$ formation and increased N$_2$ and/or N$_2$O formation. These end products were measured after a 24-hour reaction period in waters spiked with initial NHCl$_2$ concentrations of 200-, 400-, and 800 μeq Cl$_2$·L^{-1} at pH 9 under ambient and low-DO conditions in the presence and absence of 10 μM TOTDMA addition. The results are presented in Table s3-8. To help interpret these data, for each initial NHCl$_2$ dose, the TOTNH$_3$, NH$_2$Cl, N$_2$O, N$_2$, NO$_2^-$, and NO$_3^-$ were normalized by the corresponding concentration obtained in the ambient NHCl$_2$ decomposition experiment without added TOTDMA and presented in Figure 4-3.

The normalized yields for TOTNH$_3$ are presented in Figure **4-3**4-3a, and the actual measured values are presented in Table s4-8. The normalized TOTNH$_3$ yields were not impacted by 10 μM TOTDMA addition at the α = 0.05 significance level for the three initial NHCl$_2$

concentrations under ambient and low-DO conditions. However, the yields for TOTNH$_3$ were 20–40% greater under the low-DO condition compared with the ambient condition. This result implies that TOTNH$_3$ species (i.e., NH$_3$/NH$_4^+$) likely reacted with ONOOH/ONOO$^-$ or intermediates formed during its decomposition. This result is the first experimental evidence of potential cross reactions between RNS species formed by NHCl$_2$ decomposition and major species present in chloramine systems. Several studies reported the formation of HO$^\bullet$ and NO$_2^\bullet$ during ONOOH/ONOO$^-$ decomposition (Beckman et al., 1990; Gerasimov and Lymar, 1999; Hodges and Ingold, 1999). A potential cross reaction between NH$_3$ and HO$^\bullet$ was reported in the advanced oxidation literature (Hoigne and Bader, 1978; Huang et al., 2008; Cao et al., 2022) to yield NH$_2^\bullet$ which can directly react with (i) NH$_2$Cl to form NHCl$^\bullet$ and NH$_3$, (ii) NHCl$_2$ to form NCl$_2^\bullet$ and NH$_3$, (iii) HO$^\bullet$ to form NH$_2$OH, (iv) DO to form NH$_2$O$_2^\bullet$, and (v) NH$_2^\bullet$ to form N$_2$H$_4$. Many of these species are intermediates and may in turn react with various species present in chloramine systems.

The normalized yields for NH$_2$Cl are presented in Figure 4-3b and the measured values are presented in Table s3-8. The ANOVA analysis at $\alpha = 0.05$ for a given initial NHCl$_2$ concentration showed the yields for NH$_2$Cl decreased due to 10 μM TOTDMA addition and under the low-DO condition. For the ambient condition, 10 μM TOTDMA addition decreased the final NH$_2$Cl concentration by about 9-, 6- and 3% for the initial NHCl$_2$ concentrations of 200-, 400-, and 800 μeq Cl$_2 \cdot$L^{-1}, respectively. Taken together, this was evidence of a direct reaction between TOTDMA and NHCl$_2$ (i.e., P5 in Scheme 1) under ambient and low-DO conditions. For a given initial NHCl$_2$ concentration, the presence of TOTDMA resulted in less NHCl$_2$ available to form NH$_2$Cl.

132

The NH_2Cl yields were 16–20% less in the low-DO condition compared to the ambient condition for a given initial $NHCl_2$ and TOTDMA. It is therefore plausible that some NH_2Cl formation that occurs through $NHCl_2$ decomposition involved DO. According to Scheme 1, the main reactions responsible for NH_2Cl formation are U7, U8 and U1. These reactions are upstream of the reaction between HNO/NO^- and DO (i.e., R5 and R4), and therefore should not be impacted by the DO level. The fact that NH_2Cl yields were lower under the low-DO concentration implies that Scheme 1 is missing a reaction(s) involving the formation of NH_2Cl through the reaction of a $NHCl_2$ decomposition product(s) and DO.

N_2O is a stable end-product and therefore can be used as a surrogate for HNO/NO^- formation (Shafirovich and Lymar, 2002; Shafirovich and Lymar, 2003). The ANOVA analysis of the N_2O yields at $\alpha = 0.05$ indicated less N_2O formed under the ambient atmosphere compared to the low-DO condition (Table s3-8). Under ambient conditions, N_2O yields were not impacted by 10 μM TOTDMA addition ($\alpha = 0.05$, Figure 4-3c) for a given initial $NHCl_2$ concentration. This observation indicates the TOTDMA (i) predominantly reacted with a product downstream of HNO/NO^- and/or (ii) concentration used in the experiments (i.e., 10 μM) was sufficiently smaller than the initial $NHCl_2$ doses (200–800 μeq $Cl_2 \cdot L^{-1}$) and therefore did not impact the $NHCl_2$ profiles and N_2O formation.

Under low-DO conditions, N_2O yields were indistinguishable from one another at $\alpha = 0.05$ in the presence and absence of 10 μM TOTDMA addition but were greater than the N_2O yields in the ambient atmosphere (Figure 4-3c). This supports the UF+RNS reaction scheme because the amount of HNO/NO^- that reacts with DO to form $ONOOH/ONOO^-$ should decrease in the low-DO condition and is offset by an increasing amount of HNO/NO^- reacting to form N_2O through R1–R3 and N_2 through U8 and U9.

The normalized N_2 yields are presented in Figure 4-3d. The N_2 yields were unaffected by 10 μM TOTDMA addition except for the ambient condition at an initial $NHCl_2$ concentration of 200 μeq $Cl_2 \cdot L^{-1}$. Greater N_2 yields were measured for the low-DO condition compared to the ambient atmosphere, similar to the N_2O yields. This observation also supports the UF+RNS model in which more HNO/NO^- is available to form N_2 through U8 and U9 (see Scheme 1) under the low-DO condition.

Figures 4-3e and f show the normalized NO_2^- and NO_3^- yields. Under ambient DO conditions, 10 μM TOTDMA addition decreased NO_2^- by about 60–70% and decreased NO_3^- by about 40–50%. Under low-DO conditions, NO_2^- was below the method detection limit of 0.8 μM-N regardless the presence of TOTDMA, while NO_3^- formation decreased by about 50–70% in the absence of TOTDMA and about 60–80% with 10 μM TOTDMA. Overall, NO_2^- and NO_3^- yields decreased with TOTDMA addition and DO removal, which further support the UF+RNS pathway in Scheme 1. Under the ambient DO conditions, TOTDMA reacts with $ONOOH/ONOO^-$ or its decomposition products to form NDMA and DMNO and, therefore, less NO_2^- and NO_3^- are produced. Under low-DO conditions, decreased NO_2^- and NO_3^- were attributable to lower $ONOOH/ONOO^-$ formation and more TOTDMA to react with $NHCl_2$ via reaction P5 as the availability of $ONOOH/ONOO^-$ decreases.

Nitrogen Mass Balances during $NHCl_2$ Decomposition. Nitrogen mass balances were performed to determine the extent to which the nitrogen-containing species were accounted for during $NHCl_2$ decomposition. The initial total nitrogen was determined by summing the measured $NHCl_2$ and the calculated $TOTNH_3$, determined by the difference between the added NH_4Cl and measured $NHCl_2$. $TOTNH_3$ could not be accurately measured with the ammonia electrode in the presence of $NHCl_2$ because the procedure requires adjusting the sample to pH 12, which

134

accelerates $NHCl_2$ decomposition and generates HOCl that can react with $TOTNH_3$. The end-products measured following complete $NHCl_2$ decomposition were $TOTNH_3$, NH_2Cl, $NHCl_2$, N_2O, N_2, NO_2^- and NO_3^- and for the samples with added TOTDMA, NDMA and DMNO.

Practical limitations precluded the simultaneous measurement of all the nitrogenous end-products in triplicate for a given experiment, necessitating two sets of experiments, the results of which were aggregated using a linear model. In Experiment 1 (Table s3-9), NO_2^- and NO_3^-, NDMA, and DMNO were measured in triplicate, N_2O was measured in duplicate, and $TOTNH_3$ and NH_2Cl were measured once. In the Experiment 2 (Table s3-10), $TOTNH_3$, NH_2Cl, and N_2O were measured in triplicate such that all end-products were measured in triplicate in one of the experiments. A linear model was developed to aggregate Experiments 1 and 2 to calculate for the nitrogen mass balance and its corresponding 95% confidence interval. A linear model of the nitrogen recovery ratio was fitted as a function of the four treatments—Ambient, Ambient+DMA, Low-DO, and Low-DO+DMA—controlling for a binary variable to distinguish between Experiments 1 and 2 and a continuous variable to describe initial $NHCl_2$ and $TOTNH_3$ (Table s3-11) Treatment type was a significant source of variation in ratio (p = 0.0000) and the model errors passed the Shapiro-Wilk test for normal data (p = 0.1463, Table s3-12) (Shapiro and Wilk, 1965). Significant differences (p = 0.0000) were found in the ratios among the four treatment types after controlling for experiment and the initial conditions as follows: Low-DO+DMA > Low-DO > Ambient ≈ Ambient+DMA. Based on the model, 95% confidence intervals of the nitrogen recovery ratio were determined for each combination of treatment and target level of $NHCl_2$ (100-, 200- and 400 µM or 200-, 400-, 800 µeq $Cl_2 \cdot L^{-1}$). Average initial $TOTNH_3$ concentrations of 129-, 260- and 518 µM were used for initial $NHCl_2$ concentrations of 100, 200- and 400 µM, respectively.

Figure 4-4 shows the nitrogen recovery ratios generated from the linear model for the nitrogen mass balances from $NHCl_2$ decay experiments in waters with 40 mM $TOTBO_3$ at pH 9 in the presence and absence of 10 μM TOTDMA and dosed with ca. 200-, 400-, and 800 μeq $Cl_2 \cdot L^{-1}$ under ambient and low-DO conditions. In the ambient case, about 80% of the nitrogen was accounted for, regardless of the initial $NHCl_2$ dose and TOTDMA addition. In the low-DO condition, about 90% of the nitrogen was accounted for in the absence of TOTDMA addition and about 100% with 10 μM TOTDMA. The lower ratios determined for the ambient conditions compared to the low-DO conditions indicated the formation of unidentified nitrogen-containing products in the presence of DO.

Under the low-DO condition, less $ONOOH/ONOO^-$ is formed and in turn fewer decay products such as of $HO^{\bullet}$ and $NO_2^{\bullet}$ (Ferrer-Sueta and Radi, 2009). Only $HO^{\bullet}$ has been reported to react with NH_2Cl and $NHCl_2$, with rate constants of 1×10^9- and 6.2×10^8 $M^{-1}s^{-1}$, respectively (Cao et al., 2022). However, these are not the primary reactions driving the increase in ratio for the nitrogen mass balances because NH_2Cl decreased under the low-DO condition (Figure 4-3b) and $NHCl_2$ decomposition profiles were independent of the DO level (Figure 4-1). The main contributors to the closing nitrogen mass balance under low-DO condition were greater $TOTNH_3$ (Figure 4-3a) and greater N_2 (Figure 4-3d) compared to the ambient condition. Taken together, the weight of this evidence indicates that NH_3/NH_4^+ reacts with $ONOOH/ONOO^-$ or its decay products. However, the exact reaction remains unclear and requires future work in which $ONOOH/ONOO^-$ is generated and reacted with free ammonia.

Figures 4-5 and 4-6 show the UF+RNS model fits for the various nitrogen end-products. Figure 4-5a shows the simulations of $TOTNH_3$ were satisfactory although the UF+RNS model did not produce greater $TOTNH_3$ for the low-DO condition compared to the ambient condition. Figure

4-5b shows the simulations of NH_2Cl were accurate for the ambient condition but the model overpredicted NH_2Cl for the low-DO condition. Figure 4-5c shows the simulations for N_2O were underpredicted in all cases and only a weak function of the initial $NHCl_2$ concentration, in contrast to the measured concentrations. Additionally, the model was insensitive to the DO level in which the measured N_2O was greater for the low-DO condition. Figure 4-5d shows the simulations for N_2 were captured well, with higher simulated N_2 for the low-DO condition, following the measured concentrations. Figure 4-5e shows the simulations for NO_2^- were captured well for the ambient condition only. The model did not properly account for the decrease in NO_2^- upon 10 μM TOTDMA addition and overpredicted NO_2^- for the low-DO conditions. Figure 4-5f shows the simulations for NO_3^- overpredicted the measured values under all conditions, although overpredictions were greater in degree for the ambient condition. These observations indicate the UF+RNS model reactions required revisions associated with (1) $ONOOH/ONOO^-$ or its decay products which are needed to capture increased $TOTNH_3$ and decreased NH_2Cl formation under the low-DO condition, (2) greater N_2O formation and decreased NO_3^- formation, and (3) additional DMA-related reactions that involve consumption of NO_2^-.

Figure 4-6 indications the UF+RNS model was accurate for predicting the fate of NDMA under ambient and low-DO conditions for all the initial $NHCl_2$ concentrations. This result indicated that the NDMA formation pathway in the UF+RNS model is conceptually robust.

4.4-Implications

The results from this study showed that (i) all NDMA formation stemming from $NHCl_2$ decomposition in the presence of DMA went through the UF+RNS pathway in which $ONOOH/ONOO^-$ was a central node, (ii) the UF+RNS reaction scheme can be used to assess the fate of nitrogen end-products such as N_2O, N_2, NO_2^-, and NO_3^- under ambient and low-DO conditions, and (iii) less of the nitrogen was accounted for under ambient DO conditions and there is evidence of cross reactions between $TOTNH_3$ and $ONOOH/ONOO^-$ or its decay products.

Future research should include updating the UF+RNS model to accurately capture the yields of $TOTNH_3$, N_2O, N_2, NO_2^-, and NO_3^- for the ambient and low-DO conditions while maintaining the fits for $NHCl_2$, NH_2Cl, and for the samples with added TOTDMA, NDMA and DMNO. This may require experiments with $ONOOH/ONOO^-$ and $TOTNH_3$. Future experimental work should consider additional model NDMA precursors such as ranitidine, which is contained in the antacid Zantac, to assess the importance of the RNS pathway as the NDMA formation mechanism may be different from DMA (Pham et al., 2019). Besides NDMA, other *N*-nitrosamines should also be considered as their speciation in U.S. water systems may change due to the presence of the precursors like fentanyl and norfentanyl which have been linked to the opioid crisis (Gushgari et al., 2019).
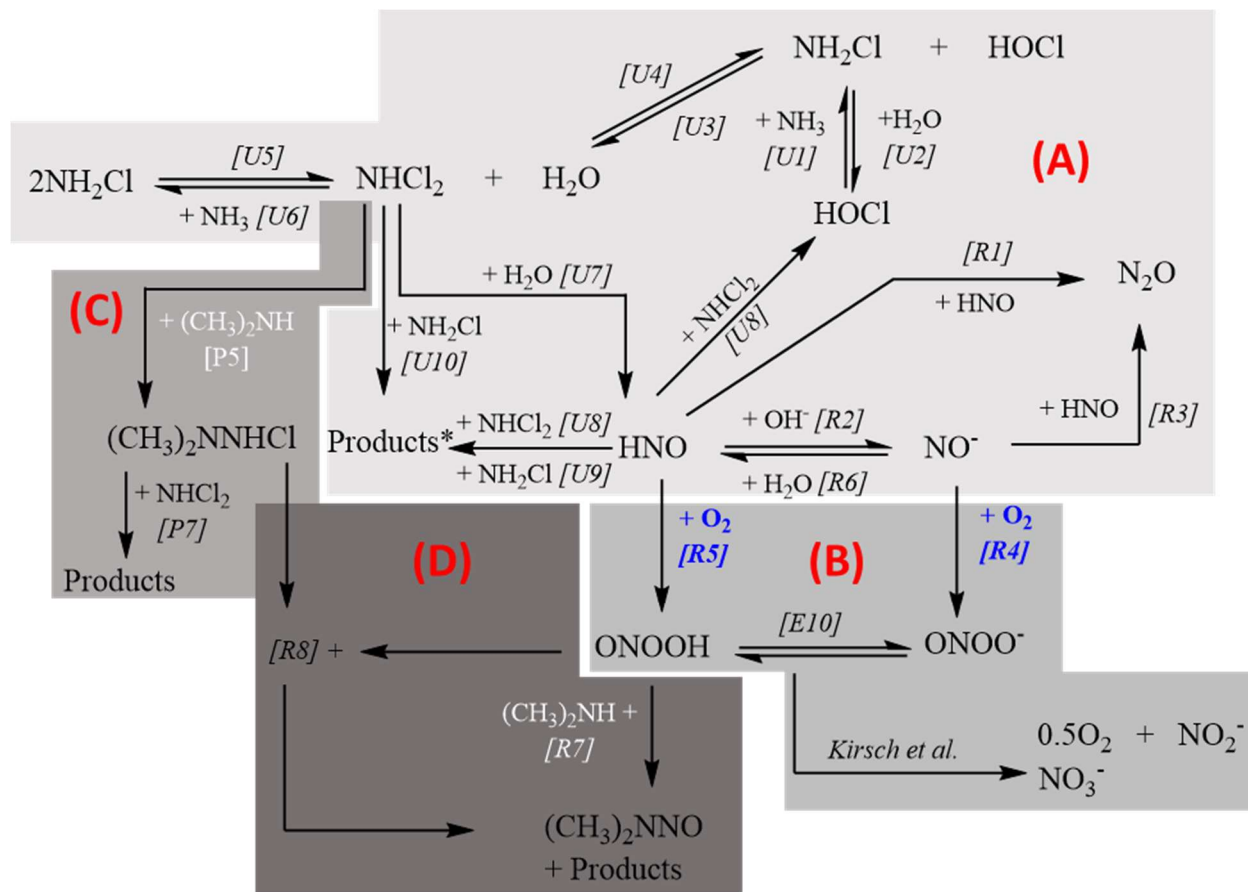
Scheme 1. Proposed reaction scheme for the UF+RNS model showing $NHCl_2$ decomposition and NDMA formation adapted from Pham et al.(Pham et al., 2021) Pathways **A** and **B** show $NHCl_2$ decay under ambient DO conditions; Pathways **C** and **D** are relevant upon total dimethylamine (TOTDMA, DMA plus dimethylammonium cation, $DMAH^+$) addition. Under low DO conditions $NHCl_2$ decay is restricted to Pathway **A** (no TOTDMA) and **A** and **C** (with TOTDMA) because DO is not available to form $ONOOH/ONOO^-$ by R4 or R5 and initiate Pathway **B**. In Pathway **A**, Products* of U8–U10 may include N_2, H_2O, HCl, NO_3^- and other unidentified products.
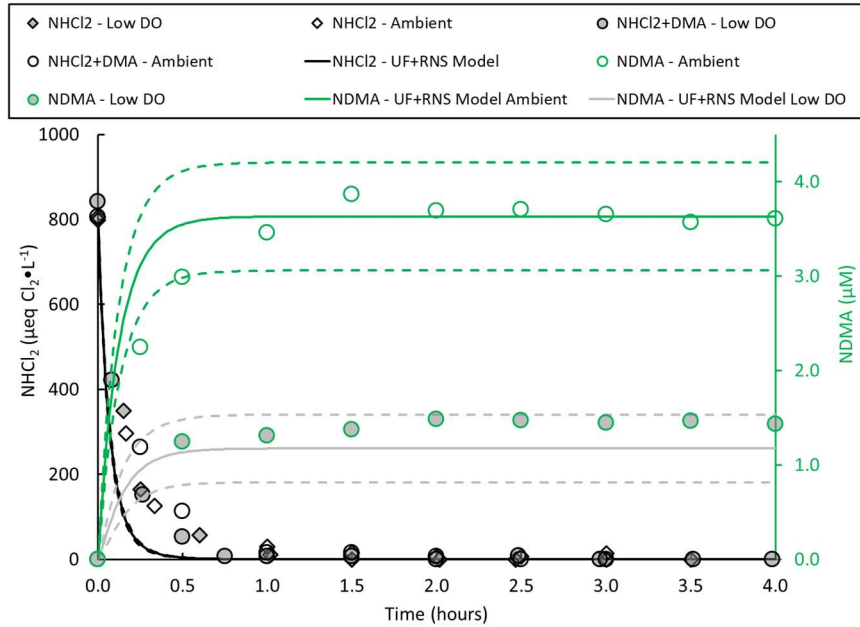
Figure 4-1. NHCl$_2$ (black, primary y-axis, measured by UV-Vis spectrometry) and NDMA (green, secondary y-axis) profiles in 40 mM TOTBO$_3$ at pH 9 with and without 10 μM TOTDMA dosed with ca. 800 μeq Cl$_2$·L^{-1} NHCl$_2$ and under an ambient atmosphere (~280 μM DO, open symbols, reported previously(Pham et al., 2021)) and the low-DO condition (≤ 20 μM DO, filled symbols). Points are measured values, lines are UF+RNS model simulations, and dashed lines are lower and upper limits for NDMA simulations calculated by one standard error in the estimated parameters.
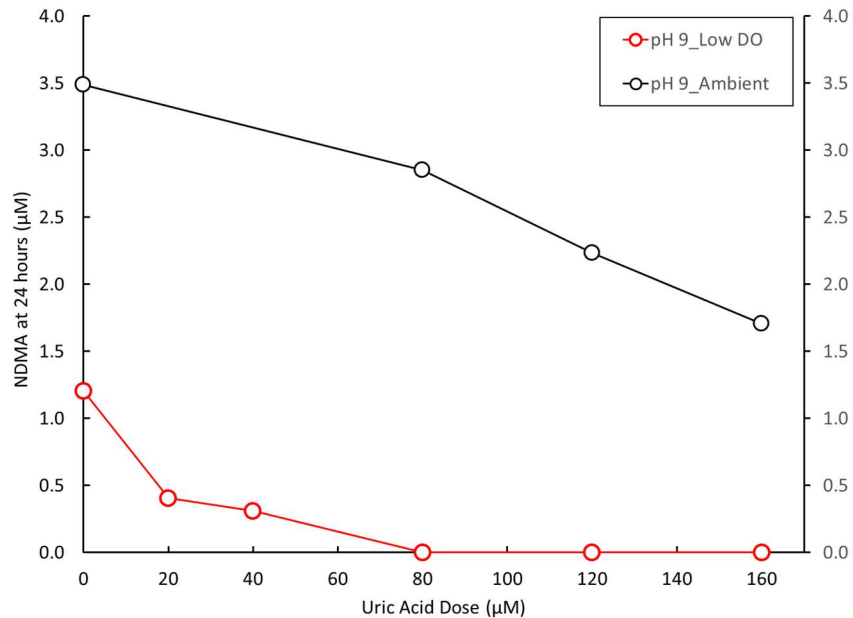
Figure 4-2. NDMA yields at 24 hours under ambient DO conditions (black, ~280 μM DO, published by Pham et al.(Pham et al., 2021)) and the low-DO conditions (red, ~20 μM DO) as a function of uric acid dose in waters spiked with about 800 μeq Cl$_2$·L^{-1} NHCl$_2$ and 10 μM TOTDMA at pH 9
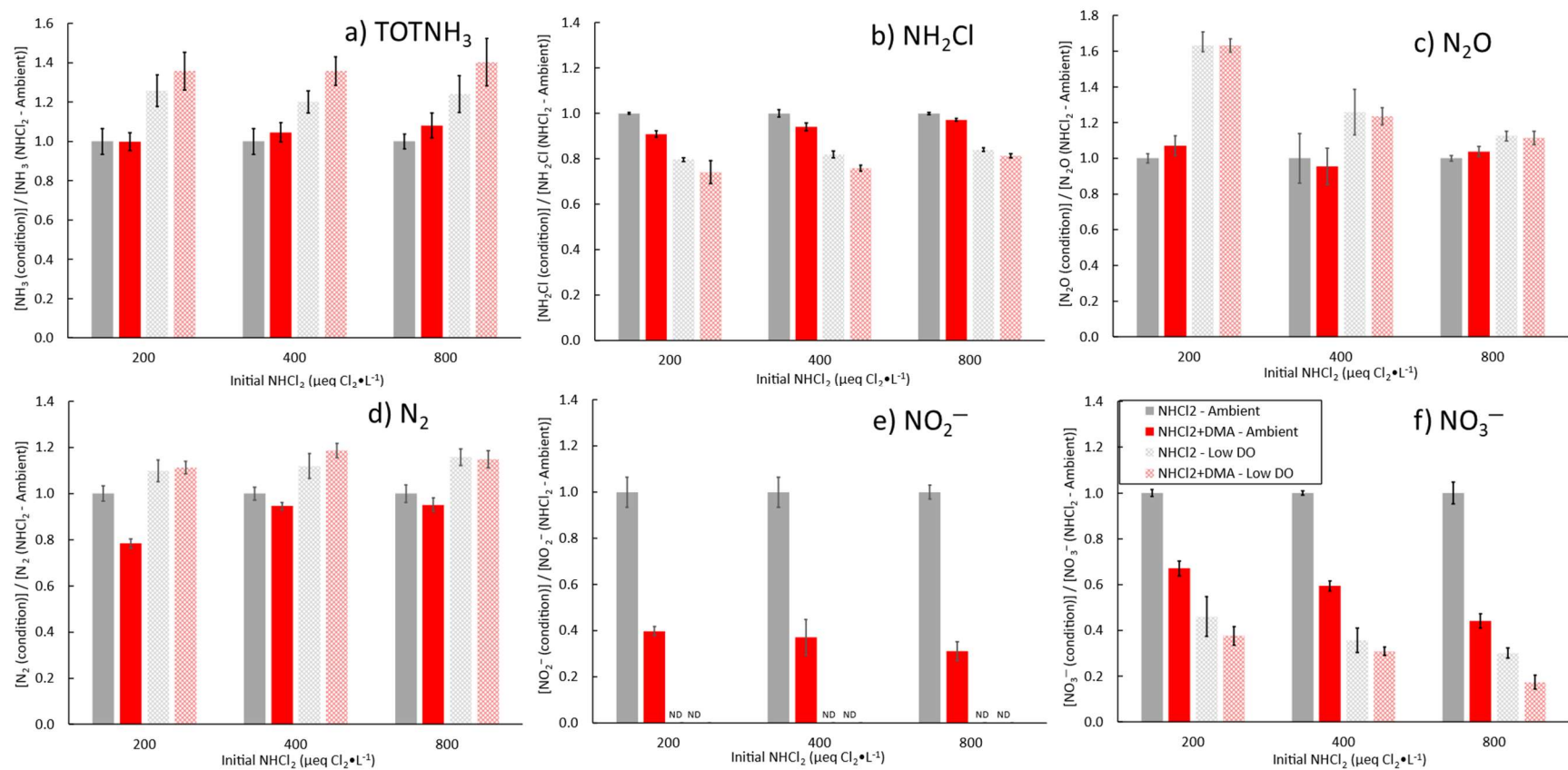
Figure 4-3. Normalized concentrations of (a) TOTNH$_3$, (b) NH$_2$Cl, (c) N$_2$O, (d) N$_2$, (e) NO$_2^-$, and (f) NO$_3^-$ measured after a 24 hour reaction time in waters dosed with ca. 200-, 400-, 800 µeq Cl$_2$·L^{-1} buffered at pH 9 with 40 mM TOTBO$_3$ under an ambient atmosphere (~280 µM DO, solid bars) and inside the glovebox (~20 µM DO, patterned bars) without added TOTDMA (grey) and with 10 µM TOTDMA (red).
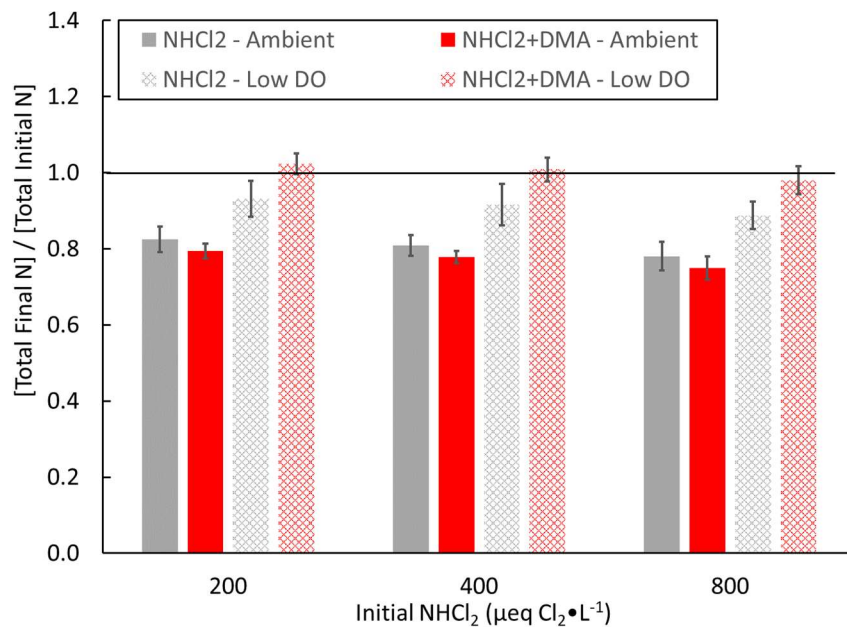
Figure 4-4. Ratios for the nitrogen mass balances generated from the linear model (Table s4-11) based on $NHCl_2$ decay Experiments 1 and 2 in 40 mM $TOTBO_3$ water buffered at pH 9 in the presence and absence of 10 µM TOTDMA addition. Samples were dosed with about 200-, 400-, and 800 µeq $Cl_2 \cdot L^{-1}$ under ambient and low-DO conditions. Error bars represent 95% confidence intervals.
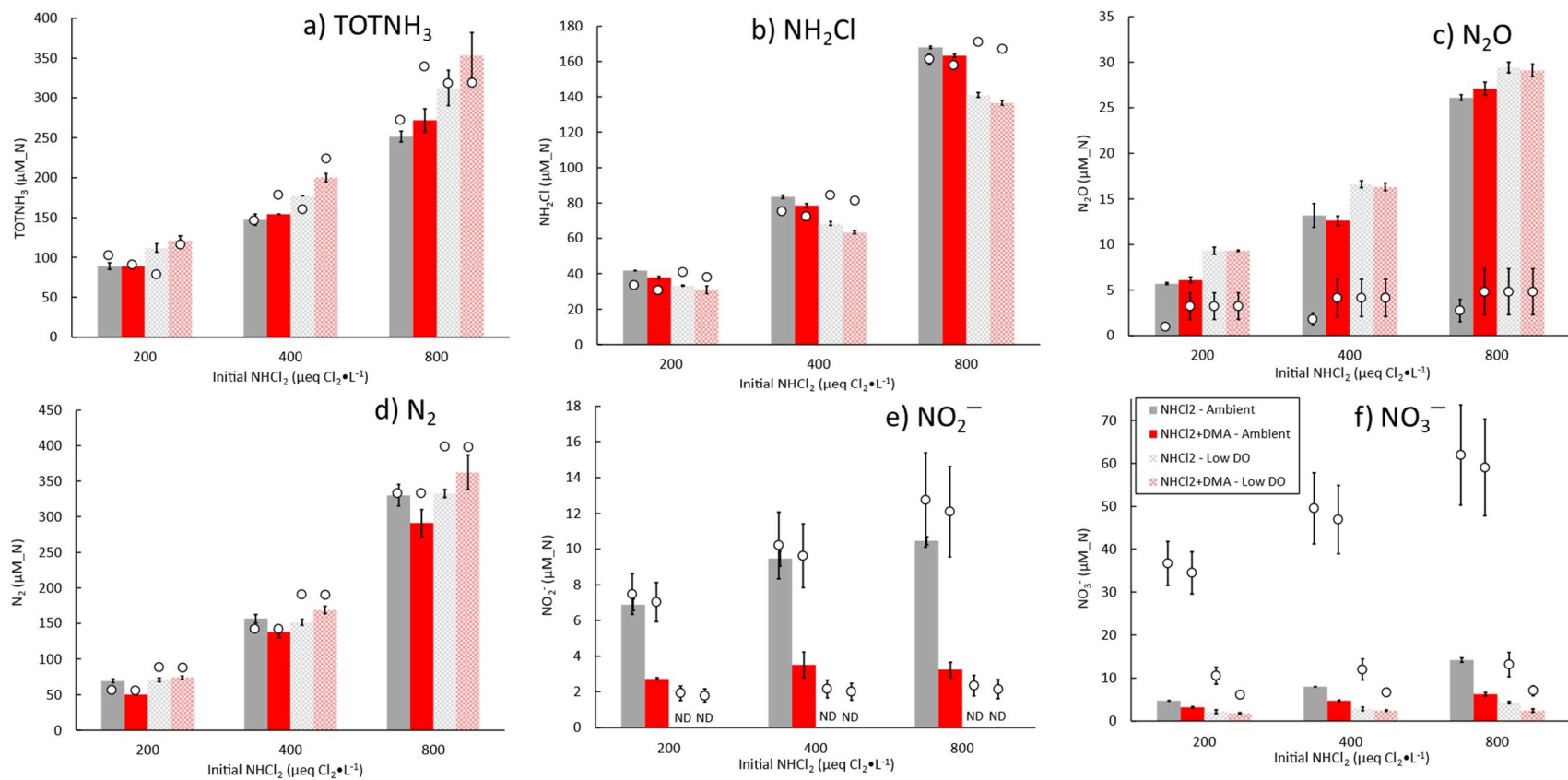
Figure 4-5. Measured (bars) and UF+RNS model simulated (circles) concentrations of (a) $TOTNH_3$, (b) NH_2Cl, (c) N_2O, (d) N_2, (e) NO_2^- and (f) NO_3^- after a 24 hour reaction time in waters dosed with ca. 200-, 400-, 800 μeq $Cl_2 \cdot L^{-1}$ buffered at pH 9 with 40 mM $TOTBO_3$ under an ambient atmosphere (~280 μM DO, solid bars) and inside the glovebox (~20 μM DO, patterned bars) without added TOTDMA (grey) and with 10 μM TOTDMA (red).
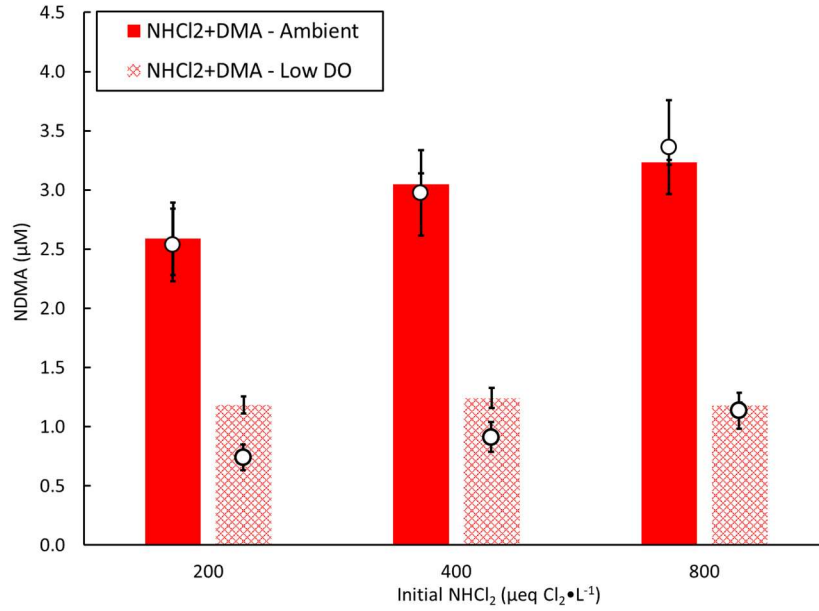
Figure 4-6. Measured (bars) and UF+RNS model simulated (circles) concentrations of NDMA after a 24 hour reaction time in waters dosed with ca. 200-, 400-, 800 µeq $Cl_2 \cdot L^{-1}$ buffered at pH 9 with 40 mM $TOTBO_3$ under an ambient atmosphere (~280 µM DO, solid bars) and inside the glovebox (~20 µM DO, patterned bars) 10 µM TOTDMA (red).

4.6-References

Beckman, J. S., Beckman, T. W., Chen, J., Marshall, P. A. and Freeman, B. A., *Proceedings of the National Academy of Sciences of the United States of America*, **87**, 1620-1624 (1990). 10.1073/pnas.87.4.1620.

Cao, Z., Yu, X., Zheng, Y., Aghdam, E., Sun, B., Song, M., Wang, A., Han, J. and Zhang, J., *Journal of Hazardous Materials*, **424**, 127341 (2022). https://doi.org/10.1016/j.jhazmat.2021.127341.

Cornwell Engineering Group. (2018). 2017 Water Utility Disinfection Survey Report,

De Laat, J., Boudiaf, N. and Dossier-Berne, F., *Water Research*, **44**, 3261-3269 (2010). https://doi.org/10.1016/j.watres.2010.03.009.

Ferrer-Sueta, G. and Radi, R., *ACS Chemical Biology*, **4**, 161-177 (2009). 10.1021/cb800279q.

Gerasimov, O. V. and Lymar, S. V., *Inorganic Chemistry*, **38**, 4317-4321 (1999). 10.1021/ic990384y.

Gushgari, A. J., Venkatesan, A. K., Chen, J., Steele, J. C. and Halden, R. U., *Water Research*, **161**, 171-180 (2019). https://doi.org/10.1016/j.watres.2019.06.003.

Hand, V. C. (1982). Kinetics and Mechanisms of the Decomposition of N-Chloro-alpha-Amino Acids and Dichloramine in Aqueous Solutions. 8310828, Ph.D., Purdue University, Ann Arbor.

Hand, V. C. and Margerum, D. W., *Inorganic Chemistry*, **22**, 1449-1456 (1983). Doi 10.1021/Ic00152a007.

Hodges, G. R. and Ingold, K. U., *Journal of the American Chemical Society*, **121**, 10695-10701 (1999). 10.1021/ja991077u.

Hoigne, J. and Bader, H., *Environ Sci Technol*, **12**, 79-84 (1978). 10.1021/es60137a005.

Hooper, D. C., Scott, G. S., Zborek, A., Mikheeva, T., Kean, R. B., Koprowski, H. and Spitsin, S. V., *The FASEB Journal*, **14**, 691-698 (2000). https://doi.org/10.1096/fasebj.14.5.691.

Hooper, D. C., Spitsin, S., Kean, R. B., Champion, J. M., Dickson, G. M., Chaudhry, I. and Koprowski, H., *Proceedings of the National Academy of Sciences of the United States of America*, **95**, 675-680 (1998). 10.1073/pnas.95.2.675.

Huang, L., Li, L., Dong, W., Liu, Y. and Hou, H., *Environ Sci Technol*, **42**, 8070-8075 (2008). 10.1021/es8008216.

Jafvert, C. T. (1985). A Unified Chlorine-Ammonia Speciation and Fate Model. Doctor of Philosophy, University of Iowa,

Jafvert, C. T. and Valentine, R. L., *Water Research*, **21**, 967-973 (1987).

Jafvert, C. T. and Valentine, R. L., *Environ Sci Technol*, **26**, 577-586 (1992). Doi 10.1021/Es00027a022.

Kean, R. B., Spitsin, S. V., Mikheeva, T., Scott, G. S. and Hooper, D. C., *The Journal of Immunology*, **165**, 6511 (2000). 10.4049/jimmunol.165.11.6511.

Kirsch, M., Korth, H. G., Wensing, A., Sustmann, R. and de Groot, H., *Archives of Biochemistry and Biophysics*, **418**, 133-150 (2003). 10.1016/j.abb.2003.07.002.

Leao, S. F. (1981). Kinetics of Combined Chlorine: Reaction of Substitution and Redox. Doctor of Philosophy, University of California, Berkeley,

Leung, S. W. and Valentine, R. L., *Water Research*, **28**, 1475-1483 (1994). Doi 10.1016/0043-1354(94)90316-6.

Montgomery, D. C., & Runger, G. C. *Applied statistics and probability for engineers*, John Wiley & Sons, New York, NY, (2013).

Pham, H. T., Wahman, D. G. and Fairey, J. L., *Environ Sci Technol*, 1740-1749 (2021). 10.1021/acs.est.0c06456.

Pham, H. T., Wahman, D. G., Zhang, W. and Fairey, J. L., *Encyclopedia of Water*, 1-14 (2019). doi:10.1002/9781119300762.wsts0037.

Ratnayaka, D. D., Brandt, M. J. and Johnson, K. M., D. D. Ratnayaka, M. J. Brandt and K. M. Johnson. *Water Supply (Sixth Edition)*. Butterworth-Heinemann. Boston: 425-461 (2009).

Saunier, B. M. (1976). Kinetics of Breakpoint Chlorination and Disinfection. Univesity of California, Berkeley, CA.

Schreiber, I. M. and Mitch, W. A., *Environ Sci Technol*, **40**, 6007-6014 (2006). 10.1021/es060978h.

Shafirovich, V. and Lymar, S. V., *Proceedings of the National Academy of Sciences of the United States of America*, **99**, 7340-7345 (2002). 10.1073/pnas.112202099.

Shafirovich, V. and Lymar, S. V., *Journal of the American Chemical Society*, **125**, 6547-6552 (2003). 10.1021/ja034378j.

Shapiro, S. S. and Wilk, M. B., *Biometrika*, **52**, 591-611 (1965). 10.2307/2333709.

Stinefelt, B., Leonard, S. S., Blemings, K. P., Shi, X. and Klandorf, H., *Annals of Clinical & Laboratory Science*, **35**, 37-45 (2005).

Valentine, R. L., Brandt, K. I. and Jafvert, C. T., *Water Research*, **20**, 1067-1074 (1986).

Valentine, R. L. and G.G, W., R. L. Jolley. *Water Chlorination: Chemistry, Enviromental Impact and Health Effects*. Lewis. Chelsea, MI**:** 819-832 (1990).

Valentine, R. L. and Jafvert, C. T., *Environ Sci Technol*, **22**, 6 (1988). 10.1021/es00171a012.

Valentine, R. L., Jafvert, C. T. and Leung, S. W., *Water Research*, **22**, 1147-1153 (1988).

Vikesland, P. J., Ozekin, K. and Valentine, R. L., *Environ Sci Technol*, **32**, 1409-1416 (1998). 10.1021/es970589a.

Wei, I. W. (1972). Chlorine Ammonia Breakpoint Reactions: Kinetics and Mechanism. Doctor of Philosophy, PhD Dissertation Harvard University, Cambridge, MA.

Yang, L., Chen, Z., Shen, J., Xu, Z., Liang, H., Tian, J., Ben, Y., Zhai, X., Shi, W. and Li, G., *Environ Sci Technol*, **43**, 5481-5487 (2009). 10.1021/es900319f.

Appendix 2

Supporting Information for

Effect of Dissolved Oxygen and Dimethylamine on Dichloramine Decomposition Products.

Evidence of Additional Reaction Pathways Revealed by Nitrogen Mass Balances

S1. Introduction

Table s4-1. The Unified (UF) model of chloramine chemistry

U#	Reaction Stoichiometry	Rate Expression	Rate Constant	Units
U1	$HOCl + NH_3 \xrightarrow{k_{u1}} NH_2Cl + H_2O$	$k_{u1}[HOCl][NH_3]$	[a] 4.2×10^6	$M^{-1}s^{-1}$
U2	$NH_2Cl + H_2O \xrightarrow{k_{u2}} HOCl + NH_3$	$k_{u2}[NH_2Cl]$	[a] 2.1×10^{-5}	s^{-1}
U3	$HOCl + NH_2Cl \xrightarrow{k_{u3}} NHCl_2 + H_2O$	$k_{u3}[HOCl][NHCl_2]$	[b] 2.8×10^2	$M^{-1}s^{-1}$
U4	$NHCl_2 + H_2O \xrightarrow{k_{u4}} HOCl + NH_2Cl$	$k_{u4}[NHCl_2]$	[b] 6.5×10^{-7}	s^{-1}
U5	$NH_2Cl + NH_2Cl \xrightarrow{k_{u5}} NHCl_2 + NH_3$	$k_{u5}[NH_2Cl]^2$	[c] k_{u5}	$M^{-1}s^{-1}$
U6	$NHCl_2 + NH_3 \xrightarrow{k_{u6}} NH_2Cl + NH_2Cl$	$k_{u6}[NHCl_2][NH_3][H^+]$	[d] 6.0×10^4	$M^{-2}s^{-1}$
U7	$NHCl_2 + H_2O \xrightarrow{k_{u7}} I$ [e]	$k_{u7}[NHCl_2][OH^-]$	[f] 110	$M^{-1}s^{-1}$
U8	I [e] $+ NHCl_2 \xrightarrow{k_{u8}} HOCl + products$ [g]	$k_{u8}[I$ [e] $][NHCl_2]$	[h] 2.7×10^4	$M^{-1}s^{-1}$
U9	I [e] $+ NH_2Cl \xrightarrow{k_{u9}} products$ [g]	$k_{u9}[I$ [e] $][NH_2Cl]$	[h] 8.3×10^3	$M^{-1}s^{-1}$
U10	$NH_2Cl + NHCl_2 \xrightarrow{k_{u10}} products$ [g]	$k_{u10}[NH_2Cl][NHCl_2]$	[i] 1.5×10^{-2}	$M^{-1}s^{-1}$
U11	$HOCl + NHCl_2 \xrightarrow{k_{u11}} NCl_3 + H_2O$	$k_{u11}[NHCl_2][HOCl]$	[d] k_{u11}	$M^{-1}s^{-1}$
U12	$NHCl_2 + NCl_3 + 2H_2O \xrightarrow{k_{u12}} 2HOCl + products$ [g]	$k_{u12}[NHCl_2][NCl_3][OH^-]$	[f] 5.6×10^{10}	$M^{-2}s^{-1}$
U13	$NH_2Cl + NCl_3 + H_2O \xrightarrow{k_{u13}} HOCl + products$ [g]	$k_{u13}[NH_2Cl][NCl_3][OH^-]$	[f] 1.4×10^9	$M^{-2}s^{-1}$
U14	$NHCl_2 + 2HOCl + H_2O \xrightarrow{k_{u14}} NO_3^- + 5H^+ + 4Cl^-$	$k_{u14}[NHCl_2][OCl^-]$	[f] 2.3×10^2	$M^{-1}s^{-1}$

U# – reaction number for the unified (UF) model of chloramine chemistry
[a] Morris and Isaac (1983)
[b] Margerum et al. (1978)
[c] Valentine et al. (1988)

$k_{u5} = k_H[H^+] + k_{H_2P}[H_2PO_4^-] + k_{H_3P}[H_3PO_4] + k_{H_2CO_3}[H_2CO_3^*] + k_{HCO_3^-}[HCO_3^-]$

where: $k_H = 6.9 \times 10^3$ $M^{-2}s^{-1}$; $k_{H_2P} = 3.6 \times 10^{-1}$ $M^{-2}s^{-1}$; $k_{H_3P} = 8.9 \times 10^2$ $M^{-2}s^{-1}$

$k_{H_2CO_3} = 7.5 \times 10^{-1}$ $M^{-2}s^{-1}$; $k_{HCO_3^-} = 2.0 \times 10^{-3}$ $M^{-2}s^{-1}$

[d] Hand and Margerum (1983)

$k_{u11} = k_{OCl^-}[OCl^-] + k_{HP}[HPO_4^{2-}] + k_{OH^-}[OH^-]$

where: $k_{OCl^-} = 9.0 \times 10^4$ $M^{-2}s^{-1}$; $k_{HP} = 1.6 \times 10^4$ $M^{-2}s^{-1}$; $k_{OH^-} = 3.3 \times 10^9$ $M^{-2}s^{-1}$

[e] I is the unidentified intermediate of dichloramine hydrolysis assumed to be nitroxyl (HNO) in this work
[f] Jafvert and Valentine (1992)
[g] may include H_2O, Cl^-, H^+, NO_3^-, N_2, and unidentified species
[h] Jafvert and Valentine (1987)
[i] Leao (1981)

149

S2. Results and Discussion

S2.1. *Correction of DO profiles and UF+RNS model*

$NHCl_2$ and NH_2Cl were assessed as possible interferences on the OX-NP microsensor. Twenty-one observations of $NHCl_2$ standards (0–1,600 µeq $Cl_2 \cdot L^{-1}$) and four observations of NH_2Cl standards (0–250 µeq $Cl_2 \cdot L^{-1}$) were prepared and measured using the OX-NP microsensor. The DI water was bubbled with ambient air for 30 minutes before using it to make NH_2Cl and dropping the pH to make the $NHCl_2$ stock solution as detailed previously.(Pham et al., 2021) The $NHCl_2$ was then prepared by adding the $NHCl_2$ stock to the oxygen saturated water and the signal measured with the OX-NP microsensor (Figure s4-1). The positive interferences of $NHCl_2$ (Figure s4-1a) and NH_2Cl (Figure s4-1b) on the DO microelectrode were linear with chloramine species concentrations. The best-fit linear regressions were used for the corrections of the DO microelectrode profiles as detailed next.
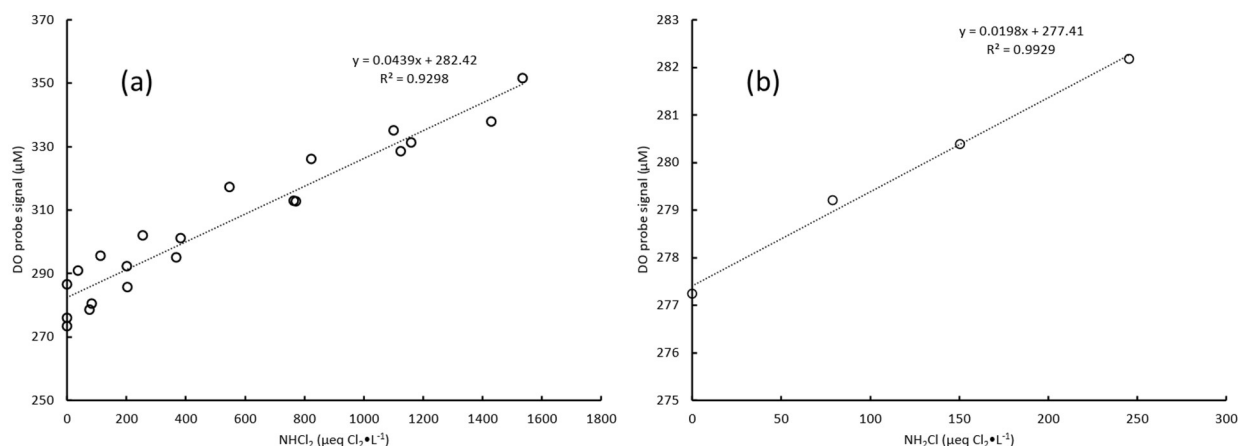
Figure s4-1. Interference signals on Unisense OX-NP microsensor produced by (a) $NHCl_2$ and (b) NH_2Cl.

In a previous study by this research group,(Pham et al., 2021) the NH_2Cl and $NHCl_2$ were measured every 30 minutes over 4 hours while DO was logged every 5 seconds with the OX-NP microsensor (Unisense). A simulation curve was therefore needed to capture the NH_2Cl and

150

$NHCl_2$ profiles over the four-hour reaction time to account for their interferences on the measured OX-NP microsensor signal. A simulation was developed using the UF model of Javert and Valentine(Jafvert and Valentine, 1992) to capture the kinetic profiles for $NHCl_2$ and NH_2Cl which were measured experimentally by the DPD-FAS titration.(Pham et al., 2021) Simulated profiles for NH_2Cl and $NHCl_2$ were used with the linear regressions in Figure s4-1 to calculate the interference on the DO microsensor. These values were subtracted from the previously reported measured DO profiles to generate the corrected DO profiles shown in Figure s4-2. The previously measured DO profiles (black lines and points in Figure s4-2) were used to estimate the rate constants for reactions U7, U8, P5, R7 and R8.(Pham et al., 2021) These were re-estimated in this current work using the corrected DO profiles (red lines and points in Figure s4-2). Table s4-2 shows the rate constants published previously and those re-estimated to account for the interferences, which were fitted using the process detailed previously.(Pham et al., 2021) The rate constant for U7 decreased by about 3%, P5 increased by about 11%, and R7b did not change. The change in the other rate constants was larger, with U8 increasing 100%, R7a increasing 86%, and R8 increasing 91%. Overall, however, the revised reaction rate constants did not change the fitting for NH_2Cl, $NHCl_2$, and NDMA (Table s4-3).
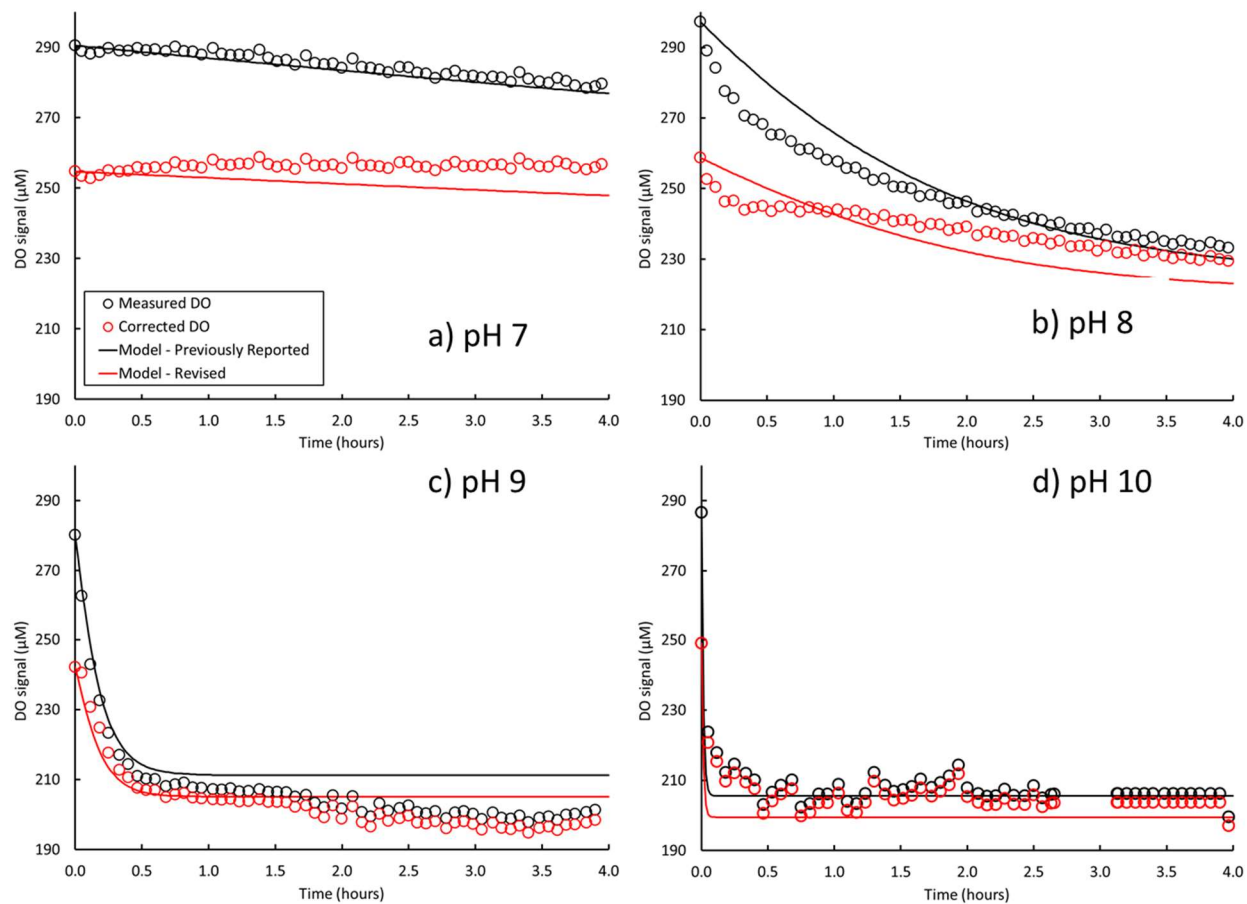
Figure s4-2. Measured DO (○) published in Pham et al. (2021) (Figure 1) and corrected DO (○) (this work) profiles during decomposition of 800 μeq Cl$_2$·L^{-1} in waters with 10 μM TOTDMA at (a) pH 7 , (b) pH 8, (c) pH 9 and (d) pH 10. At pH 10 the gap in DO microelectrode data between 2.6 and 3.2 hours was due to a lost computer connection.

152

Table s4-2. Revised Reactions Rate Constants Implemented in the UF + RNS Model

#	Reaction Stoichiometry [a]	Rate Expression [a]	Rate Constant ($M^{-1}\cdot s^{-1}$) Unless Otherwise Noted	
			Previous work (UF+RNS model) ± SE	This work (UF+RNS model) ± SE
U7	$NHCl_2 + H_2O \xrightarrow{k_{u7}} HNO + 2H^+ + 2Cl^-$	$k_{u7}[NHCl_2][OH^-]$	186 ± 6	181 ± 6
U8	$HNO + NHCl_2 \xrightarrow{k_{u8}} HOCl + products^c$	$k_{u8}[HNO][NHCl_2]$	$(8.2 \pm 0.8) \times 10^4$	$(16.4 \pm 2.2) \times 10^4$
P5	$NHCl_2 + (CH_3)_2NH \xrightarrow{k_{p5}} (CH_3)_2NNHCl + H^+ + Cl^-$	$k_{p5}[NHCl_2][(CH_3)_2NH]$	28 ± 8	31 ± 8
R7	$ONOOH + (CH_3)_2NH \xrightarrow{k_{r7}} (CH_3)_2NNO + products^f$	$k_{r7}[ONOOH][(CH_3)_2NH]$	$^g k_{r7} = k_{r7A}\left[\exp\left(-\frac{k_{r7B}}{[H^+]}\right)\right]$ $k_{r7A} = (2.1 \pm 0.4) \times 10^7\ M^{-1}\ s^{-1}$ $k_{r7B} = (4.4 \pm 0.3) \times 10^{-10}\ M$	$^g k_{r7} = k_{r7A}\left[\exp\left(-\frac{k_{r7B}}{[H^+]}\right)\right]$ $k_{r7A} = (3.9 \pm 0.8) \times 10^7\ M^{-1}\ s^{-1}$ $k_{r7B} = (4.4 \pm 0.3) \times 10^{-10}\ M$
R8	$ONOOH + (CH_3)_2NNHCl \xrightarrow{k_{r8}} (CH_3)_2NNO + products^h$	$k_{r8}[ONOOH][(CH_3)_2NNHCl]$	$^i (1.3 \pm 0.8) \times 10^7$	$(24.8 \pm 9.3) \times 10^6$

[g] Empirical formulation currently only applicable at pH 7–10, indicating that ONOOH/ONOO⁻ decomposition products may also react with $(CH_3)_2NH$ to form NDMA

Table s4-3. Weighted residual sum of squares (WRSS) and average weighted residual sum of squares (AWRSS) summary for experimental data used during UF+RNS model parameter estimation. WRSS and AWRSS are dimensionless. n represents the number of data points in each data set (total n = 528). The n listed may differ from those shown in the associated figure because zero value concentrations would result in an undefined WRSS and AWRSS

pH	Species	n	Previous work		This work	
			WRSS	AWRSS	WRSS	AWRSS
Previous work, experiments with 10 µM TOTDMA						
7	DO	58	2.3×10^{-3}	4.0×10^{-5}	1.1×10^{-2}	1.9×10^{-4}
7	NDMA	7	7.7×10^{-2}	1.1×10^{-2}	1.3×10^{-1}	1.8×10^{-2}
8	DO	58	3.3×10^{-2}	5.8×10^{-4}	4.7×10^{-2}	8.1×10^{-4}
8	NDMA	9	1.1×10^{-1}	1.2×10^{-2}	7.4×10^{-2}	8.2×10^{-3}
9	NH$_2$Cl	10	1.0	1.0×10^{-1}	9.8×10^{-2}	9.8×10^{-3}
9	NHCl$_2$	8	5.1	6.4×10^{-1}	5.3	6.6×10^{-1}
9	DO	58	1.0×10^{-1}	1.7×10^{-3}	2.2×10^{-2}	3.8×10^{-4}
9	NDMA	9	1.4×10^{-1}	1.5×10^{-2}	1.2×10^{-1}	1.3×10^{-2}
10	NH$_2$Cl	10	2.7	2.7×10^{-1}	4.1×10^{-1}	4.1×10^{-2}
10	NHCl$_2$	5	4.0	8.0×10^{-1}	4.0	8.0×10^{-1}
10	DO	54	2.0×10^{-2}	3.7×10^{-4}	1.7×10^{-1}	3.1×10^{-3}
10	NDMA	9	4.1×10^{-2}	4.6×10^{-3}	1.3×10^{-2}	1.4×10^{-3}
Previous work, experiments without TOTDMA						
7	NH$_2$Cl	9	8.3×10^{-1}	9.2×10^{-2}	8.3×10^{-1}	9.2×10^{-2}
7	NHCl$_2$	10	2.3×10^{-1}	2.3×10^{-2}	2.3×10^{-1}	2.3×10^{-2}
8	NH$_2$Cl	8	1.4	1.8×10^{-1}	1.4	1.8×10^{-1}
8	NHCl$_2$	8	1.5	1.9×10^{-1}	1.5	1.9×10^{-1}
Jafvert(Jafvert, 1985)						
6.91	NH$_2$Cl	15	2.1×10^{-2}	1.4×10^{-3}	2.1×10^{-2}	1.4×10^{-3}
6.91	NHCl$_2$	15	1.5	1.0×10^{-1}	1.5	1.0×10^{-1}
6.93	NH$_2$Cl	15	5.0×10^{-2}	3.3×10^{-3}	5.0×10^{-2}	3.3×10^{-3}
6.93	NHCl$_2$	15	1.1	7.2×10^{-2}	1.1	7.2×10^{-2}
6.95	NH$_2$Cl	15	6.6×10^{-1}	4.4×10^{-2}	9.5×10^{-1}	6.3×10^{-2}
6.95	NHCl$_2$	15	7.9×10^{-1}	5.3×10^{-2}	7.9×10^{-1}	5.3×10^{-2}
7.43	NH$_2$Cl	15	7.4×10^{-2}	4.9×10^{-3}	4.8×10^{-2}	3.2×10^{-3}
7.43	NHCl$_2$	11	3.5	3.2×10^{-1}	3.4	3.1×10^{-1}
7.47	NH$_2$Cl	15	1.0×10^{-2}	7.0×10^{-4}	4.2×10^{-3}	2.8×10^{-4}
7.47	NHCl$_2$	10	2.5	2.5×10^{-1}	2.4	2.4×10^{-1}
7.46	NH$_2$Cl	15	4.7×10^{-2}	3.1×10^{-3}	7.7×10^{-2}	5.1×10^{-3}
7.46	NHCl$_2$	12	7.1	5.9×10^{-1}	6.9	5.8×10^{-1}
6.46	NH$_2$Cl	15	2.1×10^{-1}	1.4×10^{-2}	3.4×10^{-1}	2.3×10^{-2}
6.46	NHCl$_2$	15	1.1	7.3×10^{-2}	1.2	8.1×10^{-2}

S2.1 *Impact of Buffer Strength*

Table s4-4. Final pH, NH$_2$Cl, N$_2$O, and NDMA and after a 24-hour reaction time for water containing 10 μM TOTDMA dosed with NHCl$_2$ at 800 μeq Cl$_2$·L^{-1} as a function of TOTBO$_3$. The initial pH was 9.00 ± 0.10

TOTBO$_3$ (mM)	Final pH	NH$_2$Cl (μM)			N$_2$O (μM)			NDMA (μM)		
10	8.77	NM			NM			NM		
20	8.94	146.3	159.2	148.6	11.95	12.14	12.29	3.96	4.11	4.02
30	8.98	152.0	155.4	156.5	10.11	11.76	11.50	3.91	3.93	NR
40	9.01	151.9	156.5	149.6	11.60	11.47	11.94	3.88	3.95	3.93

NM – not measured because of the final pH indicated the drift exceeded 0.10 log units.
NR – not reported due to error in sample preparation.

Table s4-5. ANOVA analysis and Turkey's test for NH$_2$Cl data shown in Table s4

Source of Variation	SS	DF	MS	F_value	p_value	F_critical
Buffer Concentration	16.238	2	8.119	0.374	0.703	5.143
Replication	130.227	6	21.704			
Total	146.465	8				

SS – Sum of Squares.
DF – Degree of Freedom.
MS – Mean Squares.

Table s4-6. ANOVA analysis and Tukey's test for N_2O data shown in Table s4

Source of Variation	SS	DF	MS	F_value	p_value	F_critical
Buffer Concentration	1.514	2	0.757	2.596	0.154	5.143
Replication	1.750	6	0.292			
Total	3.264	8				

SS – Sum of Squares.
DF – Degree of Freedom.
MS – Mean Squares.

Table s4-7. ANOVA analysis and Tukey's test for NDMA data shown in Table s4

Source of Variation	SS	DF	MS	F_value	p_value	F_critical
Buffer Concentration	0.0226	2	0.011	3.931	0.094	5.786
Replication	0.0144	5	0.003			
Total	0.0370	7				

SS – Sum of Squares.
DF – Degrees of Freedom.
MS – Mean Squares.

Table s4-8. Final pH, N_2O, N_2, NO_2^-, NO_3^-, $TOTNH_3$ and NH_2Cl measured at 24 hours at different initial concentration of $NHCl_2$ with and without the addition of 10 μM TOTDMA under ambient atmosphere (~280 μM DO) and inside the glovebox ($\leq$ ~20 μM DO).

	pH	N_2O (μM_N) n = 3	N_2 (μM_N) n = 4	NO_2^- (μM_N) n = 3	NO_3^- (μM_N) n = 3	NDMA (μM_N) n = 3	DMNO (μM_N) n = 3	$TOTNH_3$ (μM_N) n = 3	NH_2Cl (μM_N) n = 3
				Initial $NHCl2$ 200 μeq $Cl_2 \cdot L^{-1}$					
Ambient	9.10	5.7 ± 0.1^a	68 ± 1^a	6.88 ± 0.32^a	4.78 ± 0.05^a	NA	NA	89 ± 4^a	42 ± 0^a
DMA - Ambient	9.09	6.1 ± 0.3^a	50 ± 1^b	2.74 ± 0.05^b	3.20 ± 0.15^b	2.59 ± 0.06^a	$(19.8 \pm 0.5) \times 10^{-3a}$	89 ± 0^a	38 ± 1^b
Glovebox	9.11	9.3 ± 0.4^b	75 ± 3^c	ND	2.20 ± 0.42^c	NA	NA	112 ± 5^b	33 ± 0^c
DMA - Glovebox	9.11	9.3 ± 0.1^b	76 ± 2^c	ND	1.80 ± 0.19^c	1.18 ± 0.01^b	$(12.1 \pm 0.6) \times 10^{-3b}$	121 ± 7^b	31 ± 2^c
				Initial $NHCl_2$ 400 μeq $Cl_2 \cdot L^{-1}$					
Ambient	9.02	13.2 ± 1.3^a	148 ± 4^a	9.47 ± 0.44^a	8.04 ± 0.05	NA	NA	147 ± 7^a	84 ± 1^a
DMA - Ambient	9.03	12.6 ± 0.5^a	130 ± 3^b	3.51 ± 0.71^b	4.77 ± 0.18	3.05 ± 0.01^a	$(23.0 \pm 0.2) \times 10^{-3a}$	154 ± 0^a	79 ± 1^b
Glovebox	9.11	16.6 ± 0.4^b	166 ± 3^c	ND	2.86 ± 0.43	NA	NA	177 ± 0^b	68 ± 1^c
DMA - Glovebox	9.08	16.3 ± 0.4^b	176 ± 3^c	ND	2.48 ± 0.15	1.24 ± 0.01^b	$(12.1 \pm 0.1) \times 10^{-3b}$	200 ± 5^c	63 ± 1^d
				Initial $NHCl_2$ 800 μeq $Cl_2 \cdot L^{-1}$					
Ambient	8.96	26.1 ± 0.3^a	311 ± 8^a	10.46 ± 0.22^a	14.19 ± 0.48	NA	NA	252 ± 7^a	168 ± 1^a
DMA - Ambient	8.93	27.1 ± 0.7^a	274 ± 5^b	3.25 ± 0.42^b	6.27 ± 0.38	3.23 ± 0.04^a	$(29.1 \pm 1.1) \times 10^{-3a}$	272 ± 14^a	163 ± 1^b
Glovebox	9.02	29.4 ± 0.6^b	360 ± 12^c	ND	4.27 ± 0.28	NA	NA	312 ± 22^b	141 ± 1^c
DMA - Glovebox	9.04	29.1 ± 0.7^b	357 ± 10^c	ND	2.47 ± 0.42	1.18 ± 0.01^b	$(10.8 \pm 0.3) \times 10^{-3b}$	353 ± 29^b	137 ± 1^d

The uncertainty for N_2O, N_2, NO_2^-, NO_3^-, NDMA and DMNO the standard deviation of the replicate.

Values with the same letter are not significant difference from each other at $\alpha = 0.05$.

ND – Not Detected. NA – Not Appliable.

Table s4-9. Raw data for the experiment 1. Final TOTNH$_3$, NH$_2$Cl, N$_2$O, N$_2$, NO$_2^-$, and NO$_3^-$ measured at 24 hours at different initial concentration of NHCl$_2$ with and without the addition of 10 μM TOTDMA under ambient atmosphere (~280 μM DO) and inside the glovebox (≤ ~20 μM DO).

	Initial Condition		Final Condition							
	NHCl$_2$ (μM_N)	TOTNH$_3$ (μM_N)	TOTNH$_3$ (μM_N)	NH$_2$Cl (μM_N)	N$_2$O (μM_N)	N$_2$ (μM_N)	NO$_3^-$ (μM_N)	NO$_2^-$ (μM_N)	NDMA (μM_N)	DMNO (μM_N)
					Initial NHCl$_2$ 200 μeq Cl$_2$•L^{-1}					
Ambient	96.3	133.2	52.6	36.3	5.8	68.2	4.7	6.5	NA	NA
	101.8	127.6	52.6	36.3	6.3	70.7	4.8	7.1	NA	NA
	102.2	127.3	52.6	36.3	-	71.8	4.8	7.0	NA	NA
DMA – Ambient	96.1	133.4	57.8	36.4	6.5	49.5	3.2	2.7	2.54	0.020
	99.5	130.0	57.8	36.4	6.4	50.2	3.3	2.8	2.66	0.019
	100.3	129.2	57.8	36.4	-	50.6	3.1	2.8	2.56	0.020
Glovebox	104.1	121.9	98.1	32.7	7.4	70.7	1.9	ND	NA	NA
	91.8	134.3	98.1	32.7	7.3	74.1	2.0	ND	NA	NA
	105.3	120.8	98.1	32.7	-	71.1	2.7	ND	NA	NA
DMA – Glovebox	97.2	128.9	143.4	18.4	4.2	71.4	1.9	ND	1.11	0.011
	98.2	127.9	143.4	18.4	3.7	74.3	1.6	ND	1.21	0.012
	98.6	127.5	143.4	18.4	-	76.1	1.9	ND	1.22	0.013

ND – Not Detected. NA – Not Appliable.

Note: Table s4-9 is continued on the following page

Table s4-9, continued

	Initial Condition		Final Condition							
	$NHCl_2$ (μM_N)	$TOTNH_3$ (μM_N)	$TOTNH_3$ (μM_N)	NH_2Cl (μM_N)	N_2O (μM_N)	N_2 (μM_N)	NO_3^- (μM_N)	NO_2^- (μM_N)	NDMA (μM_N)	DMNO (μM_N)
			Initial $NHCl_2$ 400 μeq $Cl_2 \cdot L^{-1}$							
Ambient	204.4	254.5	106.0	75.7	12.1	148.4	8.0	9.0	NA	NA
	203.7	255.3	106.0	75.7	11.5	156.2	8.0	9.6	NA	NA
	192.6	266.4	106.0	75.7	-	162.4	8.1	9.8	NA	NA
DMA – Ambient	205.3	264.6	110.4	76.1	11.7	130.1	4.9	3.5	3.04	0.023
	203.7	266.2	110.4	76.1	13.4	134.7	4.8	3.0	3.04	0.023
	196.7	273.1	110.4	76.1	-	138.9	4.6	4.0	3.07	0.023
Glovebox	215.6	247.3	185.9	67.9	14.8	148.3	2.4	ND	NA	NA
	187.9	275.0	185.9	67.9	14.4	153.6	3.2	ND	NA	NA
	213.2	249.7	185.9	67.9	-	156.7	3.0	ND	NA	NA
DMA – Glovebox	201.9	261.0	270.2	43.4	9.3	165.6	2.4	ND	1.24	0.012
	201.0	261.8	270.2	43.4	9.1	166.3	2.5	ND	1.23	0.012
	199.0	263.9	270.2	43.4	-	174.9	2.6	ND	1.26	0.012

ND – Not Detected. NA – Not Appliable.

Note: Table s4-9 is continued on the following page

Table s4-9, continued

	Initial Condition		Final Condition							
	NHCl$_2$ (μM_N)	TOTNH$_3$ (μM_N)	TOTNH$_3$ (μM_N)	NH$_2$Cl (μM_N)	N$_2$O (μM_N)	N$_2$ (μM_N)	NO$_3^-$ (μM_N)	NO$_2^-$ (μM_N)	NDMA (μM_N)	DMNO (μM_N)
				Initial NHCl$_2$ 800 μeq Cl$_2\cdot$L^{-1}						
Ambient	413.7	515.1	232.0	155.4	25.5	311.1	14.0	10.3	NA	NA
	412.2	516.2	232.0	155.4	25.2	325.3	14.7	10.7	NA	NA
	389.7	539.1	232.0	155.4	-	341.2	13.8	10.4	NA	NA
DMA – Ambient	388.9	539.9	211.1	156.5	25.7	274.1	3.5	5.9	3.23	0.029
	402.6	526.2	211.1	156.5	25.5	279.7	3.6	6.3	3.28	0.030
	405.8	523.0	211.1	156.5	-	294.4	2.8	6.7	3.19	0.028
Glovebox	421.4	493.6	367.6	136.5	31.8	339.8	4.5	ND	NA	NA
	371.5	543.5	367.6	136.5	29.5	327.5	3.9	ND	NA	NA
	426.1	488.9	367.6	136.5	-	333.8	4.4	ND	NA	NA
DMA – Glovebox	393.4	521.6	488.2	488.2	20.7	335.8	2.9	ND	1.14	0.011
	397.4	517.6	488.2	488.2	20.3	350.4	2.1	ND	1.27	0.011
	399.1	515.9	488.2	488.2	-	372.9	2.4	ND	1.12	0.011

ND – Not Detected. NA – Not Appliable.

Table s4-10. Raw data for the experiment 2. Final $TOTNH_3$, NH_2Cl and N_2O measured at 24 hours at different initial concentration of $NHCl_2$ with and without the addition of 10 µM TOTDMA under ambient atmosphere (~280 µM DO) and inside the glovebox ($\leq$ ~20 µM DO).

	Initial Condition		Final Condition		
	$NHCl_2$ (µM_N)	$TOTNH_3$ (µM_N)	$TOTNH_3$ (µM_N)	NH_2Cl (µM_N)	N_2O (µM_N)
Initial $NHCl_2$ 200 µeq $Cl_2 \bullet L^{-1}$					
Ambient	108.8	123.4	93.0	41.6	5.7
	108.1	124.1	88.8	41.8	5.5
	107.7	124.5	84.8	41.8	5.8
DMA – Ambient	108.8	123.4	88.8	37.4	6.2
	108.1	124.1	88.8	38.6	6.3
	107.7	124.5	88.8	37.6	5.8
Glovebox	92.5	139.7	117.0	32.9	9.2
	100.5	131.7	111.7	33.5	9.8
	102.0	130.2	106.7	33.2	8.9
DMA – Glovebox	92.5	139.7	128.3	30.2	9.3
	100.5	131.7	117.0	29.2	9.3
	102.0	130.2	117.0	33.2	9.2

Note: Table s4-10 is continued on the following page

Table s4-10, continued

	Initial Condition		Final Condition		
	NHCl$_2$ (µM_N)	TOTNH$_3$ (µM_N)	TOTNH$_3$ (µM_N)	NH$_2$Cl (µM_N)	N$_2$O (µM_N)
Initial NHCl$_2$ 400 µeq Cl$_2 \cdot$L^{-1}					
Ambient	215.4	249.0	147.2	82.9	13.2
	217.6	246.8	140.6	84.7	11.9
	216.1	248.3	154.1	82.9	14.9
DMA – Ambient	215.4	249.0	154.1	79.5	13.1
	217.6	246.8	154.1	77.4	12.1
	216.1	248.3	154.1	78.6	12.6
Glovebox	204.1	260.3	176.9	69.5	17.0
	201.0	263.4	176.9	67.9	16.3
	185.1	279.3	176.9	67.7	16.5
DMA – Glovebox	204.1	260.3	203.0	63.9	15.9
	201.0	263.4	203.0	62.5	16.4
	185.1	279.3	193.9	63.9	16.7

Note: Table s4-10 is continued on the following page

Table s4-10, continued

	Initial Condition		Final Condition		
	$NHCl_2$ (μM_N)	$TOTNH_3$ (μM_N)	$TOTNH_3$ (μM_N)	NH_2Cl (μM_N)	N_2O (μM_N)
Initial $NHCl_2$ 800 μeq $Cl_2 \bullet L^{-1}$					
Ambient	435.1	493.7	255.5	168.7	25.7
	432.2	496.6	244.0	167.7	26.3
	430.7	498.1	255.5	167.7	26.2
DMA – Ambient	435.1	493.7	280.0	163.0	27.6
	432.2	496.6	280.0	164.2	26.3
	430.7	498.1	255.5	162.5	27.6
Glovebox	370.2	558.6	336.5	141.5	28.8
	401.9	526.9	307.0	139.8	29.5
	408.1	520.7	293.2	142.1	29.9
DMA – Glovebox	370.2	558.6	386.2	135.9	28.8
	401.9	526.9	336.5	138.1	28.5
	408.1	520.7	336.5	135.9	29.9

Table s4-11. ANOVA analysis for the linear model

Source	Partial SS	df	MS	F	Prob>F
Model	2.2504	6	0.3751	103.55	0.0000
$NHCl_2$	0.0209	1	0.0209	5.76	0.0193
$TOTNH_3$	0.0279	1	0.0279	7.71	
Experiments	1.7130	1	1.7130	472.92	0.0072
Treatment	0.5118	3	0.1706	47.10	0.0000
Residual	0.2354	65	0.0036		0.0000
Total	2.4859	71	0.0350		

Table s4-12. Shapiro-Wilk W test for normal data

Variable	Observation	W	V	z	Prob>z
Res	72	0.9743	1.621	1.052	0.1463

References Cited in the Supporting Information

Hand, V. C. and Margerum, D. W., *Inorganic Chemistry*, **22**, 1449-1456 (1983). Doi 10.1021/Ic00152a007.

Jafvert, C. T. (1985). A Unified Chlorine-Ammonia Speciation and Fate Model. PhD, PhD Dissertation, University of Iowa,

Jafvert, C. T. and Valentine, R. L., *Water Research*, **21**, 967-973 (1987).

Jafvert, C. T. and Valentine, R. L., *Environ Sci Technol*, **26**, 577-586 (1992). Doi 10.1021/Es00027a022.

Leao, S. F. (1981). Kinetics of Combined Chlorine: Reaction of Substitution and Redox. Ph.D. Dissertation, University of California, Berkeley,

Margerum, D. W., Gray, E. T. and Jr.; Huffman, R. P., F. E. Brinckman and J. M. Bellama. *Organometals and Organometalloids; Occurrence and Fate in the Environment;*. American Chemical Society. Washington, DC**:** 278-291 (1978).

Morris, J. C. and Isaac, R. A. *Water Chlorination Enviromental Impact and Health Effects*, Ann Arbor Science Publishers, Ann Arbor, (1983).

Pham, H. T., Wahman, D. G. and Fairey, J. L., *Environ Sci Technol*, 1740-1749 (2021). 10.1021/acs.est.0c06456.

Valentine, R. L., Jafvert, C. T. and Leung, S. W., *Water Research*, **22**, 1147-1153 (1988).

Chapter 5

Conclusion

5.1- Summary

Chapter 2 is a critical review of NDMA formation mechanism in drinking water systems, thereby addressing Objective 1. NDMA occurrence and formation pathways in drinking water systems are reviewed and NDMA yields are compared as a function of disinfectant type, water chemistry, and precursor type. NDMA formation is primarily associated with chloramination. Despite monochloramine being the predominant species between pH 7 – 9, evidence suggests that dichloramine is the primary species involved in NDMA formation. This is somewhat confounding as dichloramine is present at trace level at pH 9 while NDMA yields are maximal at this condition. The kinetic profile for NDMA formation is lacking, and that the influence of chloramine chemistry has not been carefully considered in terms of NDMA formation.

The findings in Chapter 3 demonstrated that Objective 2 was accomplished by a series of batch kinetic experiments with $NHCl_2$ and TOTDMA at pH 7, 8, 9, and 10 under ambient atmosphere in headspace free vials. NDMA, N_2O, DO, $NHCl_2$ and NH_2Cl were kinetically quantified. $NHCl_2$, N_2O and DO profiles suggested the formation of RNS during $NHCl_2$ decomposition, including HNO/NO^- and $ONOOH/ONOO^-$. The presence of uric acid led to the decreased of NDMA yields implicated $ONOOH/ONOO^-$ as a central node for NDMA formation, which was further supported by concomitant DMNO formation. The UF+RNS kinetic model accurately simulated $NHCl_2$, NH_2Cl, NDMA and DO profiles and yields. The UF+RNS model included (1) the unified model of chloramine chemistry revised with HNO as a direct product of $NHCl_2$ hydrolysis, (2) HNO/NO^- then reacting with (i) HNO to form N_2O, (ii) DO to form $ONOOH/ONOO^-$, or (iii) $NHCl_2$ or NH_2Cl to form nitrogen gas, and (3) NDMA formation via $ONOOH/ONOO^-$ or their decomposition products reacting with (i) DMA and/or (ii) chlorinated unsymmetrical dimethylhydrazine (UDMH-Cl), the product of $NHCl_2$ and DMA.

Objective 3 was addressed in Chapter 4. The role of DO in this reaction scheme was examined at pH 9 by assessing kinetic profiles of $NHCl_2$ and NDMA and nitrogen mass balances under ambient DO (~280 μM) and low-DO (< 20 μM) conditions in the presence and absence of 10 μM TOTDMA. Uric acid, an $ONOOH/ONOO^-$ scavenger, completely shut down NDMA formation under the low-DO condition, validating $ONOOH/ONOO^-$ as the central node in NDMA formation. Yield experiments with initial $NHCl_2$ of 200-, 400-, and 800 μeq $Cl_2 \cdot L^{-1}$ tracked the formation of NH_3/NH_4^+, NH_2Cl, N_2O, N_2, NO_2^-, and NO_3^-. NH_3/NH_4^+ yields were 20–40% greater under the low-DO condition, implying a reaction occurred between NH_3/NH_4^+ and $ONOOH/ONOO^-$ or its decomposition products. NH_2Cl yields were 16–20% lower under the low-DO condition, revealing a previously unknown NH_2Cl formation reaction. Under ambient DO conditions, about 80% of the nitrogen was accounted for compared to the low-DO conditions in which nitrogen recoveries were 90- and 100% in the absence and presence of 10 μM TOTDMA, respectively. An existing mechanistic model accurately predicted NH_3/NH_4^+, NH_2Cl, and N_2 under ambient conditions but underpredicted N_2O and overpredicted NO_2^- and NO_3^-. The results provide a framework to guide future experiments with $ONOOH/ONOO^-$ generators and revise the mechanistic model to better capture the nitrogenous end-products.

5.2- Significance and Future Work

The findings from this work provide mechanistic insights into the chloramine chemistry and its impact on formation of NDMA. The formation of HNO/NO^- and $ONOOH/ONOO^-$ during $NHCl_2$ decomposition had not yet been considered or experimentally confirmed. This work confirmed the formation of reactive nitrogen species during $NHCl_2$ decomposition and delineated their role in the NDMA formation.

Future work should include other NDMA precursors such as ranitidine because the mechanism for NDMA formation from ranitidine is suspected to be different from the formation of NDMA from DMA. Aside from NDMA, speciation of N-nitrosamines in U.S water systems may change due to the presence of the precursors linked to the opioid crisis. For example, N-nitrosopiperidine (NPIP) was not found during a 2010 nationwide survey of chloramine utilities. Our preliminary data, however, show NPIP can form from the chloramination of water containing the powerful synthetic opioid fentanyl (FEN) and its major metabolite norfentanyl (NFEN).

Future work also should include simplifying the peroxynitrite decomposition model to only include relevant reactions under drinking water conditions.